EXAMENSARBETE INOM TEKNIK,
GRUNDNIVÅ, 15 HP
STOCKHOLM, SVERIGE 2020

Property Prediction Of Super Strong Nanocellulose Fibers

[Fiber and polymer technology]

MARIA ABADA, LOUISE BRANDT

ELIN FOSSUM, ANTON ÅKESSON

KTH
SKOLAN FÖR KEMI, BIOTEKNOLOGI OCH HÄLSA

Abstract

The innovative technology behind production of strong biofilaments involves the process of spinning filaments from nanoparticles extracted from wood. These nanoparticles are called cellulose nanofibrils (CNFs). The spun filaments can have high mechanical properties, rivaling many other plant based materials, and could be an environmentally friendly replacement for many materials in the future such as fabrics and composites. Before mass production might be possible, the optimal dispersion properties must be determined for the intended use, with regard to concentration, method of oxidation (TEMPO-oxidation or carboxymethylation) and pretreatment through sonication and centrifugation.

In this bachelor's thesis attributes of spun filaments were investigated in order to find a correlation between mechanical properties and the effects of concentration, method of oxidation as well as sonication and centrifugation of the dispersions. The mechanical properties were also compared to the fibrils' ability to entangle and align during flow-focusing. A variety of analytical methods: flow-stop, tensile testing, scanning electron microscopy (SEM) and wide angle X-ray scattering (WAXS) were implemented for the dispersions and filaments.

The results from this study show that flow-stop analysis could be used to determine which CNF dispersions are spinnable and which are non-spinnable, along with which spinnable dispersion would yield the strongest filament. It was also concluded that crystallinity of fibrils affects the mechanical properties of filaments and that TCNFs are generally more crystalline than CMCs. Pretreatment through sonication and centrifugation seems to have a negative impact on spinnability and sonication in combination with low concentration seems to lead to non-spinnable conditions. On the other hand, sonicated dispersions seem to yield a greater number of samples without aggregates than non-sonicated ones. Aggregates, however, seem to only affect ultimate stress out of the measured mechanical properties. Furthermore, concentration and viscosity affect spinnability and CMC dispersions seem to yield thicker filaments than TCNF dispersions. However, due to lack of statistically validated data any definitive conclusions could not be drawn.

Acknowledgements

As a group, we would like to express our sincere gratitude to Tomas Rosén (Treesearch, KTH Royal institute of Technology, Sweden), Korneliya Gordeyeva (KTH Royal institute of Technology, Sweden), Daniel Söderberg (Treesearch, KTH Royal institute of Technology, Sweden) and Lars Wågberg (KTH Royal institute of Technology, Sweden) for giving us the opportunity to perform this project. We pay a special regard to Tomas and Korneliya, for their encouragements and infinite support and guidance. We would also like to express our deepest appreciation to Åsa Engström and Karl Håkansson at RISE, from whom we have received immense help and many valuable inputs.

1. Introduction

The aim of this study is to investigate and compare the mechanical properties of filaments spun from different types of nanocellulose dispersions. These dispersions contain cellulose nanofibrils (CNFs), that can also sometimes be referred to as nanocellulose fibrils (NFCs) or cellulose microfibrils (CMFs). This study compares CNF filaments spun from dispersions of TEMPO-oxidized CNFs (TCNFs) and carboxymethylated CNFs (CMCs), of different concentrations as well as different combinations of pretreatment through sonication and centrifugation. By using different types of analytical instruments the alignment, crystallinity and mechanical properties of the filaments are investigated. Furthermore, results from a new form of analytical instrument, called flow-stop, are analyzed and potential connections to spinnability are investigated.

The overall aim of this study is to investigate possible connections between the internal filament structures and the mechanical properties of the filaments.

Sub-questions to help reach conclusions on the study are listed below.

- *Which conditions led to spinnable dispersions?*
- *Which conditions led to higher degree of alignment of fibrils inside the filaments?*
- *Can obvious differences in filament surface structure depending on treatment be determined?*
- *How did the internal structure of cellulose inside fibrils change with treatment?*
- *Which conditions yielded filaments with highest values of mechanical properties?*

2. Theoretical background

2.1 Cellulose and nanocellulose

Cellulose is a chain polymer built of (1→4)-β-glucose monomers. Cellulose nanofibril (CNF) consists of cellulose chains packed parallel to each other in a specific manner and are linked through van der Waals forces and hydrogen bonds. (Ek et. al., 2011) The crystallinity of the CNF is dependant on the amassed interface of the fibrils and the degree of order of single chains. A non-crystalline region forms in between fibrils and is made of amorph, unaligned cellulose. (Daicho *et. al.,* 2018)

Derivatization, substitution of at least one hydroxyl group into another functional group, changes the features of the cellulose. As the functional groups are changed, the force of the intermolecular bonds also changes through derivatization. (Ek *et. al.*, 2011)

Through high-pressure homogenization of pulp, wood based CNFs can be produced, as pulp in general has a high weight percentage (wt%) of cellulose. At the same time mechanical extraction of CNFs from wood pulp may result in a significant decrease of cellulose crystallinity. In order to decrease clogging, which often occurs in this process and preserves native cellulose crystallinity, hydrophilic cellulose polymers and other swelling agents can be added to pulp prior to treatment or charged groups can be introduced within the wood fibers by chemical pre-treatments. (Klemm *et. al.*, 2011)

2.1.1 TEMPO-oxidized Cellulose (TCNF)

When oxidizing cellulose with 2,2,6,6-tetramethylpiperidine-1-oxyl radical (TEMPO), various systems can be used. For the TEMPO/NaClO/NaBr system under alkaline conditions, the primary hydroxyl of C^6 is selectively converted into a carboxylate group. TEMPO and NaBr act as catalysts while NaClO acts as an oxidant. The mechanism is illustrated in Fig.1 below. Further, selective reduction of aldehyde groups that have not been converted into carboxylates can be done using $NaBH_4$. (Saito *et. al.*, 2006)

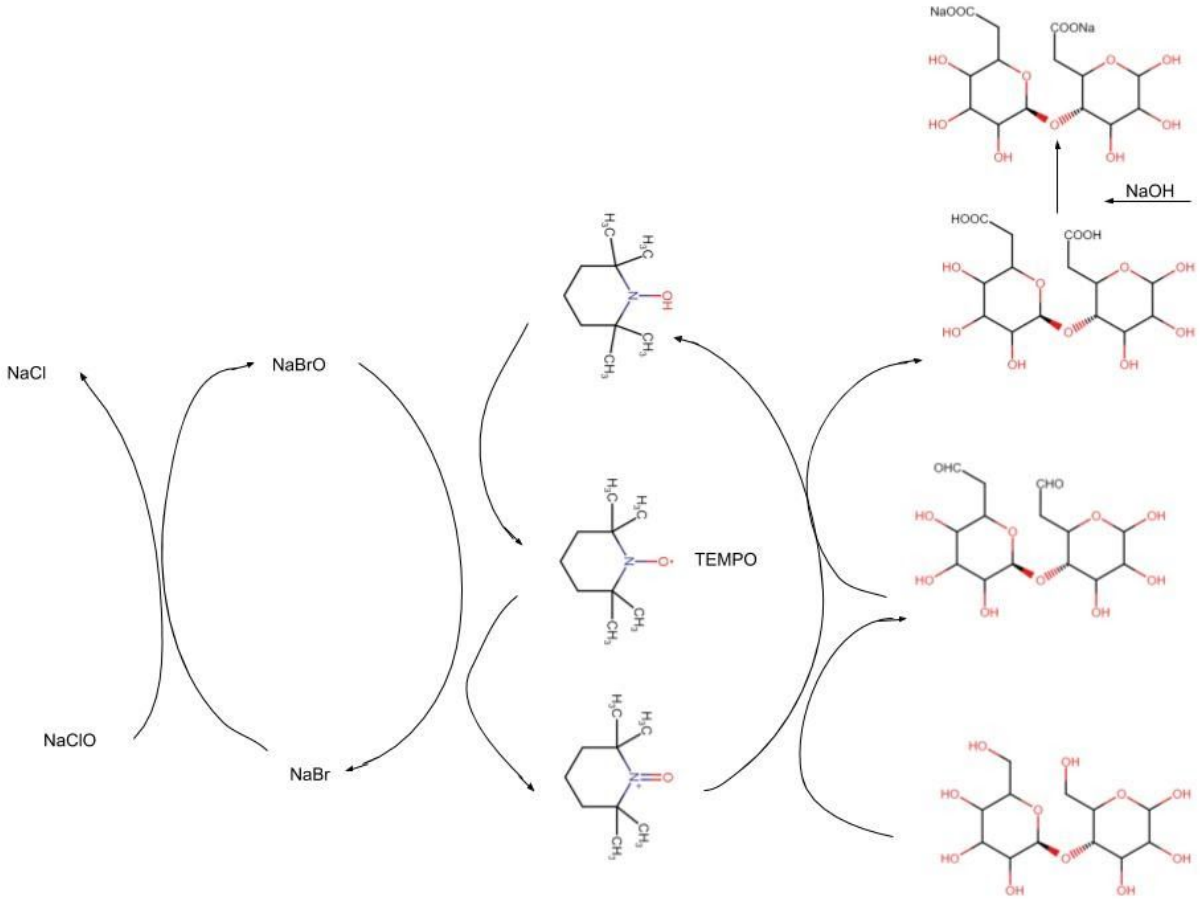

Figure 1. Illustration of mechanism for TEMPO/NaClO/NaBr system oxidation adapted from Saito *et. al.* (2006).

It has been found that using a higher concentration of NaClO during oxidation results in CNFs with higher fibrillation yield and increased carboxylate content. The reason for the higher fibrillation yield is, among others, the high content of carboxylate. Carboxylates cause the CNFs to repel each other, through electrostatic repulsion. It has also been observed that usage of higher concentrations of NaClO result in stronger networks of CNFs as it increases the specific area of the cellulose which results in entanglements of CNF. (Bettaieb *et. al.*, 2015)

TEMPO-oxidation does not affect the crystallinity of the cellulose as the substitution of functional groups does not occur inside the cellulose crystallites but rather on the surface of them. (Saito *et. al.*, 2006)

2.1.2 Carboxymethylated Cellulose (CMC)

Under alkaline conditions, cellulose dispersed with NaOH in an organic liquid, the hydroxyl groups of cellulose can undergo etherfication with monochloroacetic acid (C2H3ClO2) or sodium monocholoacetic acid (SMAC) as described below. This process can be repeated with the product of the foregoing step. (Aguir *et. al.*, 2005)

$$CellONa + C2H3ClO2 \rightarrow CellOCH_2COONa$$

Several carboxymethyl groups can be substituted onto the alkaline cellulose depending on the the conditions of the reaction. The determining factors of the degree of substitution (DS) are reagent concentrations, type of solvent and amount of times carboxymethylation has occurred. (Aguir *et. al.*, 2005) DS defines how many functional groups per repeating unit that are substituted within a polymer. (No author, 2011) For the reagent concentrations, the amounts of NaOH and C2H3ClO2 are relevant. An optimum DS can be reached with increasing concentration of NaOH and the higher the concentration of C2H3ClO2 the higher the DS. For the solvent, the DS increases with decreasing polarity of the organic solvent. The more times that the carboxymethylation is done, the higher the DS. (Aguir *et. al.*, 2005)

When NaOH is introduced during carboxymethylation, it affects the crystallinity of the cellulose as it reacts in the amorphous regions of it. The reactions between NaOH and cellulose results in cellulose-II replacing some of the cellulose-I. It has been found that the overall crystallinity increases when increasing the amount of NaOH used. (Bhandari *et. al.,* 2011)

2.2 Rheology of CNF Dispersions

Viscosity of CNF dispersions are in direct correlation to shear rate, which is the propagation of movement through a liquid. (Naderi et. al., 2016) A CNF dispersion is a shear thinning liquid, meaning it is non-Newtonian and the viscosity of the liquid decreases during shear strain. (Meng et. al., 2016) The CNF dispersions typically obtain some elastic properties above a certain overlap concentration, typically around 0.01-0.05 wt%, due to increasing fibril-fibril interactions. (Geng et. al., 2018) The overlap concentration thus signifies the critical concentration separating the semi-dilute and dilute regions of the dispersion. (Onyianta et. al., 2017) A semi-dilute CNF dispersion is also known to be thixotropic, meaning that the viscosity is not only dependent on the instantaneous shear rate, but also on the shear history, for example if dispersion has been pre-sheared or not. (Naderi et. al., 2016) At higher concentration, such as 0.3 wt% for a dispersion of 980 μmol/g charge, the connectivity between nanofibrils is so high that the dispersion transitions to a volume-spanning arrested gel-like state. (Geng et. al., 2018)

It has been proven that for CMC an increase of the system's ionic strength leads to a decrease in viscosity as well as gel stiffness. (Naderi *et. al.,* 2016) The viscosity of TCNF follows the same trend. (Moberg *et. al.*, 2017)

2.3 Sonication and centrifugation

Sonication and centrifugation are two processes that can be used to homogenize dispersions. The sonication process disrupts aggregates in a dispersion by applying high energy ultrasonic frequencies through a liquid sample. The process agitates the nanofibrils through rapid compression and disturbs clotting. (Thanu *et. al.,* 2019) A probe is inserted in the sample and emits focused acoustic energy evenly throughout the sample. (Covaris, 2020) Centrifugation can, in turn, be performed to separate fibrils of different lengths and aggregates to prevent abnormally big objects from entering the machinery or threads, and thereby causing clogging or defects within filaments, respectively. (Yang, *et. al.,* 2019)

2.4 Flow-focusing

Cellulose nanofibrils (CNFs) can be organized and spun into strong macroscale fibers by ensuring fibril alignment in the structure, which can be achieved using a method called flow-focusing spinning. (Mittal *et. al.*, 2018)

Flow-focusing spinning is performed using a double flow-focusing channel geometry, which consists of six different channels: one for the CNF dispersion (marked by 1 in Fig.2), two each for deionized water (marked by 2 in Fig.2) and acid at low pH (marked by 3 in Fig.2), and one that serves as outlet (marked by 4 in Fig.2). The CNF dispersion is injected in the core flow channel, while sheath flows of water and acid are injected in channels perpendicular to the flow of the CNF dispersion. The principle for the double flow-focusing spinning method is shown in Fig.2. (Mittal *et. al.*, 2018)

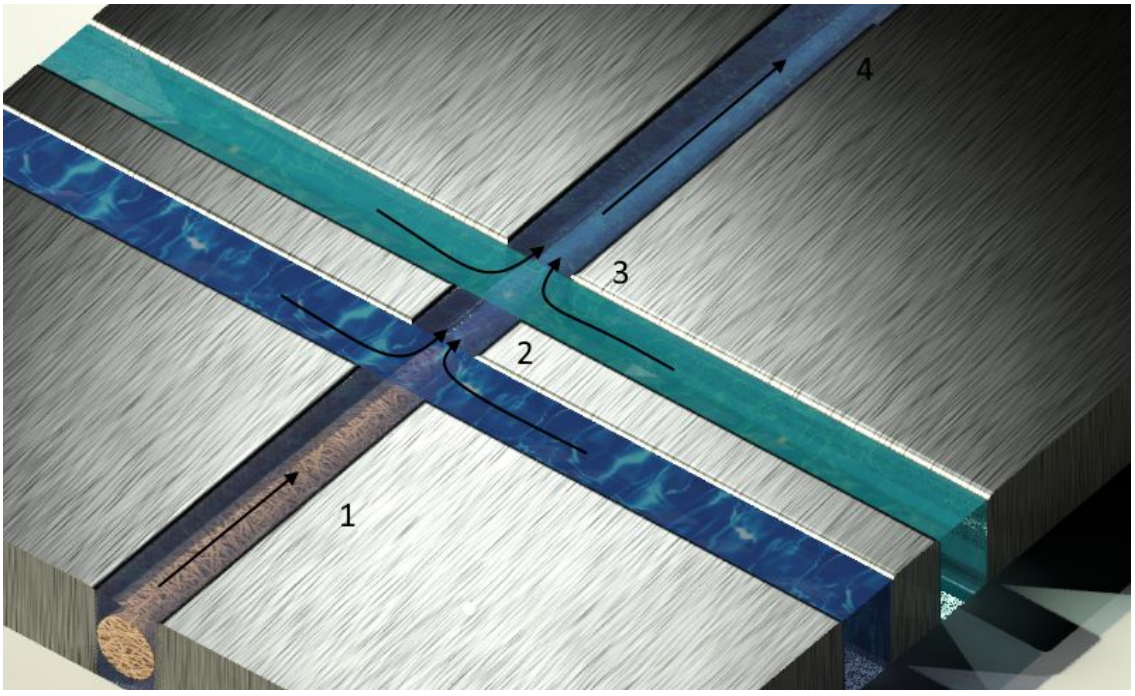

Figure 2. Illustration of the principle structure of a double flow-focusing channel that is used in order to align cellulose nanofibrils (CNFs) into macroscale fibers. A CNF dispersion is injected in the core flow (marked by 1), while deionized water (marked by 2) and acid at low pH (marked by 3) are injected perpendicular to the CNF dispersion flow. This figure is adapted from Mittal *et. al.*, 2018

When the nanocellulose dispersion comes in contact with the sheath flows of water (marked by 2 in Fig.2), hydrodynamically induced fibril alignment is obtained in the direction of the flow. (Håkansson *et. al.*, 2014) As a direct effect of introducing acid at low pH, the alignment is then locked in, what is described by Mittal *et. al.* (2018) as, a metastable colloidal glass structure. When the nanocellulose dispersion comes in contact with the acid, the carboxylate (COO^-) groups become protonated and the electrostatic repulsions are reduced and overcome by van der Waals and hydrophobic forces. The resulting metastable structure prevents loss of alignment, that would otherwise occur due to Brownian motion. (Mittal *et. al.*, 2018)

The deionized water flowing along the walls of the flow-focusing channel prevents transition of the CNF dispersion into the glass state in contact with the walls, which could otherwise lead to clogging of the cell. (Mittal *et. al.*, 2018)

2.5 Analytical methods

2.5.1 Flow-stop

A similar flow-focusing setup to the one explained in section 2.4 above can be combined with a flow-stop procedure, in order to measure birefringence in cellulose nanofibril (CNF) dispersions and thereby provide information on the fibril alignment in relation to Brownian motion. The single flow-focusing setup is in this case consisting of four main channels as can be seen in Fig.3. The CNF dispersion is injected in the core channel and deionized water is injected in the two sheath flow channels perpendicular to the flow of CNF. The fourth channel serves as an outlet. This setup ensures an extensional flow of the CNF dispersion, which causes the CNFs to align in the direction of the flow. The flow cell is mounted in between two cross polarizers, and a high-speed camera is installed to measure red laser light passing through the setup. The birefringence properties of the CNF dispersions allow for measuring fibril alignment in the system by observing changes in birefringence of the red laser light. Once the flows of CNF dispersion and deionized water reach a steady state, the flows are rapidly stopped by closing the valves (marked with V in Fig.3) connected to the pumps. Brownian motion then causes the system to de-align, which can be observed as a decay of birefringence. The collected data is compared to a reference, whereupon comparisons can be made between different dispersions. (Brouzet *et. al.*, 2019)

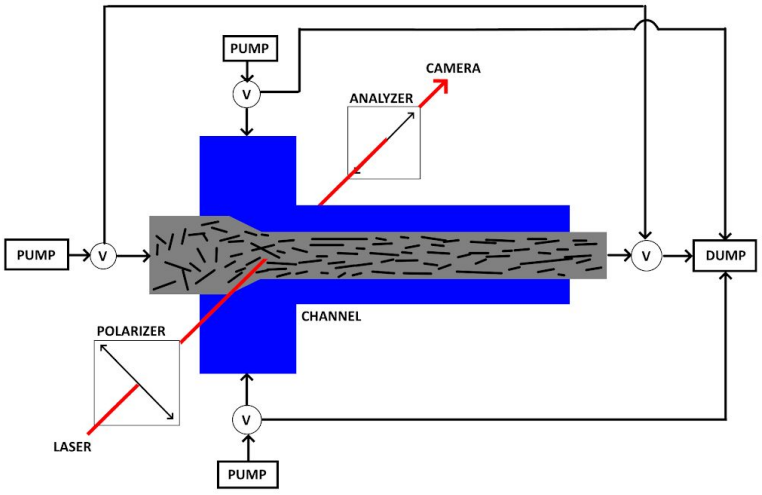

Figure 3. Illustration of the setup used for flow-stop analysis of CNF dispersions, where a flow cell with a single flow-focusing geometry is mounted in between two cross polarizers. The CNF dispersion (grey) flows in the center channel of the cell, while deionized water (blue) flows in the two channels perpendicular to the flow of CNF. The stopping of the flows is controlled by three-way valves, marked by V. This figure is adapted from Brouzet *et. al.*, 2019 (Supporting information).

The definition for birefringence used when performing flow-stop analysis is presented in equation 1 below.

$$Birefringence = \sqrt{\frac{I}{t_{exp}}} \quad (1)$$

where I is the intensity of the collected red laser light and t_{exp} is the exposure time used when performing the analysis.

2.5.2 Tensile test

To examine the mechanical properties, attributes and, by extension, the real-world applications of finished filaments stress-strain (tensile) testing can be performed. Stress-strain testing is the procedure of dislocating two points of a sample's length from each other to the point of full fracture. The main values sought are the overall load withstood before fracture, ultimate stress, and the force withstood without altering the filament geometry. In addition, the extruded force for a deformation to occur may be relevant, if noticeably high for a sample, depending on the filaments intended use, and should be taken into account. Tensile testing plots the Engineering Stress (σ_e) with respect to the Engineering Strain (ε_e). The implemented equations are listed below (equations 2 and 3), along with their completions. (Tu, S. *et. al.*, 2020)

Engineering Strain (ε_e), displacement of the sample (δ) over the original length of the sample (L_0), is calculated as seen in equation 2.

$$\varepsilon_e = \frac{\delta}{L_0} \quad (2)$$

Engineering Stress (σ_e), which is load applied divided by the original cross-section area is seen below in equation 3.

$$\sigma_e = \frac{P}{A_0} \quad (3)$$

Where P is load applied by the machine and A_0 is the original cross-section area of the sample.

An example of the final graph provided can be seen below in Fig.4.

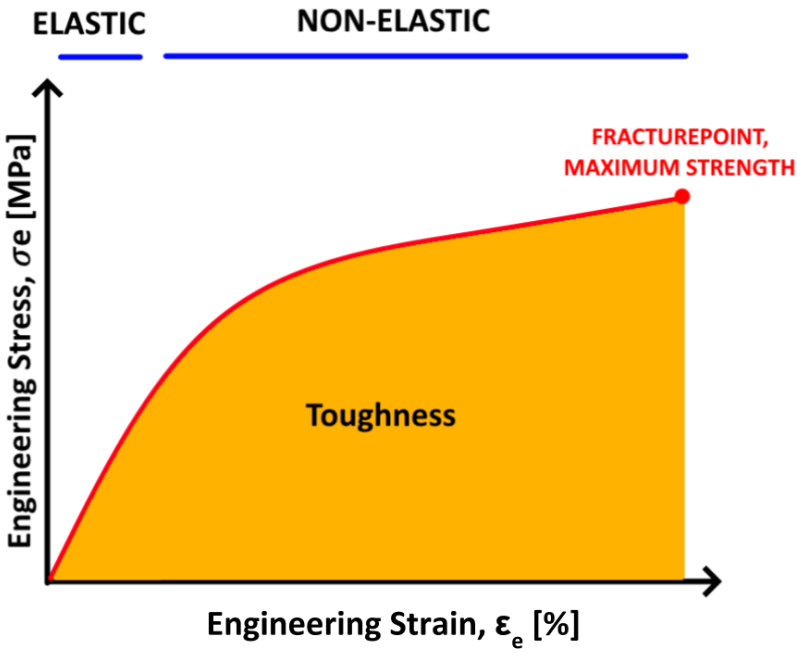

Figure 4. A typical stress-strain test curve that could be seen from tensile testing of a filament thread.

At lower loads applied, the filament thread will act according to Hooke's law, as a brittle, elastic material, which is reflected in the linear part of the graph in Fig.4, referred to as the elastic modulus (*E*). At higher loads however, the sample takes on a ductile property, irreversibly stretching with the displacement until fracturing. The strain required for fracture is referred as strain at break. The elastic modulus is the constant proportionality between strain and stress at lower loads and can be calculated as follows in equation 4. (Roylance, 2001)

$$\sigma_e = E\varepsilon_e \tag{4}$$

The area below the graph represent the total energy requirement for fracture, namely, the toughness of the sample. (Roylance, 2001)

Chemical cross-linking has proven to be a, to some degree, replication of the natural cross-linking between cellulose and lignin/hemicellulose by introducing bonds between fibrils. This leads to an improvement in connectivity and stress transfer. (Mittal *et. al.,* 2018)

2.5.3 Scanning electron Microscopy

In order to assess the topography and alignment of individual filaments, scanning electron microscopy (SEM) can be utilized. This method allows for analysis of the electron patterns emitted of microscopic regions on a sample when focusing an electron beam on it. The microscope can determine so called secondary, back-scattered, electrons diffracted in a thin specimen such as nanocellulose filament. These electron-diffractions along with emitted X-rays show dislocations, defects, interfaces and second phase particles in the sample. (Clarke *et. al.*, 2002)

2.5.4 Wide-angle X-ray scattering

Wide-angle X-ray scattering (WAXS) is a method that could be used to analyze the structure of a filament, as well as the alignment and crystallinity of the fibrils inside the filament. (Clarkson *et. al.*, 2018) Alignment refers to the orientation of crystalline regions, amorphous regions or both. (Bunsell, *et. al.*, 2018) Crystallinity refers to the periodic ordering of the cellulose chains inside the fibrils. (Fahlman, 2018) The process involves scattering of a sample. First an X-ray beam is fired towards the sample. A collimator narrows the beam further towards the sample in several layers to parallelize the beam of the X-rays while removing the excess X-rays. Any and all density irregularities of the sample, including the sample in its entirety will scatter the primary beam away from its source. The detector then picks up the scattered X-rays while a physical object, called beamstop, between the sample and detector prevents the unscattered parts of the primary beam from damaging the detector. (Pauw, 2007) This characterization method can reveal information on crystallinity, orientation and alignment. (Clarkson *et. al.*, 2018)

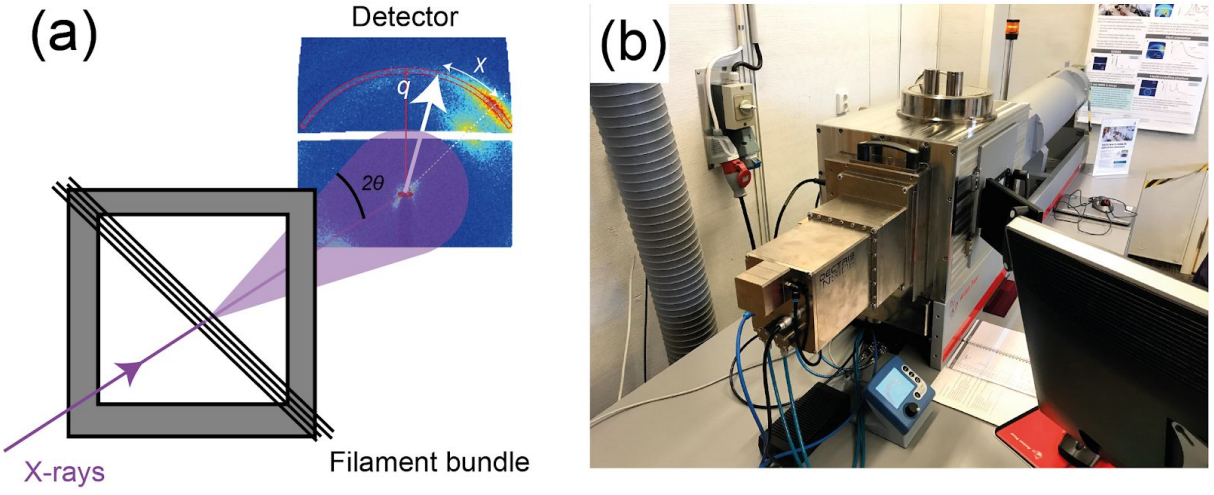

Figure 5. Illustration of WAXS analysis. Figure a.) shows a schematic of the basics for WAXS analysis and b.) shows a WAXS analysis instrument.

The scattering intensity, I, is analyzed at various scattering vectors, q, defined as follows in equation 5. (Björn, 2018)

$$q = \frac{4\pi}{\lambda} \cdot sin(\theta) \tag{5}$$

where 2θ is the scattering angle between primary beam and scattered X-rays, see Fig. 5 a.), and λ is the wavelength of the X-ray beam. (Björn, 2018)

The scattering intensity at a given q, is reflecting the degree of periodic ordering at a certain length scale, d, which is defined in equation 6. (Björn, 2018)

$$d = \frac{2\pi}{q} \tag{6}$$

where q is the scattering vector. (Björn, 2018)

Furthermore, if the scattering intensity pattern is displaying ordered properties it may be seen as dependant of the Azimuthal angle χ, see Fig. 5 a.). (Björn, 2018)

2.5.4.1 WAXS analysis of CNF filaments

A crystalline material or region can be represented by viewing it as a lattice of atoms intersected by its crystal planes and corresponding Miller indices. The indices represent the geometric orientation of the crystal planes by three numbers, correlating to the axis coordinates intersected by the plane and the amount of planes per crystal facete. (Björn, 2018)

Three Miller indices for cellulose are $(1\,\bar{1}\,0)$, (110), and (200) which translate to angles where q is approximately 1.02 nm^{-1}, 1.16 nm^{-1} and 1.59 nm^{-1}, respectively. These numbers correlate to known crystal planes for cellulose. (Han *et. al.* 2013)

2.5.4.2 Equations for WAXS analysis

From the data given through WAXS analysis of a sample a crystallinity index and an orientation index can be calculated. The crystallinity index is calculated using the intensity data calculated as a function of the scattering vector, q, and gives an idea of the crystallinity of a sample. Crystallinity indices can be used to compare the crystallinity of different samples, providing that the crystallinity index is computed the same way for all of them. A crystallinity index of one hundred percent indicates complete crystallinity of the sample, while a crystallinity index of zero percent indicates that the structure is completely amorphous. In this report equation 7 below is used as the definition for crystallinity index.

$$C = 100 \cdot \frac{I_{200} - I_{non-cr}}{I_{200}} \quad [\%] \tag{7}$$

where C denotes the crystallinity index, I_{200} is the maximum intensity of the peak corresponding to the crystal plane in the sample with the Miller indices 200 and I_{non-cr} is the intensity of the valley between the peaks, which represents the intensity of diffraction of the non-crystalline material. (Terinte *et. al.*, 2011)

The orientation index of a sample is calculated using the intensity data calculated as a function of the azimuthal angle, and provides a measurement for the degree of alignment in the samples. Orientation indices of different samples can be compared to each other in order to get an idea of the difference in alignment. An orientation index of one indicates that there is full alignment in the sample, while an orientation index of zero indicates that the structure of the sample is completely random. The definition used for orientation index in this report is provided in equation 8 below.

$$f_c = \frac{180^\circ - fwhm}{180^\circ} \tag{8}$$

where f_c stands for orientation index and $fwhm$ represents the full width at half-maximum of the peak. (Mittal *et. al.*, 2018)

3. Experimental setup

The experimental setup used for spinning filaments from nanocellulose dispersions consisted of a flow-focusing cell, a flowing water bath, rollers, pumps, syringes and tubes. Two 20 ml syringes were filled with deionized water, another two 20 ml syringes were filled with hydrochloric acid at pH 2 and one 5 ml syringe was filled with CNF dispersion. The syringes were then placed on pumps and connected to the cell. The flow-focusing cell was mounted so that the outlet was in contact with the flowing water bath. This allowed for spun filaments to be ejected into the flowing water, whereupon they could be extracted manually and put on a turning roller. The speed of the water flow, as well as the speed of the roller, was adjusted to match the rate of the filament ejection.

4. Method

4.1 Dispersions tested for spinning

Different dispersions with different conditions were tested for spinning, all seven of which are presented in table 1 below. Note that at sample preparation, all dispersions originally had the same concentration and these were adjusted by diluting with deionized water.

Table 1. The table presents the dispersions that were tested for spinning.

Assigned name	**Dispersion type and weight conc.**	**Sonicated**	**Centrifuged**	**Charge (µmoles/g)**
TCNF(0.2 wt%)	TCNF 0.2 wt%	No	No	1000
$TCNF_{sc}$(0.2 wt%)	TCNF 0.2 wt%	Yes	Yes	1000
$TCNF_{sc}$(0.27 wt%)	TCNF 0.27 wt%	Yes	Yes	1000
$TCNF_{sc}$(0.3 wt%)	TCNF 0.3 wt%	Yes	Yes	1000
CMC_{sc}(0.3 wt%)	CMC 0.3 wt%	Yes	Yes	1600
CMC(0.3 wt%)	CMC 0.3 wt%	No	No	1600
CMC(0.2 wt%)	CMC 0.2 wt%	No	No	1600

It was intended to spin CMC_{sc} of varying concentrations as done with CMC, however due to shortage of time that was not done.

4.2 Spinning

The pre-made CNF-dispersion was placed on the magnetic stirrer for 20 minutes to remove eventual aggregates which could form due to self-assembling nature of cellulose after long storage. Bubbles were removed through sonication bath, vacuum suction or centrifugation. It depended on what was accessible. During the stirring the cell was mounted and attached to the set up. The rest of the apparatus was prepared by filling the water bath with deionized water and the pump was turned on to fill the water channel. Syringes were filled with deionized water, 0.01M hydrochloric acid (pH 2) and the CNF-dispersion. Two large syringes (20 ml) were filled with deionized water and hydrochloric acid respectively and a small syringe (5 ml) was filled with the CNF-dispersion. The syringes were mounted on the pumps and the rates of the pumps were adjusted to the values shown in table 2. These flow-rates were identical to previous work performed by Håkansson *et. al.* (2014).

Table 2. Flow rates for specified channels of the cell.

Liquid	**Rate [ml/h]**
Deionized water	4.4
Hydrochloric acid (pH 2)	24.6
CNF-dispersion	4.1

The tubes were attached to the flow-focusing cell and the liquids were pushed through the cell in the right order to avoid clogging. Water was first pushed through, then CNF-dispersion, water again, then acid and at last water again. If CNF-dispersion and acid were pumped through directly after one another, clogging would occur. When there were no bubbles in the channel the cell was lowered into the flowing water and the pumps were turned on. The filament was ejected into the flowing water bath, where it was picked up by hand with a tweezer and placed on a roller. The filaments were then left to dry. Each dried filament was then taped on to a sample holder of paper with a squared U-shape (outer dimensions 2 x 2 cm^2 and inner dimensions 1 x 1 cm^2). Around 60 samples per dispersion were prepared for microscopy and tensile tests for more statistically validated results. One sample per dispersion was prepared for WAXS tests by taping approximately 20 filaments on the diagonal of a sample holder of paper with the shape of a hollow square (outer dimensions 1 x 1 cm^2 and inner dimensions 0.5 x 0.5 cm^2). The samples were placed in Petri dishes marked with necessary information.

If there were particles in the CNF-dispersion before spinning it needed to be homogenized with a Polytron/Thurrax at 5300/10000 rpm for 3 min. If the particles were not dispersed enough a centrifugation of the dispersion was performed to remove the largest particles, while still preserving the CNFs, at 4000 rpm for 15 min. The concentration was determined again by weighing and drying three cups containing approximately 2 ml respectively. The concentration was then calculated. If the concentration was too low it needed to be top concentrated using an Ultrafiltration setup (Ultracel® 100 kDa filter). After the dispersion was dewatered it was mixed again with the Polytron/Thurrax and bubbles were removed with a vacuum desiccator. If there were only bubbles in the CNF-dispersion the vacuum desiccator was sufficient.

If it was not possible to spin filaments from a dispersion the concentration was increased by dewatering it using Ultrafiltration setup (Ultracel® 100 kDa filter) and continuing with the same procedure described in the section above.

4.2 Optical Microscopy

Samples were carefully moved from the Petri dish to a small glass-plate which was placed under the optical microscope. The programme *Streambasic* was opened and the focus of the microscope was adjusted. An approximate value of the minimum width of the filaments was determined. Images of the thinnest part of the filaments and eventual aggregates or deformations were saved in a folder. The thinnest widths were examined in order to see if there was a correlation between width and breakage.

To estimate filament lengths, samples were placed under a USB-microscope connected to a computer. The programme *Dino capture* was opened and the microscope was calibrated and the focus was adjusted. The length of the filament was measured and noted.

4.3 Flow stop

The flow stop analysis was conducted by supervisors. Two syringes were filled with deionized water and one with CNF dispersion and mounted on the flow cell. The pumps were started and flow stop analysis was initiated by turning on the camera. The flow was then stopped by redirecting it to not go through the flow cell and decrease of alignment was documented. This was performed 5 times each on every dispersion, including the non-spinnable ones.

4.4 Tensile testing

The samples were inserted into an ElectroPuls 1000 Instron® tensile tester paired with the corresponding program, WaveMatrix. The samples were clamped to the base of the machine and to the pulling arm, at that point the paper frame for the filament was cut so that the anchor points on the machine were the only things keeping the filament sample in place. The machine was reset and the algorithms were initiated to start the test. All samples were displaced, with the deformation rate 3 mm/min, until fracture.

The data was imported into MatLab, whereupon graphs were constructed and used to calculate values for E-modulus, strain at break, ultimate stress and toughness.

5. Difficulties resulting from COVID-19

Unfortunately due to the pressing pandemic caused by the 2020 COVID-19 outbreak a significant number of cancellations or delays occurred during the experimental phase of this project. As the labs were closed off to prevent spreading the virus, many tests including SEM, WAXS and flow-stop were not able to be performed directly by us but were performed by our supervisors. Other dispersion variants that would otherwise have been analyzed had to be abandoned, since the laboratories were closed due to health and safety concerns.

6. Results

6.1 Spinning

During the spinning process some dispersion were spinnable and some were not. The table below shows which were and which were not.

Table 3. List of dispersions and their spinnability.

Dispersion	**Spinnable (Yes/No)**
TCNF(0.2 wt%)	Yes
$TCNF_{sc}$(0.2 wt%)	No
$TCNF_{sc}$(0.27 wt%)	No
$TCNF_{sc}$(0.3 wt%)	Yes
CMC_{sc}(0.3 wt%)	No
CMC(0.3 wt%)	Yes
CMC(0.2 wt%)	Yes

For all four spinnable dispersions, all intended analytical methods were performed and data was collected, except for CMC(0.2 wt%). There was no time to make a WAXS-sample for CMC(0.2 wt%) and therefore, this sample has no WAXS-analysis data.

The $TCNF_{sc}$(0.3 wt%) dispersion in table 3 was a more recent version of another previous dispersion ($TCNF_{sc}$(0.3 wt%)*). The older dispersion did not seem fit for spinning as it showed signs of contamination or faulty pretreatment, and it was therefore chosen to spin the more recently prepared dispersion instead.

6.2 WAXS-analysis

The WAXS analysis resulted in raw data that could be combined into a mean value detector image for each sample. These images are shown below in Fig.6, where the first image to the left corresponds to analysis of TCNF(0.2 wt%), the image in the middle corresponds to analysis of $TCNF_{sc}$(0.3 wt%) and the image to the right corresponds to analysis of CMC(0.3 wt%). Each image shows areas of higher and lower light intensities, where the areas of higher intensities correspond to crystal planes in the nanocellulose structures. The area of highest intensity in each image in Fig.6 (seen in the upper right of each image) corresponds to the crystal plane (200), whereas the other intensity peak directly adjacent to it corresponds to the two crystal planes (110) and $(1\,\bar{1}\,0)$. This connection can be made by studying the q-values for each of the intensity peaks seen in Fig.6 and comparing them to the values for the crystal planes provided in section 2.5.4.

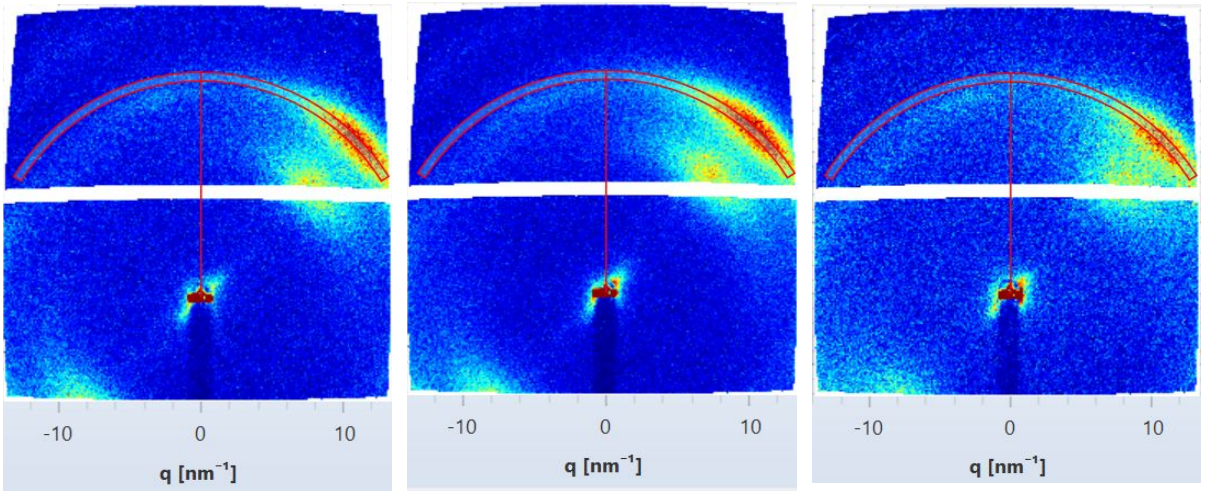

Figure 6. Mean value of detector images from WAXS analysis. The image to the left corresponds to analysis of TCNF(0.2 wt%), the one in the middle $TCNF_{sc}$(0.3 wt%) and the one to the right CMC(0.3 wt%).

The raw data for radial intensity has been processed and the mean value has been calculated as a function of the scattering vector, *q*, for each sample. The averaged graphs are presented in Fig.7 below, where the red graph corresponds to the analysis of CMC(0.3 wt%), the green graph corresponds to TCNF(0.2 wt%) and the blue graph corresponds to $TCNF_{sc}$(0.3 wt%). The highest peak of each graph represents the crystal plane (200), while the lower peak of each graph corresponds to both of the crystal planes (110) and $(1\,\bar{1}\,0)$.

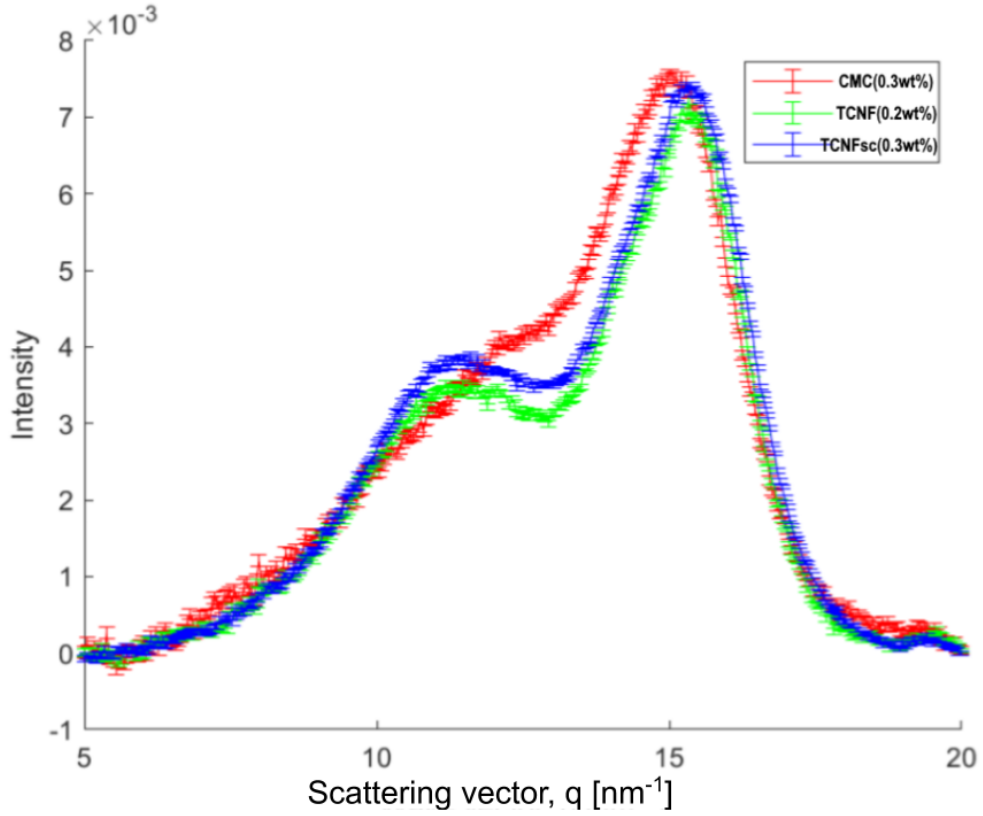

Figure 7. Illustration of an average of radial intensity as a function of the scattering vector, calculated from raw data received during WAXS analysis of the samples. The green graph corresponds to analysis of TCNF(0.2 wt%), while the blue graph corresponds to analysis of $TCNF_{sc}$(0.3 wt%) and the red graph corresponds to CMC(0.3 wt%).

Crystallinity indices of each sample were calculated according to equation 7 in the theoretical background, section 2.5.4.2. The full calculations can be found in appendix, section 10.1.1, and the resulting indices are presented in table 4 below.

Table 4. The table presents the calculated crystallinity indices of the samples.

Sample	TCNF(0.2 wt%)	$TCNF_{sc}$(0.3 wt%)	CMC(0.3 wt%)
Crystallinity index, CI	56.4%	53.4%	45.3%

An average of the intensity as a function of the azimuthal angle is illustrated in Fig.10 below, where the red graph corresponds to the analysis of CMC(0.3 wt%), the green graph corresponds to TCNF(0.2 wt%) and the blue graph corresponds to $TCNF_{sc}$(0.3 wt%). The averages were calculated from raw data received during WAXS-analysis.

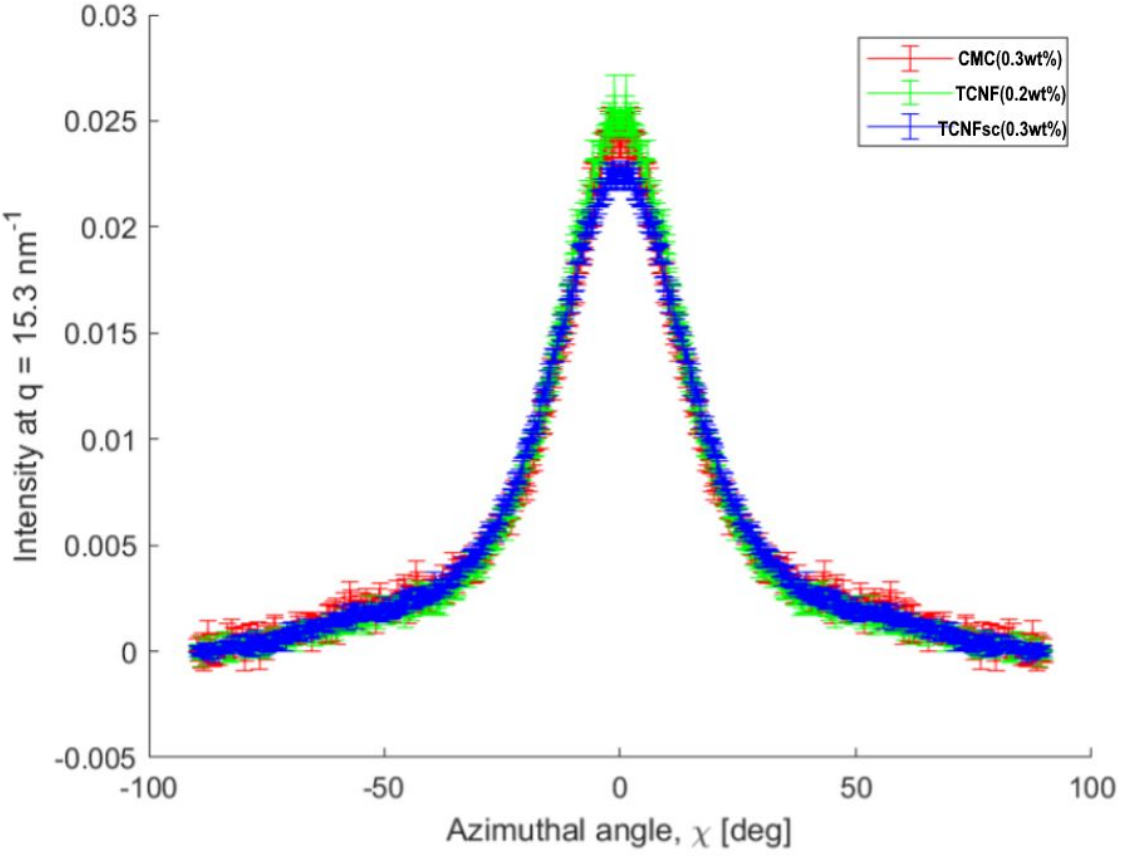

Figure 8. Illustration of an average of the intensity as a function of the azimuthal angle, calculated from raw data received during WAXS analysis of the samples. The green graph corresponds to analysis of TCNF(0.2 wt%), while the blue graph corresponds to analysis of $TCNF_{sc}$(0.3 wt%) and the red graph corresponds to CMC(0.3 wt%).

Orientation indices were calculated for each of the samples according to equation 8 in the theoretical background, section 2.5.4. The full calculations can be found in appendix, section 10.1.2, and the resulting values are presented in table 5 below.

Table 5. The tables present the calculated orientation indices of the samples.

Sample	TCNF(0.2 wt%)	$TCNF_{sc}$(0.3 wt%)	CMC(0.3 wt%)
Orientation index	0.832	0.806	0.823

6.3 SEM

Filaments from all four of the spinnable dispersions were analysed with scanning electron microscopy (SEM). The results from analysis of the $TCNF_{sc}$(0.3 wt%) dispersion are presented in Fig.9. In Fig.9.a) a zoomed in image of the filament is shown, and the width of the filament is marked. In Fig.9.b) an image of a bigger portion of the sample is displayed.

a) 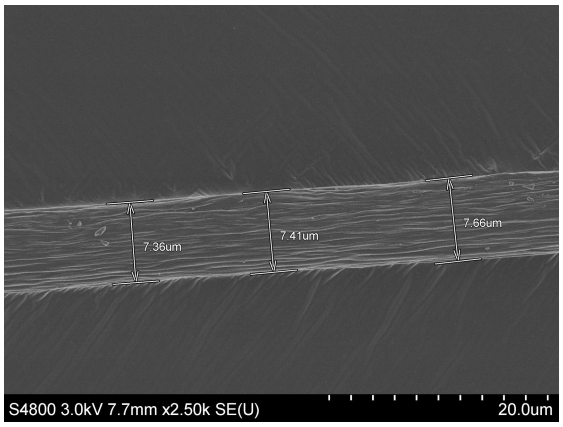

b) 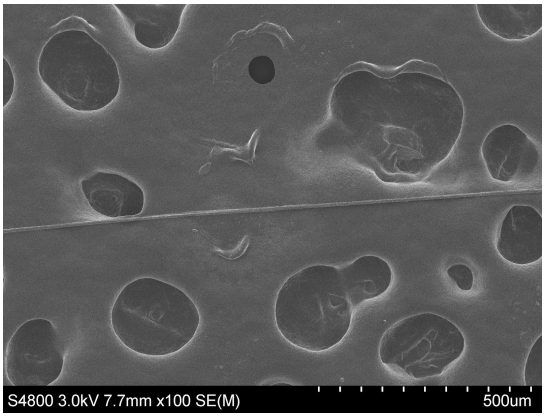

Figure 9. Results from scanning electron microscopy on $TCNF_{sc}$(0.3 wt%). In a) is a zoomed in image of the sample and in b) is an image of a bigger portion of the sample.

In Fig.10 the results from SEM-analysis of TCNF(0.2 wt%) are presented. An image of the whole sample and the width of it is displayed in Fig.10.a). In Fig.10.b) is a zoomed in picture of the surface of the filament. The individual fibrils are not visible, only the rough surface of the filament. In Fig.10.c) is an image of the cross section of the filament presented, along with the width of it.

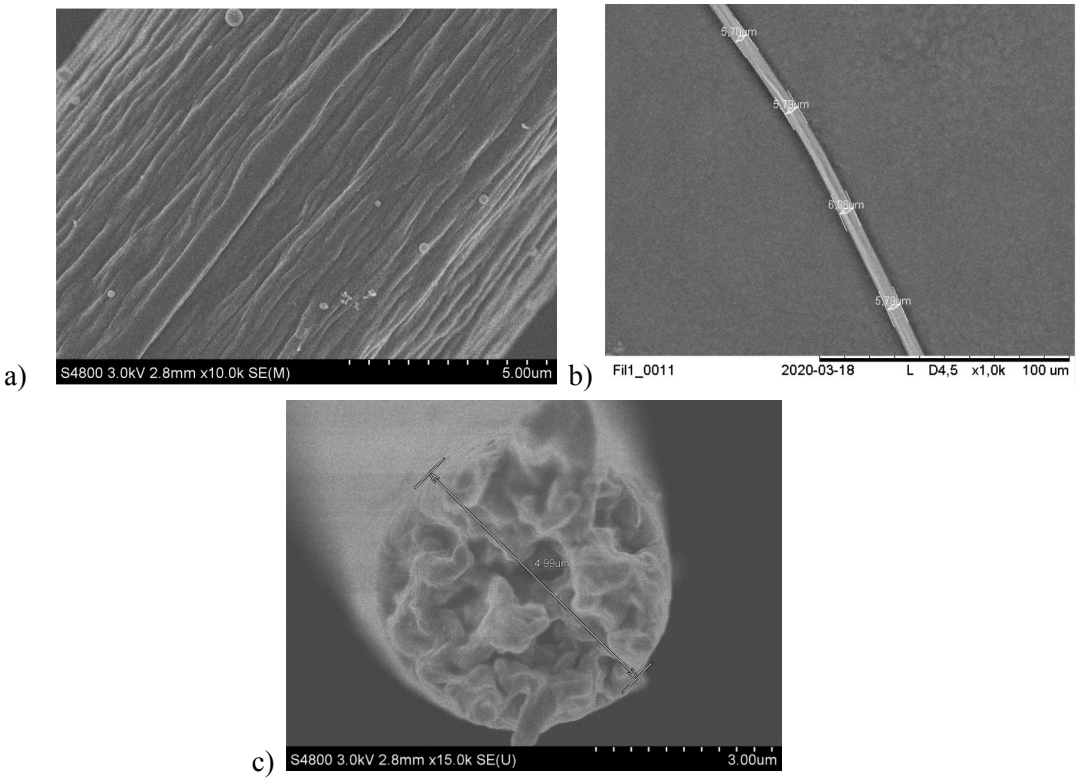

Figure 10. Results from scanning electron microscopy on TCNF(0.2 wt%). In a) is a zoomed in image of the sample. In b) an image of a bigger part of the sample is displayed. The width of the sample is marked. In c) a cross section of the filament is presented. The width of the cross section is marked.

The results from SEM analysis of filaments spun from the two CMC dispersions are presented in Fig.11. Filament spun from CMC(0.3 wt%) is displayed in Fig.11.a) and filament spun from CMC(0.2 wt%) in Fig.11.b). The approximate width of the filaments can be derived from the length scale at the bottom of the images.

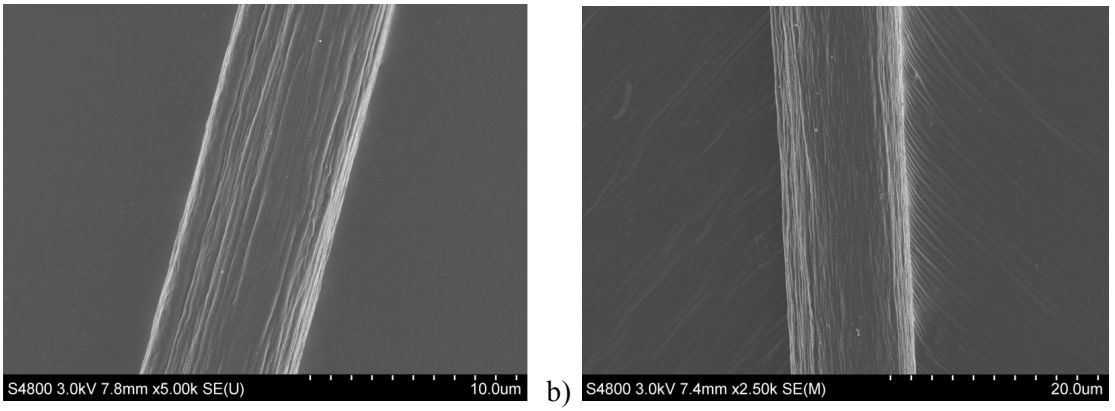

Figure 11. Results from SEM analysis of filaments spun from CMC dispersion. In a) CMC(0.3 wt%) and in b) CMC(0.2 wt%).

6.4 Flow-stop

Flow-stop analysis was performed on all but one of the dispersions tested for spinning and a few more that were not tested for spinning.

By using MatLab to analyze the collected data, images illustrating certain properties were collected. One of these images shows how fast the decay in birefringence was at different parts of the flow-focusing channel, during the first 50 ms after stopping the flow through the channel. This decay, during the first 50 ms, was given the variable name $D_{r,fast}$ and has the unit [rad^2/s]. Another image shows where the decay in birefringence was slowest, this was done by creating an image of the slowest measurable decrease in alignment. This decay was given the variable name $D_{r,slow}$ and has the unit [rad^2/s]. A third image was collected, showing the birefringence of the dispersion throughout the channel. The birefringence was calculated from the intensity of the red laser light collected by the detector, according to the definition presented in equation 1, in section 2.5.1.

Five experiments were performed on each dispersion and mean value images were collected for $D_{r,fast}$, $D_{r,slow}$ and birefringence, along with mean value intensity profiles for each of the mentioned variables, calculated along the flow-focusing channel centerline. The resulting images and graphs are all presented in appendix, section 10.2.1, and an example is given in Fig.12 below. The example figure shows the results of analysis performed on TCNF(0.2 wt%), which was tested for spinning, where the mean value images are shown on the left and the corresponding intensity profiles are shown on the right. The mean value images and the mean value intensity profiles both follow the same order, where the results for $D_{r,fast}$ are presented on top, the results for $D_{r,slow}$ are presented in the middle and the results for birefringence are shown on the bottom. The colour legend to the right of the images shows that a red colour represents a high value and a blue colour represents a low value. In the images for $D_{r,fast}$ and $D_{r,slow}$ this refers to the rate of dealignment and in the birefringence image it refers to how much birefringence there is at different parts along the channel.

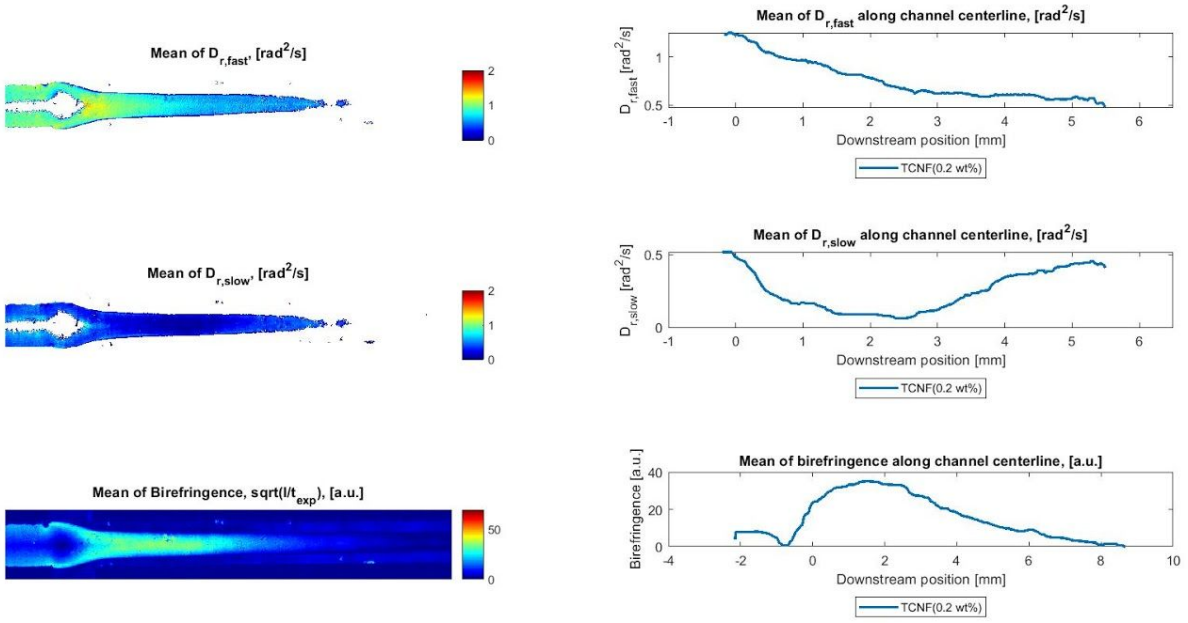

Figure 12. The figure shows an example of the resulting images and graphs given by flow-stop analyses of the dispersions, where these particular results are those given by analysis of TCNF(0.2 wt%), which was tested for spinning. The left side of the figure shows mean value images for $D_{r,fast}$, $D_{r,slow}$ and birefringence, where the first mentioned image is shown at the top of the figure, the second in the middle and the last on the bottom. On the right side of the figure mean value intensity profiles for the middle of the flow-focusing channel are presented, for each of the mentioned variables, where the order of the graphs follows that of the images to the left.

The mean value intensity profiles for the 6 dispersions tested for spinning, calculated along the flow-focusing channel centerline, are presented again in Fig.13 through 17 below, where the intensity profiles for the different dispersions are presented in the same figures. A legend illustrating which graph belongs to which sample is shown in the top right corner of each figure. The dispersions represented by solid lines are the ones that proved spinnable and the dispersions marked with dotted lines are the ones that were not spinnable. In Fig.13 below, the intensity profiles regarding $D_{r,fast}$ are presented for the 6 analyzed dispersions that were tested for spinning.

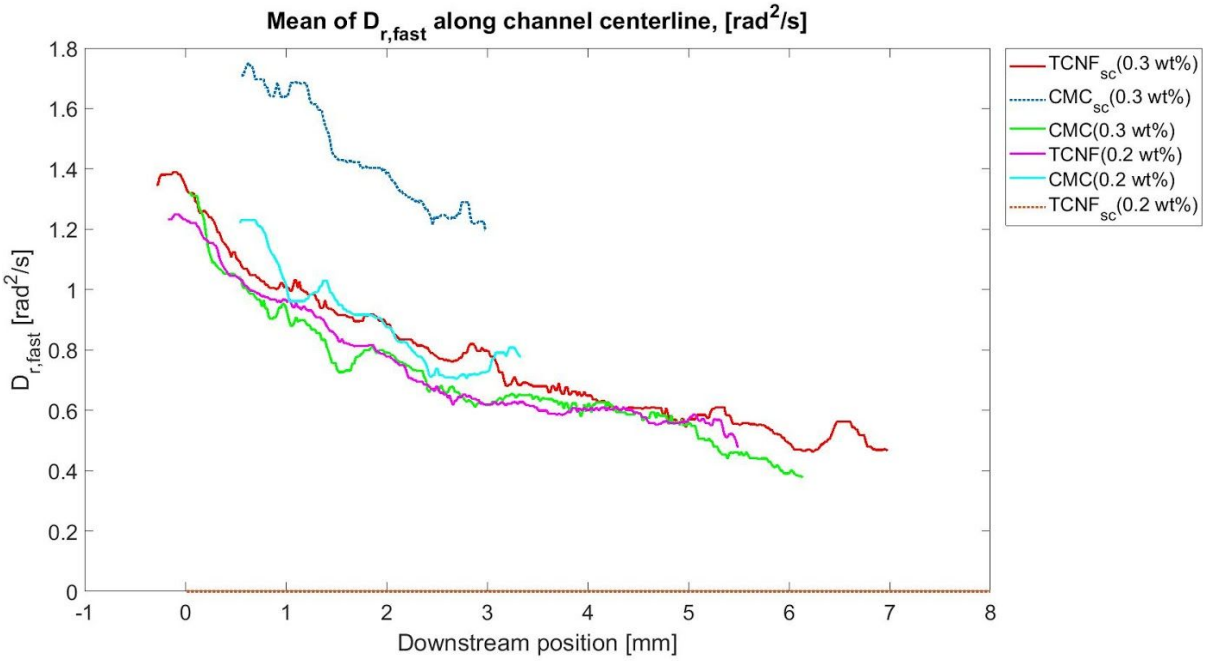

Figure 13. Illustration of the intensity profiles given for $D_{r,fast}$ along the flow-focusing channel centerline, for the 6 dispersions analyzed that were tested for spinning. A legend illustrating which graph belongs to which dispersion is shown in the top right corner of the figure. The dispersions represented by solid lines were spinnable and the dispersions marked with dotted lines were not spinnable.

Fig.14 below shows the intensity profiles regarding $D_{r,slow}$, for the 6 dispersions that were tested for spinning, both on a linear scale, in Fig.14.a), and on a logarithmic scale, in Fig.14.b). The conversion from the linear scale to the logarithmic scale was made to allow for easier analysis of the graphs, later performed in section 7.4.

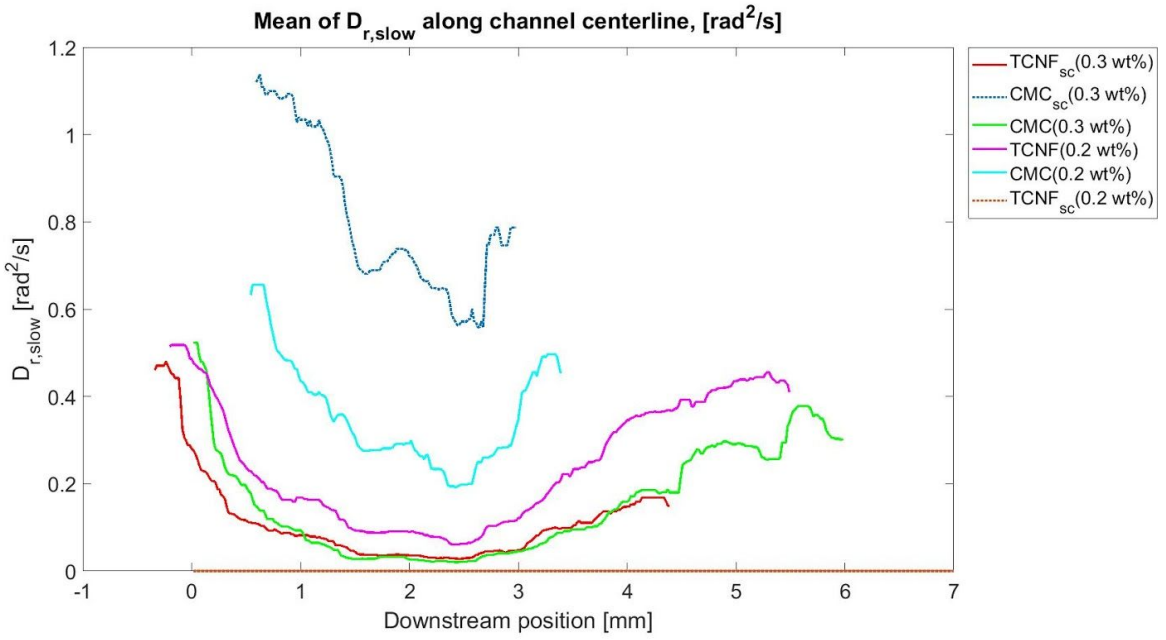

a.)

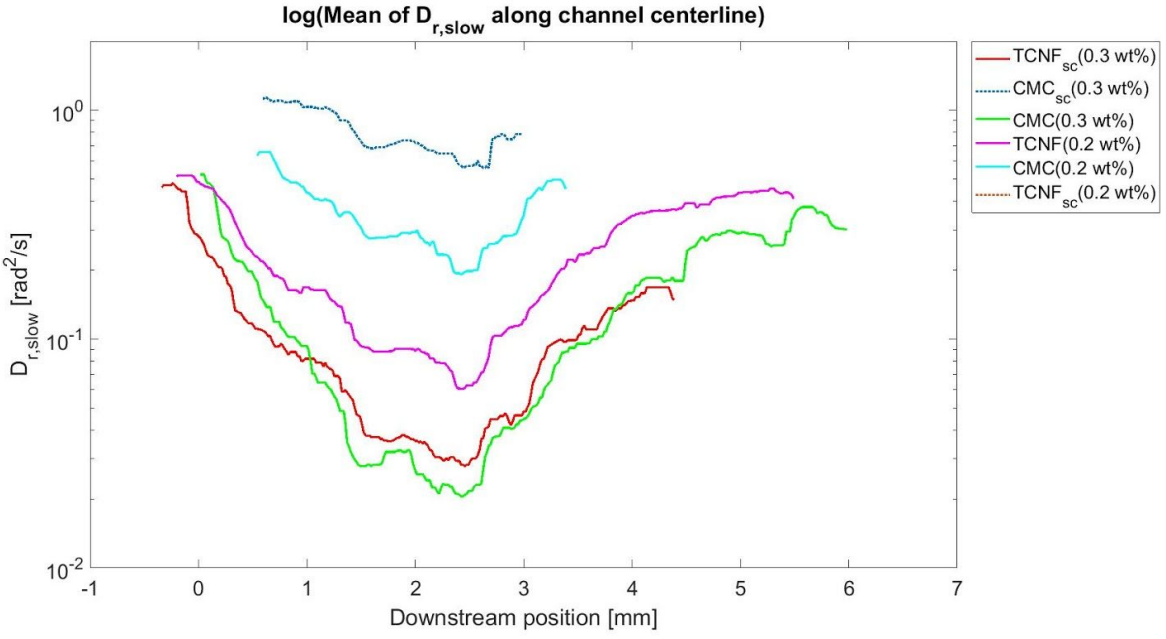

b.)

Figure 14. In the figure intensity profiles given for $D_{r,slow}$ along the flow-focusing channel centerline are presented, for each of the 6 analyzed dispersions that were tested for spinning. In Fig.14.a) the intensity profiles are presented on a linear scale, while the intensity profiles are presented on a logarithmic scale in Fig.14.b). A legend illustrating which graph belongs to which dispersion is shown in the top right corner of each figure. The dispersions represented by solid lines were spinnable and the dispersions marked with dotted lines were not spinnable.

In Fig.15 below the intensity profiles regarding birefringence are presented, for the 6 dispersions that were tested for spinning.

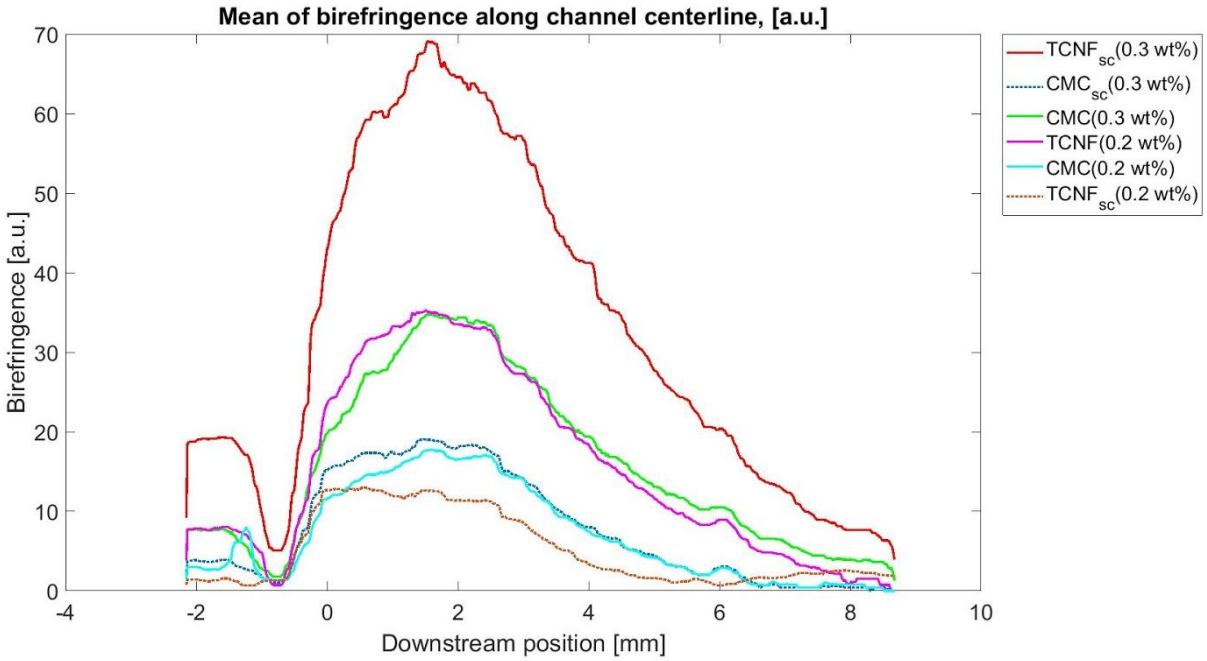

Figure 15. The figure shows the resulting intensity profiles for birefringence along the flow-focusing channel centerline, for the 6 dispersions analyzed that were tested for spinning. A legend illustrating which graph belongs to which dispersion is shown in the top right corner of the figure. The dispersions represented by solid lines were spinnable and the dispersions marked with dotted lines were not spinnable.

By using MatLab, key values were extracted for the properties investigated with flow-stop analysis, for each of the 6 dispersions that were tested for spinning. The key values are maximum rate of decay in birefringence, that is max($D_{r,fast}$), minimum rate of decay in birefringence, that is min($D_{r,slow}$), and maximum birefringence. The values are presented in table 6 below.

Table 6. In the table key values for the properties investigated with flow-stop analysis are presented for the 6 analyzed dispersions that were tested for spinning. The key values listed are maximum rate of decay in birefringence, seen as max($D_{r,fast}$), minimum rate of decay in birefringence, seen as min($D_{r,slow}$), and maximum birefringence.

Dispersion name	**max($D_{r,fast}$)**	**min($D_{r,slow}$)**	**Maximum birefringence**
$TCNF_{sc}$(0.3 wt%)	1.39	0.0278	69.1
CMC_{sc}(0.3 wt%)	1.75	0.559	19.0
CMC(0.3 wt%)	1.32	0.0206	34.8
TCNF(0.2 wt%)	1.25	0.0605	35.3
CMC(0.2 wt%)	1.23	0.191	17.8
$TCNF_{sc}$(0.2 wt%)	Non-measurable	Non-measurable	13.0

Figures showing the intensity profiles for the 4 dispersions analyzed with flow-stop that were not tested for spinning, were also created. These figures are presented below in Fig.16 through 20, where the intensity profiles for the 4 mentioned dispersions are presented. A legend illustrating which graph

belongs to which sample is shown in the top right corner of each figure. The star following a dispersion name marks that the dispersion in question was not tested for spinning. In Fig.16 below, the intensity profiles regarding $D_{r,fast}$ are presented for the 4 analyzed dispersions that were not tested for spinning.

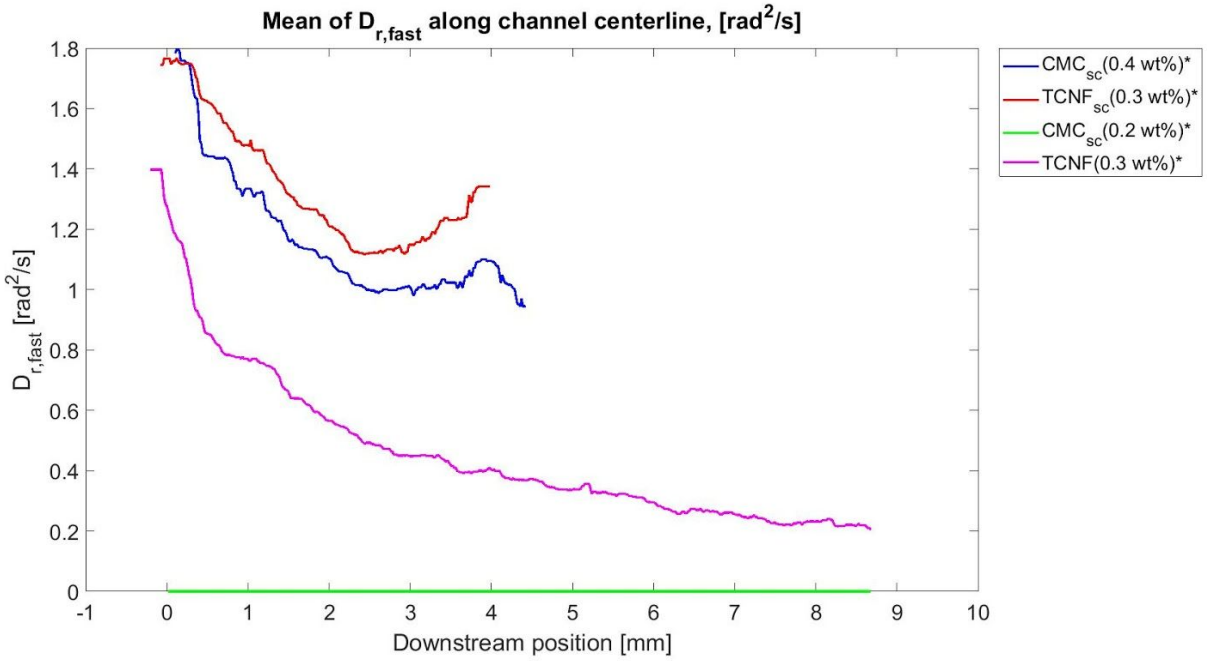

Figure 16. Illustration of the intensity profiles given for $D_{r,fast}$ along the flow-focusing channel centerline, for the 4 dispersions analyzed that were not tested for spinning. A legend illustrating which graph belongs to which dispersion is shown in the top right corner of the figure. The star following a dispersion name marks that the dispersion in question was not tested for spinning.

Fig.17 below shows the intensity profiles regarding $D_{r,slow}$, for the 4 dispersions that were not tested for spinning, both on a linear scale, in Fig.17.a), and on a logarithmic scale, in Fig.17.b). As for Fig.14, the conversion from the linear scale to the logarithmic scale was made to allow for easier analysis of the graphs, later performed in section 7.4.

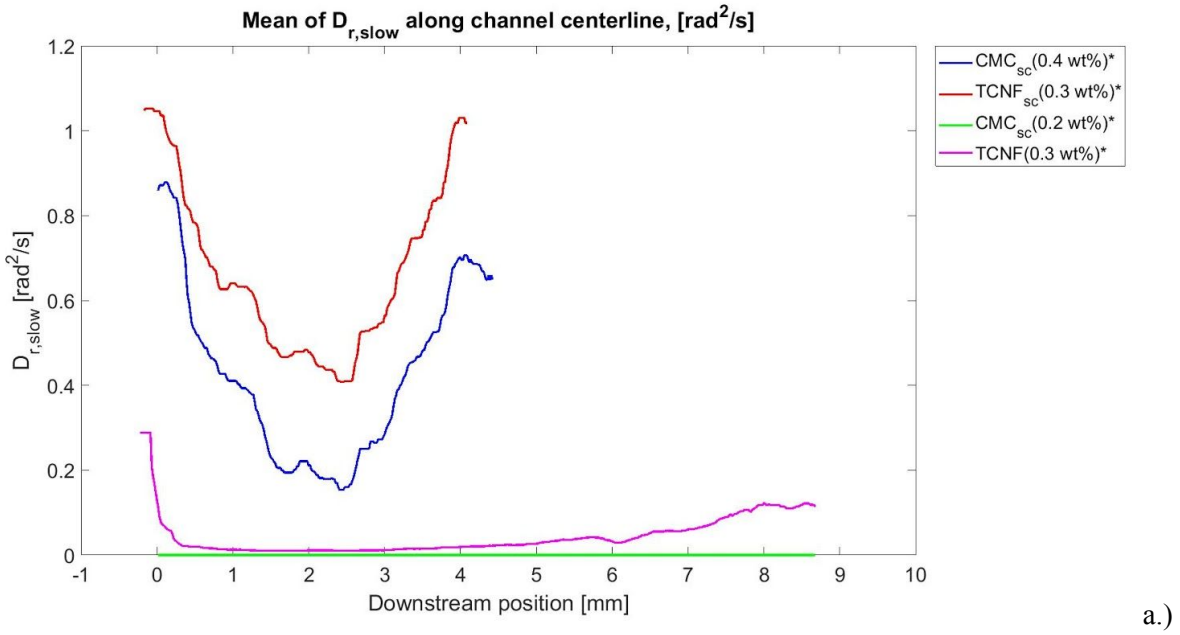

a.)

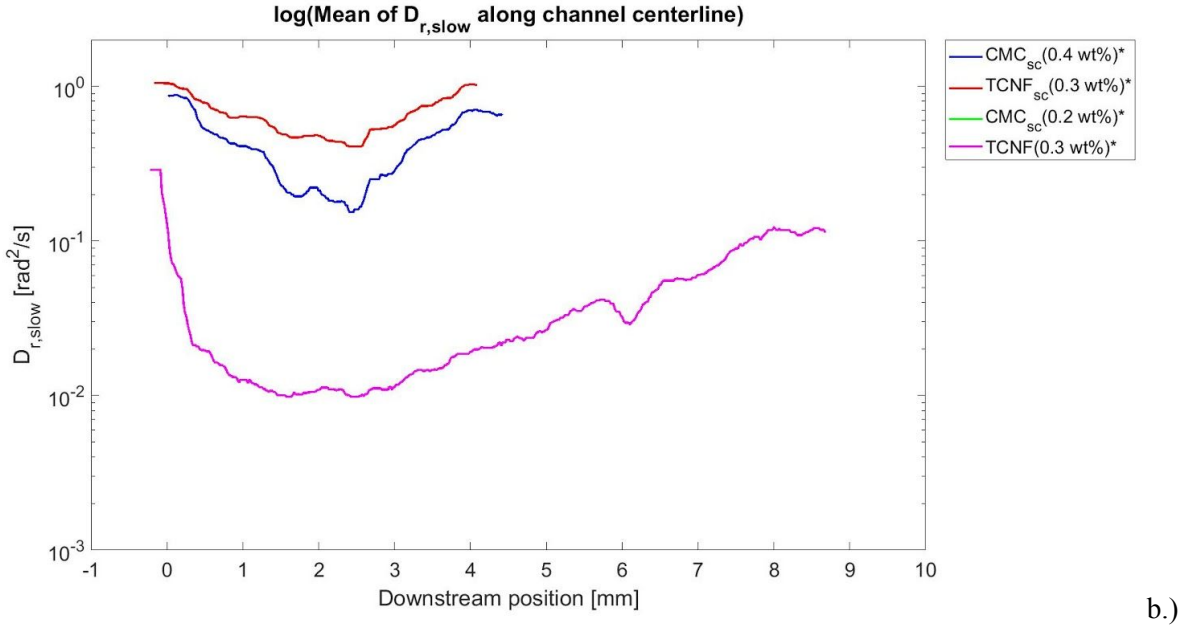

b.)

Figure 17. In the figure intensity profiles given for $D_{r,slow}$ along the flow-focusing channel centerline are presented, for each of the 4 analyzed dispersions that were not tested for spinning. In Fig.17.a) the intensity profiles are presented on a linear scale, while the intensity profiles are presented on a logarithmic scale in Fig.17.b). A legend illustrating which graph belongs to which dispersion is shown in the top right corner of each figure. The star following a dispersion name marks that the dispersion in question was not tested for spinning.

In Fig.18 below, the intensity profiles regarding birefringence are presented for the 4 analyzed dispersions that were not tested for spinning.

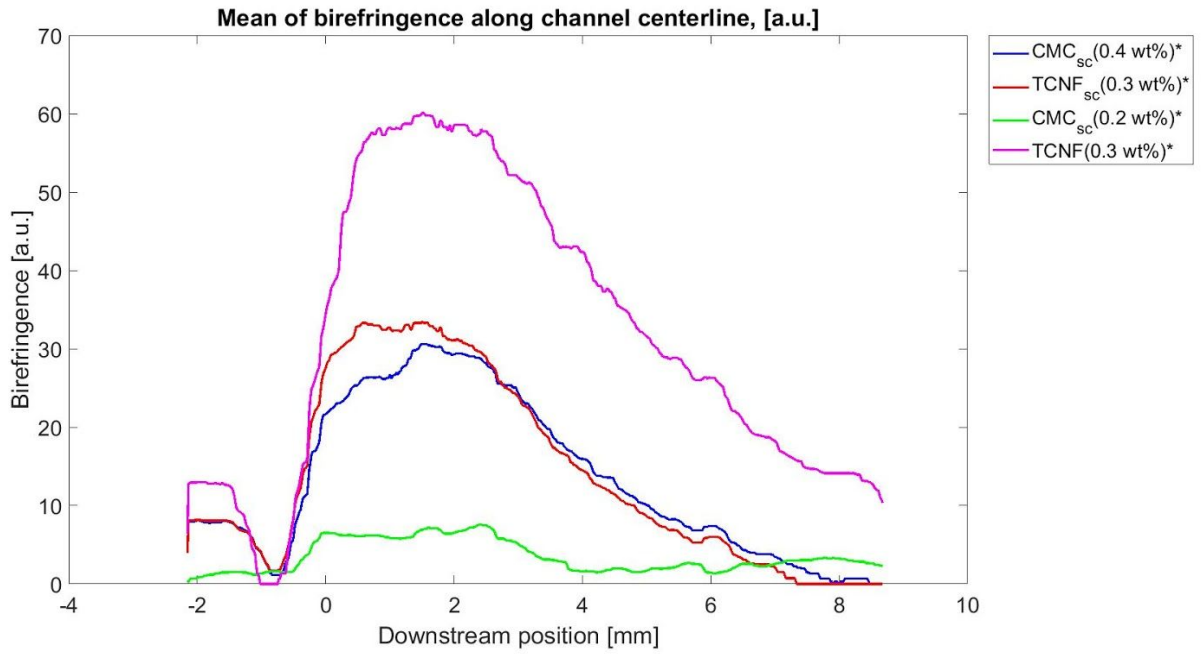

Figure 18. The figure shows the resulting intensity profiles for birefringence along the flow-focusing channel centerline, for the 4 dispersions analyzed that were not tested for spinning. A legend illustrating which graph belongs to which dispersion is shown in the top right corner of the figure. The star following a dispersion name marks that the dispersion in question was not tested for spinning.

As for the dispersions tested for spinning, MatLab was used to extract key values for the properties investigated with flow-stop analysis, for each of the 4 dispersions that were not tested for spinning. The key values are maximum rate of decay in birefringence, that is max($D_{r,fast}$), minimum rate of decay in birefringence, that is min($D_{r,slow}$), and maximum birefringence. The values are presented in table 7 below, where the stars following the dispersion names mark that the dispersions were not tested for spinning.

Table 7. In the table key values for the properties investigated with flow-stop analysis are presented for the 4 analyzed dispersions that were not tested for spinning. The key values listed are maximum rate of decay in birefringence, seen as max($D_{r,fast}$), minimum rate of decay in birefringence, seen as min($D_{r,slow}$), and maximum birefringence. The stars following the dispersion names mark that the dispersions were not tested for spinning.

Dispersion name	**max($D_{r,fast}$)**	**min($D_{r,slow}$)**	**Maximum birefringence**
CMC$_{sc}$(0.4 wt%)*	1.79	0.154	30.6
TCNF$_{sc}$(0.3 wt%)*	1.77	0.408	33.4
CMC$_{sc}$(0.2 wt%)*	Non-measurable	Non-measurable	7.57
TCNF(0.3 wt%)*	1.40	0.0098	60.1

6.5 Tensile testing and microscopy

All filaments were analyzed with optical microscopy, both to find the thinnest width of each sample and to find possible aggregates and contaminations on them. The collection of samples that did not have any contaminants or aggregates are referred to as clean. The width of the thinnest part of each sample is presented in tables AI through AIV in appendix, section 10.3.

When calculating the statistical data, the samples included in the calculations had to fulfill certain requirements. All samples that had broken at the grip were excluded, as their breakage could depend on the stickiness of the tape rather than the filaments mechanical properties. All values that were not in the interval of the highest and lowest value of the clean filaments were also excluded. Calculations were done firstly on the clean samples and secondly on the clean ones together with the ones that had aggregates and fulfilled the requirements stated above. Table 8 describes how many samples were included for each calculation of each dispersion.

Table 8. Amounts of data points used in statistical calculation for each dispersion, where clean refers to samples without aggregates or contaminations on the filaments and mix refers to a mix of clean and non-clean samples.

Dispersion	**Amount of data clean**	**Amount of data mix**	**Amount of samples tested**	**Percentage of clean [%]**
TCNF(0.2 wt%)	10	24	64	15.6
$TCNF_{sc}$(0.3 wt%)	18	32	60	30.0
CMC(0.3 wt%)	11	21	56	19.6
CMC(0.2 wt%)	1	16	34	2.94

The mean values, standard deviations and standard deviations in percent of the minimum widths of the filaments for each dispersion are presented in the table 9 below.

Table 9. Statistical values of minimum widths of filaments of each dispersion.

Dispersion	**Mean value of clean [µm]**	**Stdav of clean [µm]**	**Stdav of clean [%]**	**Mean value of mix [µm]**	**Stdav of mix [µm]**	**Stdav of mix[%]**
$TCNF_{sc}$(0.3 wt%)	8.3	1.6	19.8	9.1	2.1	22.6
TCNF(0.2 wt%)	7.7	2.0	26.1	8.1	2.8	34.8
CMC(0.3 wt%)	8.7	1.5	17.7	9.6	2.5	25.6
CMC(0.2 wt%)	--	--	--	9.3	2.3	24.8

Tensile testing was executed on filaments spun from all four spinnable dispersions. MatLab was used to analyse and visualize collected data. The received diagrams are presented in section 10.2.2 in appendix.

The mean values and standard deviations of elastic modulus, toughness and ultimate stress for each dispersion was calculated using excel. The values were calculated for all clean samples of each dispersion and for all clean together with some aggregated samples, the values are shown in the tables 9 through 12 below.

In tables 10 through 12 below, "clean" indicates that the value calculated only includes clean samples and "mix" indicates that the value calculated includes clean samples and samples containing aggregates that fulfill the requirements written in section 4.4. Table 10 shows the calculated mean values, standard deviations and standard deviations in percent of the E-modulus, ultimate stress, strain at break and toughness in the indicated units for samples spun from dispersion $TCNF_{sc}$(0.3 wt%).

Table 10. The mean values and standard deviations (SDs) for $TCNF_{sc}$(0.3 wt%).

Value	Mean of clean	SD of clean	SD [%] of clean	Mean of mix	SD of mix	SD [%] of mix
E-modulus [GPa]	26	8.0	30.7	26	6.8	26.5
Ultimate stress [MPa]	427	91.2	21.3	405	78.7	19.4
Strain at break [%]	5.9	1.6	26.6	5.8	1.7	29.1
Toughness [MJ/m^3]	17.8	5.70	32.1	16.6	4.73	28.4

Table 11 shows the calculated mean values, standard deviations and standard deviations in percent of the E-modulus, ultimate stress, strain at break and toughness in the indicated units for samples spun fråm dispersion TCNF(0.2 wt%).

Table 11. The mean values and standard deviations (SDs) for TCNF(0.2 wt%).

Value	Mean of clean	SD of clean	SD [%] of clean	Mean of mix	SD of mix	SD [%] of mix
E-modulus [GPa]	22	4.4	20.6	22.6	4.8	21.3
Ultimate stress [MPa]	323	73.9	22.9	354	71.9	20.3
Strain at break [%]	4.4	1.6	35.3	4.5	1.3	29.2
Toughness [MJ/m^3]	10.3	5.19	50.4	11.8	4.29	38.4

Table 12 shows the calculated mean values, standard deviations and standard deviations in percent of the E-modulus, ultimate stress, strain at break and toughness in the indicated units for samples spun fråm dispersion CMC(0.3 wt%).

Table 12. The mean values and standard deviations (SDs) for CMC(0.3 wt%).

Value	Mean of clean	SD of clean	SD [%] of clean	Mean of mix	SD of mix	SD [%] of mix
E-modulus [GPa]	21	3.5	16.6	21	3.4	16.0
Ultimate stress [MPa]	392	77.5	19.8	386	68.1	17.7
Strain at break [%]	7.4	1.4	18.5	7.3	1.4	18.4
Toughness [MJ/m^3]	20.6	7.16	34.7	20.4	6.70	32.9

For dispersion CMC 0.2wt% there was only one clean sample and therefore no mean values or standard deviations could be calculated. The values for the clean sample were:

- E-modulus [GPa]: 31
- Ultimate stress [MPa]: 534
- Strain at break [%]: 6.2
- Toughness [MJ/m^3]: 24

Table 13 shows the mean values of and standard deviations for the results of the tensile test for the mixed samples, that is the clean sample along with the ones containing aggregates, for the samples spun from dispersion CMC(0.2 wt%).

Table 13. The mean values and standard deviations (SDs) for CMC(0.2 wt%).

Value	Mean of mix	SD of mix	SD [%] of mix
E-modulus [GPa]	22	4.1	18.3
Ultimate stress [MPa]	417	68.3	16.4
Strain at break [%]	7.3	2.3	31.3
Toughness [MJ/m^3]	21.7	7.76	35.7

6.6 Combined results

All relevant key characteristics that could be quantitatively determined are presented in table 14. The SEM results could not be quantitatively determined and are therefore not included. It is presented in the table whether the dispersion was spinnable. From WAXS analysis, crystallinity index (CI) and orientation index are included. From flow-stop analysis the values for maximum and minimum rate of decay in birefringence along with maximum birefringence are included, where the maximum has been named max($D_{r,fast}$) [rad^2/s] and the minimum min($D_{r,slow}$) [rad^2/s]. The mean values of minimum width for clean and mix sample collections are presented as a result from optical microscopy. Values for E-modulus, ultimate stress, strain at break and toughness of the clean and mix collections of data are presented as results from tensile testing.

Table 14. Summary of the results from WAXS analysis, Flow stop, optical microscopy and tensile testing for each dispersion. All relevant key characteristics are listed. The spinnable dispersions are sorted by values for ultimate stress where CMC(0.2 wt%) has the highest value. The non-spinnable dispersion have been sorted by amount of data collected, where $TCNF_{sc}$(0.27 wt%) has the least amount of data. CI stands for crystallinity index, max($D_{r,fast}$) [rad^2/s] stands for maximum rate of decay in birefringence and min($D_{r,fast}$) [rad^2/s] for minimum rate of decay in birefringence. The values for mechanical properties and minimum widths are presented as mix/clean, where clean refers to samples without aggregates or contaminations on the filaments and mix refers to a mix of clean and non-clean samples.

Dispersion/ Key characteristics	CMC (0.2 wt%)	TCNFsc (0.3 wt%)	CMC (0.3 wt%)	TCNF (0.2 wt%)	CMCsc (0.3 wt%)	TCNFsc (0.2 wt%)	TCNFsc (0.27 wt%)
Spinnability	Yes	Yes	Yes	Yes	No	No	No
CI [%]	--	53.4	45.3	56.4	--	--	--
Orientation index	--	0.81	0.82	0.83	--	--	--
max($D_{r,fast}$) [rad^2/s]	1.23	1.39	1.32	1.25	1.75	Non-measurable	--
min($D_{r,slow}$) [rad^2/s]	0.191	0.0278	0.0206	0.0605	0.559	Non-measurable	--
Maximum birefringence [a.u.]	17.8	69.1	34.8	35.3	19.0	13.0	--
Mean minimum width [µm]	9.3/--	8.1/8.3	9.6/8.7	9.1/7.7	--	--	--
E-Modulus [GPa]	22/31	26/26	21/21	23/22	--	--	--
Ultimate stress [MPa]	417/534	405/427	386/392	354/323	--	--	--
Strain at break [%]	7.3/6.2	5.8/5.9	7.3/7.4	4.5/4.4	--	--	--
Toughness [MJ/m^3]	21.7/24	16.6/17.8	20.4/20.6	11.8/10.3	--	--	--

7. Discussion

7.1 Spinning

There were several restricting factors of the laboratory work that, in some way and to varying extent inhibited the spinning of filaments. To begin with, it was not possible to spin filaments from dispersions containing bubbles or visible particles. If there were bubbles in the dispersion used for spinning an inconsistent inflow was obtained, which would cause inconsistencies in the resulting filaments. Too big particles in the dispersion would result in difficulties during alignment of fibrils in the flow-focusing channel and could also contribute to clogging in the cell. In the beginning of the project an ultrasonic bath was used to remove bubbles from dispersions. However, it was later revealed that this resulted in the fibrils being merged into bigger particles, which is why only a vacuum desiccator was later used to remove bubbles. Contaminants could also affect the quality of the dispersions.

One of the most frequent problems occuring during spinning was clogging in the flow cell. One main reason for this happening was that the different liquids were pushed through the channel-geometry in the wrong order, so that the acid came in contact with the CNF dispersion before spinning started. However, this was carefully avoided as much as possible and mainly happened when the water pump was not started properly, so that no water entered the channel-geometry. Another reason for clogging was inadequate cleaning of the flow cell, which could mean that contaminants or dispersion remains, from earlier spinning sessions, were left in the channels, creating blockage.

In some cases it seemed like spinning was not possible due to the concentration of the dispersions being too low and viscosity being too low. The low viscosity affected the spinning in such a way that the fibrils in the dispersions could not bond to each other due to lack of contact points between CNFs. The filaments could not be retrieved from the water bath. In other cases the dispersion seemed to be too charged for the spun filaments to stick to the roller and thereby being collected. Another problem noticed with these dispersions was that the filaments were attracted by the plexiglass wall of the water bath and the plate of the roller, so that the filaments constantly broke instead of being rolled up. In conclusion, in order to spin filaments dispersions with high enough concentration and a charge that allowed the filaments to be collected as samples, were needed.

7.2 WAXS

WAXS analysis provided data that can be correlated to structures of the nanocellulose fibrils. The structure refers to two main factors, the first being how the cellulose chains inside the fibrils are organized in relation to each other. This provides information on the crystallinity of the fibrils. The second factor is the alignment of the cellulose chains in the filament, which also reveals information on alignment of the fibrils in the filaments, since the alignment of the cellulose chains is proportional to the alignment of the fibrils.

7.2.1 Crystallinity

In Fig.7, in section 6.2, it is visualised that the two TCNF samples have higher crystallinity than the CMC(0.3 wt%) sample, since they have more defined, thinner peaks. The figure was used to calculate

the crystallinity index of each of the three samples, which can be seen in table 4, section 6.2. As earlier mentioned, the crystallinity indices describe the crystallinity of the fibrils. Table 4 shows that the crystallinity indices between the samples do not largely differ. However, there are differences. The TCNF samples have higher crystallinity indices and can therefore be assumed to have higher crystallinity than the CMC sample. This agrees with the theories for the two oxidation methods, found in section 2.1.1. Furthermore, the sonicated and centrifuged TCNF sample has a somewhat lower crystallinity than the non-treated TCNF sample. The reason for this might be that sonication is a pretty drastic treatment, it not only breaks aggregates but also the cellulose itself, decreasing its crystallinity. However, the fact that the difference in crystallinity between the treated and non-treated samples was small shows that such breakage is insignificant in comparison to the amount of preserved crystalline cellulose.

In general, we can conclude that TCNFs seem to be more crystalline than CMC fibrils and that pretreatment through sonication and centrifugation seems to lower the crystallinity of the CNFs.

However, sources of error might have had an impact on the results. Examples of sources of error might be contamination of dispersions and/or filaments, aggregates on filaments and instrument failures during WAXS analysis. In order to minimize the effects of error sources, certain measures have been taken:

- When selecting filaments for WAXS sampling, the thinnest, most even ones were chosen.
- When applying the filaments on sample holder, a USB-microscope was used in order to be able to place them on top of each other with as much precision as possible.

In order to draw a more statistically validated conclusion every experiment and minimize the effects of error sources even further we would need to:

- Perform every experiment several times.
- Prepare dispersions with different conditions with regard to oxidation method, pretreatment and orginiating batch, and analyze filaments from these.
- More samples should be prepared so that a representative mean value could be obtained.
- Multiple dispersions of the same sort should be prepared in order to minimize the risk for contamination of dispersions affecting the final results.

In future analyses, it would be interesting to further investigate the impact of the following correlations:

1. Crystallinity and pretreatment (sonication and centrifugation).
2. Crystallinity and type of oxidation of the CNF dispersions.
3. Crystallinity and combinations of the factors named in case 1 and 2.

7.2.2 Alignment

Fig.8, section 6.2, was used to calculate orientation indices of the three samples. The orientation indices, presented in table 5 in section 6.2, provide information on the alignment of the cellulose chains in the filaments, which in turn provides information on the alignment of the fibrils within the filaments. In the table it can be seen that the filaments from the three dispersions have approximately the same orientation index, which means that their degrees of alignment are also approximately the same.

A comparison between the results for the TCNFs shows that pretreatment through sonication and centrifugation does not seem to have an impact on alignment. Sonication and centrifugation are performed in order to remove aggregates from the dispersions, but since both of the TCNF samples have approximately the same orientation index ($TCNF_{sc}$(0.3 wt%) even has a slightly lower value) the pretreatments do not seem to have an impact on the alignment. The results demonstrate that the amount of mis-oriented aggregates is not significant in comparison to the amount of aligned CNFs. The results for CMC also show that the majority of the crystalline parts of CMC are aligned, which suggests that the spinning was efficient in aligning the fibrils in the direction of the flow.

However, in order to draw a more statistically validated conclusion, more statistically supported results would have been needed. In order to gain these type of results, additional studies would need to be performed as described in section 6.2.1 above.

An additional source of error, not mentioned in section 6.2.1, that only affects alignment, and not crystallinity, is uneven mounting of filaments on WAXS sample holders. For future studies this source of error would need to be minimized along with the previous mentioned ones.

7.3 SEM

The scanning electron microscopy images offers some insight to the differing appearances of the filaments when oxidized through TEMPO or CMC. Comparing Fig.9.a) and Fig.11.b) it is evident that the grooves on the filament vary in thickness. CMC filaments have a smoother surface than their counterpart, TCNF filaments. The cause of this could be a myriad of factors, most likely it is dissolved cellulose filling the grooves due to the high degree of substitution from CMC treatment where some of the cellulose breaks down to its monomer, lacks crystallinity and coats the filament.

Furthermore, looking at the different concentrations of the dispersions in Fig.11.a) and 13.b) it is evident that a concentration of 0.2 wt% yields a much more sleek surface as opposed to the same treatment at a concentration of 0.3wt%. This could be because of the varying shear rate and the fact that when a higher concentrated dispersion is spun, less hydrochloric acid is able to protonize the fibrils to bond them together. The correlation applies to both oxidizing treatments tested.

To summarize, not enough data were readily available to make a definitive conclusion. The most one can gather is that the lower concentration leads to a sleeker surface of the filament and that CMC will dissolve some parts of the filament into free cellulose molecules. What this means mechanically is yet to be investigated.

7.4 Flow-stop

When studying the images Fig.AIII through AXII in appendix, section 10.2.1.1 and 10.2.1.2, it is visible that the decay in birefringence is always slowest in the same spot, namely where the extensional flow begins after water is injected in the channel. In the images this is visible from the fact that that spot is always a colour that represents a lower value, on the colour scale to the right of the images, than other parts of the channel.

As discussed by Rosén *et. al.* (2020), the desired property when performing flow-stop is primarily to have a dispersion with long fibrils with high degree of entanglement, leading to a slow decay in

birefringence, shown by low values of $D_{r,fast}$ and $D_{r,slow}$. As also mentioned by Rosén *et. al.* (2020), the value of $D_{r,fast}$ represent the effective length of the shortest (primarily non-entangled) fibrils in the dispersion, and the value of $D_{r,slow}$ represent the longest fibrils and their degree of entanglement. Furthermore, slow decay in birefringence typically leads to a high degree of alignment, which is represented by high values of birefringence. However, the concentration of the dispersions also have an effect on the birefringence, in such a way that higher concentration brings higher values for birefringence. Another factor affecting the birefringence is the degree of crystallinity in the fibrils in the dispersions, since crystalline regions cause birefringence to a greater extent than amorphous regions. Hence, birefringence can not be directly correlated to the degree of alignment.

To start off, the flow-stop results for the dispersions that were tested for spinning are discussed. The results for $D_{r,fast}$ (the rate of decay in birefringence during the first 50 ms after stopping the flow through the flow-focusing channel), provided in [rad^2/s], are illustrated in Fig.13, section 6.4, for the 6 dispersions tested for spinning. Regarding the values for maximum rate of decay in birefringence, given by max($D_{r,fast}$) and presented in table 6, section 6.4, all dispersions tested for spinning show similar results except for CMC_{sc}(0.2 wt%) and $TCNF_{sc}$(0.2 wt%). The CMC_{sc}(0.3 wt%) dispersion gave the highest value and the value for $TCNF_{sc}$(0.2 wt%) was non-measurable, meaning that the rate of decay in birefringence was to fast to be measured. The results for $D_{r,slow}$ (the slowest measurable rate of decay in birefringence), provided in [rad^2/s], are illustrated in Fig.14, section 6.4, for the 6 dispersions tested for spinning. Regarding the minimum rate of decay in birefringence, given by min($D_{r,slow}$) and presented in table 6, section 6.4, the dispersions $TCNF_{sc}$(0.3 wt%), CMC(0.3 wt%) and TNCF(0.2 wt%) all show values below 0.1 rad^2/s, representing a slow decay in birefringence. The CMC_{sc}(0.3 wt%) and CMC(0.2 wt%) dispersions both gave minimum values higher than 0.1 rad^2/s, but CMC(0.2 wt%) had a lower value than CMC_{sc}(0.3 wt%). The value for $TCNF_{sc}$(0.2 wt%) was non-measurable, for the same reason as mentioned for $D_{r,fast}$. The results for birefringence of the 6 dispersions tested for spinning are presented in Fig.15, section 6.4. Regarding the maximum values for birefringence, presented in table 6, section 6.4, the $TCNF_{sc}$(0.3 wt%) has the highest value by far, a value almost double that of the dispersion with the second highest value. Reasons for this value being so high, apart from a high degree of alignment, could be that the concentration is relatively high and that the crystallinity might be high as well. Apart from the $TCNF_{sc}$(0.2 wt%) dispersion, the TCNF dispersions gave higher values than the CMC dispersions. However, the $TCNF_{sc}$(0.2 wt%) mentioned gave the lowest values for maximum birefringence. This can be correlated to the fact that $D_{r,fast}$ and $D_{r,slow}$ for this dispersion were too fast to measure, as can be seen for the key values in table 6 and the in Fig.AVIII in appendix, section 10.2.1.1, where the data for $D_{r,fast}$ and $D_{r,slow}$ is shown as straight lines at 0 rad^2/s.

To continue, the flow-stop results for the dispersions that were not tested for spinning are discussed. In Fig.16, section 6.4, the results for $D_{r,fast}$ (the rate of decay in birefringence during the first 50 ms after stopping the flow through the flow-focusing channel), provided in [rad^2/s], are presented. The values for maximum rate of decay in birefringence, given by max($D_{r,fast}$), are presented in table 7, section 6.4. It can there be seen that TCNF(0.3 wt%)* has the lowest value and that the value for CMC_{sc}(0.2 wt%)* was non-measurable. The $TCNF_{sc}$(0.3 wt%)* and CMC_{sc}(0.4 wt%)* gave very similar values. The results for $D_{r,slow}$ (the slowest measurable rate of decay in birefringence), provided in [rad^2/s], are presented in Fig.17, section 6.4. The values for minimum rate of decay in birefringence, given by min($D_{r,slow}$), are presented in table 7, section 6.4. It can there be seen that the TCNF(0.3 wt%)* gave the lowest value of all dispersions analyzed with flow-stop, including the ones

that were tested for spinning. This dispersion gave a value lower than 0.01 rad^2/s, indicating a very slow decrease in alignment. The highest value was measured for $TCNF_{sc}$(0.3 wt%)* and the value for CMC_{sc}(0.2 wt%)* was non-measurable. The results for birefringence of the dispersions not tested for spinning are presented in Fig.18, section 6.4. The maximum values for birefringence of the different dispersions are presented in table 7. In table it can be found that the TCNF(0.3 wt%)* dispersion has the second highest value of all dispersions analyzed with flow-stop, including the ones that were tested for spinning. The CMC_{sc}(0.2 wt%)* dispersion gave the absolute lowest maximum value of birefringence out of all the dispersions analyzed. This can be correlated to the fact that the values for $D_{r,fast}$ and $D_{r,slow}$ were too fast to measure, as can be seen for the key values in table 7, section 6.4, and the in Fig.XI in appendix, section 10.2.1.2, where the data for $D_{r,fast}$ and $D_{r,slow}$ is shown as straight lines at 0 rad^2/s.

When comparing the flow-stop results for two sonicated and centrifuged TCNF dispersions of 0.3 wt%, that is $TCNF_{sc}$(0.3 wt%) and $TCNF_{sc}$(0.3 wt%)*, it can be seen that their results are very different. While $TCNF_{sc}$(0.3 wt%) gave relatively low values for $D_{r,fast}$ and $D_{r,slow}$, $TCNF_{sc}$(0.3 wt%)* gave significantly higher values, especially for $D_{r,slow}$. The results for birefringence are also differing, where $TCNF_{sc}$(0.3 wt%) gave the highest value of all dispersion tested with flow-stop and $TCNF_{sc}$(0.3 wt%)* gave a value about half that size. That these two dispersions that supposedly are the same gave such differing results in flow-stop, probably means that the $TCNF_{sc}$(0.3 wt%)* dispersion was indeed contaminated and it was therefore a good choice spin $TCNF_{sc}$(0.3 wt%) instead, as was reasoned in section 6.1.

When comparing the values of $D_{r,slow}$ and $D_{r,fast}$ for dispersions with the same concentrations and that have been oxidized in the same manner, listed in table 6 and 7 in section 6.4, a correlation between pretreatment and dealignment rate can be found. The values for the dispersions that were not pretreated with sonication and centrifugation yield lower values for $D_{r,slow}$ and $D_{r,fast}$ than their pretreated counterparts every time. This suggests that pretreatment of dispersions results in a more rapid loss of alignment. This could be due to the shortening of fibrils during the pretreatment processes which might lead to less entanglement and therefore faster dealignment.

7.5 Tensile testing and microscopy

When looking at table 9 in section 6.5, it can be observed that the TCNF dispersions yield thinner threads than CMC dispersions, both when observing clean and aggregated samples. This might depend on the higher charge of the CMC dispersions since the structure will keep more water within. Another option is that CMC is more branched compared to TCNF. This due to the less selective type of oxidation, which drops CNF crystallinity creating branched and disordered regions, making bending of CNF more probable. These factors might result in less dense packing of CNFs within a filament upon drying. A comparison between filaments spun from dispersions of the same oxidation method, shows that a higher concentration yields thicker filaments. This might be because, higher concentration leads to more fibrils being next to each other while alining, leading to thicker filaments. However, all mean values of the thinnest widths exceeded the expected values by almost double, which suggests that the samples studied consist of two or more filaments that have adhered to one another. Furthermore, the optical microscopy analysis revealed that spinning of the pretreated dispersion $TCNF_{sc}$(0.3 wt%) yielded the greatest percentage of clean samples out of the spun dispersions. These results are presented in table 8. Centrifugation separates fibrils of different lengths,

stated in section 2.3, while sonication agitates the fibrils through oscillations. It seems like sonication removes aggregates and that sonicated dispersions thereby yield a larger number of clean samples than non-sonicated ones.

In this study the desired filaments are the strongest ones, that are the ones with highest values in the tensile testing, with regard to E-modulus, ultimate stress, strain at break and toughness. The values in tables 9 through 12 were extracted, as described in section 6.5, from the graphs in Fig.AXIII through AXVI in appendix, section 10.2.2, as well as in Fig.16 in section 6.5.

When comparing the mean values and standard deviations of the clean samples with the corresponding values of the mixed samples it is revealed that the values do not differ largely, except for the values of ultimate stress. Therefore it can be said that the aggregates can be neglected when observing E-modulus, strain at break and toughness. However, the comparison between the values for clean and mix cannot be performed for the CMC(0.2 wt%) samples as only one clean sample of this dispersion was available to test.

When comparing the results of tensile testing for all the different samples of the different dispersions it can be seen that:

- E-modulus: TCNF filaments show higher values than CMC filaments.
- Toughness and Strain at break: CMC filaments show higher values than TCNF filaments.
- Ultimate stress: Similar for filaments from all dispersions except for TCNF(0.2 wt%), which stands out with its low value.

The values for the mechanical properties for filaments spun from dispersions with the same oxidation method are similar, the values do not differ largely. Ultimate stress is an exception for this since these values vary more widely between the filaments of different dispersions. As earlier mentioned, ultimate stress is the only property where the values significantly vary between clean and mix of each dispersion. Therefore, it could be said that aggregates have a greater impact on the ultimate stress than on the other measured properties. This indicates that the tensile tests of non-clean samples have measured the aggregates' effect on the filaments, rather than how much stress the filaments actually can withstand before breaking. Because of this it is assumed that the filaments break at the aggregates, which is why the values for ultimate stress are uncertain to a greater extent than the values for the rest of the properties. For this reason the values for clean samples are taken into account when discussing ultimate stress.

It can also be said that the TCNF dispersions seem to yield stiffer filaments than CMC dispersions, as the E-modulus for TCNF filaments are higher while strain at break and toughness are lower than for CMC filaments. This will be further discussed in section 7.6.

Furthermore, the statistical data of this study might be a great source of error as the amount of samples tested and included in calculations for each dispersion varies. The reasons being either that not enough filaments were spun due to lack of time, samples were broken before tested or results of tests did not fulfill requirements to be included.

7.6 Combined discussion

All quantitative results discussing in this section are presented in table 14, section 6.6. To start off, the combined results for each individual dispersion will be discussed.

- The CMC(0.2 wt%) dispersion was spinnable. However, this dispersion was the most difficult to spin out of the spinnable ones, which can be distinguished by the fact that fewer samples were made for this dispersion. This coincides with the fact that the minimum rate of decay in birefringence (min($D_{r,slow}$)) was higher than for the other spinnable dispersions, meaning that the loss of alignment was faster for this dispersion. The fact that this dispersion was spinnable, yet hard to spin and had a value for min($D_{r,slow}$) that was more than double those for the other spinnable dispersions, implies that it can be counted as an outlier. This is why we do not consider this dispersion when drawing our conclusions. In the flow-stop results it can also be seen that the maximum value for birefringence is relatively low, suggesting a lower degree of alignment. However, this low value might also depend on the relatively low concentration and the fact that CMC dispersions have lower crystallinity than TCNF dispersions, as discussed in section 7.2.1. WAXS analysis was never performed on samples from this dispersions, so the degree of crystallinity cannot be definitely determined. However, that this dispersion has a lower crystallinity than the TCNF dispersions is strengthened by the fact that the values for strain at break and toughness are higher, and the E-modulus is lower. This means that the CMC filaments from this dispersion are less stiff, which indicated that they are less crystalline. For ultimate stress no reliable value was obtained since only one clean sample was obtained.

- The $TCNF_{sc}$(0.3 wt%) dispersion was also spinnable. This coincides with the results from flow-stop analysis, which shows that the dispersion has a relatively low value for minimum rate of decay in birefringence (min($D_{r,slow}$)), and therefore a slow loss of alignment. The maximum value for birefringence is very high, suggesting a high degree of alignment. However, this might also depend on the fact that this dispersion has a relatively high concentration as well as crystallinity. The fact that the crystallinity is relatively high is shown by the crystallinity index from WAXS analysis. The results from tensile testing indicates that the filaments from this dispersion are relatively stiff (as discussed in section 7.5), since the E-modulus is relatively high and toughness and strain at break gave relatively low values. This corresponds to the results from WAXS analysis. A mean value for ultimate stress was obtained. However, as discussed in section 7.5, no conclusions can be drawn from this.

- The CMC(0.3 wt%) was another spinnable dispersion. This seems to agree with the results from flow-stop analysis, as the values for minimum rate of decay in birefringence (min($D_{r,slow}$)) are the lowest out of all dispersions tested for spinning. The maximum birefringence value was rather average. A reason for this value being lower than that of $TCNF_{sc}$(0.3 wt%), which has the same concentration, might be that the degree of crystallinity is lower, indicated by the crystallinity index obtained from WAXS analysis. As for the CMC(0.2 wt%) dispersion, the results from tensile testing seem to agree with the fact that CMC dispersions are not as stiff as TCNF dispersions. This also coincides with the results from WAXS analysis.

- The TCNF(0.2 wt%) was also spinnable, which agrees with the results from flow-stop analysis where min($D_{r,slow}$) was relatively low, suggesting a slow enough decrease in alignment for spinning to be enabled. The value for maximum birefringence is the second highest, but still half as high as that of $TCNF_{sc}$(0.3 wt%). This could be due to the concentration being lower, since the crystallinity index is actually higher than for samples from the other TCNF dispersion. The results from tensile testing show that the mean values from this dispersion gave the second highest E-modulus and the absolute lowest values for strain at break and toughness, indicating that samples from this dispersion are very stiff. This is confirmed once again by WAXS analysis.

- The CMC_{sc}(0.3 wt%) was non-spinnable, which coincides with the fact that min($D_{r,slow}$) from flow-stop analysis gave the highest value of the measurable ones, suggesting a relatively fast loss of alignment. The value for maximum birefringence is the third lowest, in the same range as CMC(0.2 wt%). One reason for this value being low might be that the fibrils in the dispersion are not very crystalline.

- The $TCNF_{sc}$(0.2 wt%) was also non-spinnable. This was confirmed by the fact that values for neither min($D_{r,fast}$) or min($D_{r,slow}$) was measurable due to a very rapid decrease of alignment. This dispersion also gave the lowest value for maximum birefringence, which suggest that it was difficult to obtain alignment during flow-focusing.

- The $TCNF_{sc}$(0.27 wt%) was not spinnable. No other analyses were performed on this dispersion, hence no other results were obtained.

In general, TCNFs are more crystalline than CMC fibrils. This has an affect on the mechanical properties tested with tensile testing, in such a way that E-modulus is higher, due to the fact that more energy is required to deform it, and strain at break and toughness give lower values, for the reason that filaments from more crystalline CNFs can absorb less energy before breaking. A reason for filaments spun from CMC dispersions being less stiff than filaments spun from TCNF dispersions might be that the CNFs in the filaments spun from CMC dispersions have a greater contact surface and are more cross-linked. This, as described in section 2.5.2, improves the connectivity and stress transfer. More efficient distribution of mechanical impact over the filament postpones the breakage of the filament and will allow it to absorb more energy resulting in higher ultimate stress and toughness. This might be due to the CMC dispersions containing dissolved cellulose molecules which can function as binders between the CNFs and increase the contact surface.

As earlier discussed in section 7.4, dispersions pretreated through sonication and centrifugation yield flow-stop results that suggest that they are less spinnable than their not pretreated counterparts. This agrees with the results of spinning, section 6.1, where the pretreated dispersions were not spinnable while their not pretreated counterparts were. Since centrifugation only separates fibrils of different lengths from aggregates, stated in section 2.3, it can be reasoned that the reason for the dispersions being less spinnable is sonication, which through oscillations of the dispersions agitates the fibrils themselves, see section 2.3. The difficulties during spinning of sonicated dispersions seemed to be a result of the fibrils in the dispersion being too short, see section 7.4. This made the dispersions more difficult to spin since it was more difficult to obtain alignment during flow-focusing, and since the

dealignment seemed to be very rapid as a result of brownian motion. Therefore, it seems like non-sonicated dispersions are to prefer when spinning. Two examples of where sonication seems to have had this effect is for the CMC_{sc}(0.3 wt%) and $TCNF_{sc}$(0.2 wt%) dispersions, which were not spinnable. The first names dispersion gave high values for $D_{r,fast}$ and $D_{r,slow}$, while the second mentioned gave non-measurable values, from flow-stop analysis. This indicates that the fibrils in both cases were highly susceptible to brownian motion. This, in turn, indicates that the fibrils in these two dispersions were shorter than in other dispersions. In addition, shorter particles also have fewer contact points, which means that dispersions containing these fibrils will turn into a gel-like structure, and thereby be spinnable, at higher concentrations than dispersions containing longer fibrils. Since the CMC_{sc}(0.3 wt%) dispersion has a higher concentration than the $TCNF_{sc}$(0.2 wt%) dispersion it seems like the CMC dispersion contains even shorter fibrils than the TCNF one, suggesting that the CMC fibrils were shorter to start with, even before sonication. This is supported by the fact that the CMC dispersion had a higher charge than the TCNF one, and that carboxymethylation is less selective than TEMPO oxidation.

From the flow-stop results of the dispersions that were not tested for spinning, provided in table 7, an initial prediction about their spinnability might be made. The TCNF(0.3 wt%)* gave the lowest value for min($D_{r,slow}$) of all dispersions tested through flow-stop analysis, which indicates that it would be easy to spin since the loss of alignment is slow. The birefringence for this dispersion is also very high, which indicates that alignment of this dispersion through flow-focusing would be efficient. From these results it seems like spinning of this dispersion would be very successful. However, a prediction about mechanical properties cannot be made. These factors would be interesting to investigate in further analyses. The CMC_{sc}(0.2 wt%)* dispersion gave non-measurable values for both $D_{r,fast}$ and $D_{r,slow}$, suggesting a very rapid loss of alignment. The low value for maximum birefringence in turn, suggests that the degree of alignment was not very high to start with, which indicates that alignment through flow-focusing is not very efficient for this dispersion. Therefore this dispersion is assumed to be non-spinnable, something that would be interesting to test in further analyses. A prediction on the spinnability of CMC_{sc}(0.4 wt%)* dispersion is slightly more difficult to make since the values given by flow-stop analysis did not stand out in either direction. However, the value for min($D_{r,slow}$) is similar, even slightly lower, to that of the spinnable dispersion CMC(0.2 wt%) and a hypothesis would therefore be that even this one is spinnable. This contrasts the results given for the CMC_{sc}(0.3 wt%) dispersion, which was not spinnable. This is probably due to the higher concentration of 0.4 wt%, which allows for more contact points between the fibrils and thereby enables the creation of the gel-like structure needed for spinning.

As discussed in section 7.4, flow-stop could be used to see a difference between the two sonicated and centrifuged TCNF dispersions of 0.3 wt%, $TCNF_{sc}$(0.3 wt%) and $TCNF_{sc}$(0.3 wt%)*, even though they are supposedly the same. The differing results suggest that something happened to the one dispersion making it different than the other one. The fact that this can be seen with flow-stop analysis suggest that this new characterisation method can be used for easy prediction on the spinnability of different dispersions, rather than using a method of trial and error to determine spinnability.

When studying the resulting values for min($D_{r,slow}$) from flow-stop analysis of the spinnable dispersions and excluding the data for the outlier CMC(0.2 wt%), it can be seen that the two dispersions with the lowest values for min($D_{r,slow}$) are the two dispersions with best performing samples in tensile testing with regard to ultimate stress, where both dispersions gave an average of

about 400 MPa. It can also be seen that the dispersion with the highest measurable min($D_{r,slow}$), out of the three dispersions included in this discussion, gave the samples with the lowest values for ultimate stress, an average of about 350 MPa. This indicates that $D_{r,slow}$ might be used to predict mechanical properties of filaments spun from different dispersions.

In the SEM analysis it is seen that the CMC filaments had a smoother surface than TCNFs. The cause of this could be the high degree of substitution from CMC dissolving some cellulose chains to its monomers. This would then coat the filaments with non-crystalline cellulose and smoothing the surface. The WAXS analysis reaches the same conclusion as TCNF had a higher degree of crystallinity due to the lack of the amorphous cellulose monomers.

8. Conclusions

When combining all different factors that were studied through WAXS, flow-stop, tensile testing and observations during spinning, the following conclusions can be drawn:

- The results from this study show that flow-stop analysis could be used to determine which CNF dispersions are spinnable and which are non-spinnable.

- The slowest measurable decrease in alignment, $D_{r,slow}$, from the flow-stop analysis seems to be a good indicator to determine which of the CNF dispersions are spinnable and which of the spinnable dispersions would lead to good mechanical properties of the filaments.

- High crystallinity of fibrils in a filament yields high E-modulus and low values for strain at break and toughness for the filament.

- Low crystallinity of fibrils in a filament yields low E-modulus and high values for strain at break and toughness for the filaments.

- TCNFs are generally more crystalline than CMC fibrils.

- Dispersions pretreated through sonication and centrifugation seem to yield less spinnable dispersions than their not pretreated counterparts.

- Sonication in combination with low concentration seems to lead to non-spinnable conditions.

- Sonication of dispersions seems to result in spinning of more filaments without aggregates.

- Aggregates have a greater impact on the ultimate stress than on the other measured mechanical properties.

- Concentration and viscosity of the dispersions seem to have an affect on their spinnability, in such a way that a too low concentration and a too low viscosity seem to yield non-spinnable conditions.

- CMC dispersions appear to yield thicker samples than those spun from TCNF.

Due to a lack of statistically validated data all of the above named conclusions are somewhat uncertain and more extensive investigations would be required for more definitive conclusions.

9. References

Aguir, C. *et. al.* (2005). Experimental Study on Carboxymethylation of Cellulose Extracted from Posidonia oceanica. *Journal of Applied Polymer Science*. doi: 10.1002/app.22713. Available at: https://onlinelibrary-wiley-com.focus.lib.kth.se/doi/full/10.1002/app.22713 (Retrieved: 2020-05-17).

Bettaieb, F. *et. al.* (2015). Effect of the oxidation treatment on the production of cellulose nanofiber suspensions from Posidonia oceanica: The rheological aspect. *Carbohydr. Polym.* doi: 10.1016/j.carbpol.2015.07.091. Available at: https://www-sciencedirect-com.focus.lib.kth.se/science/article/pii/S0144861715007201#tblfn0010 (Retrieved: 2020-05-17).

Bhandari, P. (2011). Carboxymethylation of cellulose using reactive extrusion. *Carbohydr. Polym.* doi: 10.1016/j.carbpol.2011.10.056. Available at: https://www-sciencedirect-com.focus.lib.kth.se/science/article/pii/S0144861711009623 (Retrieved: 2020-05-19).

Björn, L. (2018). Characterisation of Injection Moulded Polymer Materials using SAXS and WAXS. Göteborg: Department of Physics, Chalmers University of Technology. p. 4, 12-13. Available at: http://publications.lib.chalmers.se/records/fulltext/256180/256180.pdf (Retrieved: 2020-05-07).

Brouzet, C. *et. al.* (2019). Characterizing the Orientational and Network Dynamics of Polydisperse Nanofibers on the Nanoscale. *Macromolecules.* doi: 10.1021/acs.macromol.8b02714 .

Brouzet, C. *et. al.* (2019). Supporting information: Characterizing Orientational and Network Dynamics of Polydisperse Nanofibers on the Nanoscale. Available at: https://pubs.acs.org/doi/suppl/10.1021/acs.macromol.8b02714/suppl_file/ma8b02714_si_001.pdf (Retrieved: 2020-02-08).

Bunsell, A.B. (2018). Handbook of Properties of Textile and Technical Fibres. Second Edition. Cambridge, UK: Elsevier. p.21-55. doi:10.1016/B978-0-08-101272-7.00002-X

Clarke, A.R. *et. al.* (2002). Microscopy techniques for materials science. Cambridge, UK: Elsevier. p.343.

Clarkson, C. M. *et. al.* (2018). Melt Spinning of Cellulose Nanofibril/Polylactic Acid (CNF/PLA) Composite Fibers For High Stiffness. *ACS Applied Polymer Materials.* doi: 10.1021/acsapm.8b00030 Available at: https://pubs.acs.org/doi/10.1021/acsapm.8b00030 (Retrieved: 2020-05-21)

Covaris. AFA Technology vs. Probe/ Bath Sonicator (N.D). Available at: https://covaris.com/pre-analytical/afa-vs-sonicators/ (Retrieved:2020-05-08).

Daicho, K. *et. al*. (2018). The Crystallinity of Nanocellulose: Dispersion-Induced Disordering of the Grain Boundary in Biologically Structured Cellulose. *ACS Appl. Nano Mater*. doi: 10.1021/acsanm.8b01438. Available at:

https://pubs-acs-org.focus.lib.kth.se/doi/10.1021/acsanm.8b01438 (Retrieved: 2020-04-9).

EK, M. *et. al.* (2011). Introduktion till cellulosateknologi. Stockholm: Institutionen för fiber och polymerteknologi, KTH Royal Institute of Technology. p.14-18, 20.

Fahlman, B. D. (2018), Materials Chemistry, Second Edition, *Springer* ISBN: 94-024-1255-7 p. 13

Geng, L. *et. al.* (2018) Understanding the Mechanistic Behavior of Highly Charged Cellulose Nanofibers in Aqueous Systems, *Macromolecules*. doi: 10.1021/acs.macromol.7b02642, Available at: https://pubs.acs.org/doi/abs/10.1021/acs.macromol.7b02642. (Retrieved: 2020-05-21)

Han, J. et. al. (2013) Self-Assembling Behavior of Cellulose Nanoparticles during Freeze-Drying: Effect of Suspension Concentration, Particle Size, Crystal Structure, and Surface Charge: doi: 10.1021/bm4001734 (Retrieved: 2020-05-18)

Håkansson, K.M.O. *et. al.* (2014). Hydrodynamic alignment and assembly of nanofibrils resulting in strong cellulose filaments. *Nat. Commun.* 5:4018 doi: 10.1038/ncomms5018.

Klemm, D. *et. al.* (2011). Nanocelluloses: A New Family of Nature‐Based Materials. *Angew. Chem*. doi:10.1002/anie.201001273. Available at: https://onlinelibrary-wiley-com.focus.lib.kth.se/doi/full/10.1002/anie.201001273 (Retrieved: 2020-02-08).

Meng, Q. *et. al.* (2016). The role of heteropolysaccharides in developing oxidized cellulose nanofibrils. *Carbohydr. Polym.* Available at: https://doi.org/10.1016/j.carbpol.2016.02.058 (Retrieved: 2020-05-07).

Mittal, N. *et. al.* (2018). Multiscale Control of Nanocellulose Assembly: Transferring Remarcable Nanoscale Fibril Mechanics to Macroscale Fibers. *ACS Nano.* doi: 10.1021/acsnano.8b01084.

Moberg, T. *et. al.* (2017). Rheological properties of nanocellulose suspensions: effects of fibril/particle dimensions and surface characteristics. *Cellulose.* doi: 10.1007/s10570-017-1283-0. Available at: https://link-springer-com.focus.lib.kth.se/article/10.1007/s10570-017-1283-0 (Retrieved: 2020-04-12).

Naderi, A. *et. al*. (2016). A comparative study of the rheological properties of three different nanofibrillated cellulose systems. *Nord. Pulp Pap. Res. J*. Journal volume 31 no (3). Available at: https://www-degruyter-com.focus.lib.kth.se/view/journals/npprj/31/3/article-p354.xml (Retrieved: 2020-04-11).

No author. (2011). Degree of Substitution. In Encyclopedia of Polymer Science and Technology, (Ed.). doi:10.1002/0471440264.pst445. Available at: https://onlinelibrary-wiley-com.focus.lib.kth.se/doi/abs/10.1002/0471440264.pst445 (Retrieved: 2020-05-18).

Onyianta, A.J. *et. al.* (2017) The Use of Sedimentation for the Estimation of Aspect Ratios of Charged Cellulose Nanofibrils, *Advances in Natural Fibre Composites: Raw Materials, Processing and Analysis,* Edinburgh: School of Engineering and Built Environment, Edinburgh Napier University.

p.195-202. doi: 10.1007/978-3-319-64641-1 Available at: https://link.springer.com/chapter/10.1007/978-3-319-64641-1_17 (Retrieved: 2020-05-19)

Pauw, B.R. (2007-08-15). A Short Introduction to Small-Angle X-Ray Scattering [Online]. *lookingatnothing.com.* 1:13. Available at: https://lookingatnothing.com/index.php/videos (Retrieved: 2020-05-07).

Rosén *et. al.* (2020). Flow Fields Control Nanostructural Organization in Semiflexible Networks. Soft Matter, accepted May 2020. Pre-print available at arXiv:1801.07558.

Saito, T. *et. al.* (2006). TEMPO-mediated oxidation of native cellulose: Microscopic analysis of fibrous fractions in the oxidized products. *Carbohydr. Polym.* doi: 10.1016/j.carbpol.2006.01.034. https://www-sciencedirect-com.focus.lib.kth.se/science/article/pii/S0144861706000622#fig1 (Retrieved: 2020-05-17).

Saito, T. *et. al.* (2006). Wet Strength Improvement of TEMPO-Oxidized Cellulose Sheets Prepared with Cationic Polymers. *Industrial & Engineering Chemistry Research.* doi: 10.1021/ie0611608. Available at: https://pubs-acs-org.focus.lib.kth.se/doi/full/10.1021/bm0497769 (Retrieved: 2020-05-17).

Terinte, N. *et. al.* (2011). Overview on native and microcrystalline cellulose I structure studied by X-ray diffraction (WAXD): Comparison between measurement techniques. doi: Lenzinger Berichte 89 118-131. p.121-122.

Thanu, D.P.R. *et. al.* (2018). Developments in Surface Contamination and Cleaning: Applications of Cleaning Techniques, Vol. 11, Elsevier, Amsterdam: Materials science and engineering, University of Arizona , ch.1, p.41.

Tu, S. *et. al.* (2019). Stress–strain curves of metallic materials and post-necking strain hardening characterization: A review. *Fatigue & Fracture of Engineering Materials & Structures*. p. 3-19. doi: 10.1111/ffe.13134. Available at: https://onlinelibrary-wiley-com.focus.lib.kth.se/doi/full/10.1111/ffe.13134 (Retrieved: 2020-05-07).

Roylance, D. (2001). STRESS-STRAIN CURVES. Cambridge: Department of Materials Science and Engineering, Massachusetts Institute of Technology. p.6-7. Available at: http://web.mit.edu/course/3/3.11/www/modules/ss.pdf (Retrieved: 2020-05-08).

Yang, X. *et. al.* (2019). Eco-Friendly Cellulose Nanofibrils Designed by Nature – Effects from Preserving Native State. *ACS Nano*. doi: 10.1021/acsnano.9b07659.

10. Appendix

10.1 Calculations

10.1.1 Calculation of crystallinity index

The intensities I_{200} and $I_{non\text{-}cr}$ for each sample were read from the graphs in Fig.7, in section 6.2, as illustrated in Fig.AI below and used in equation 7 (written below) from section 2.4.2 in order to calculate the crystallinity indices.

$$C = 100 \cdot \frac{I_{200} - I_{non-cr}}{I_{200}} \quad [\%]$$

I_{200}(TCNF(0.2 wt%)) = 7.05*10^{-3}
I_{200}(TCNFsc(0.3 wt%)) = 7.30 *10^{-3}
I_{200}(CMC(0.3 wt%)) =7.40*10^{-3}

$I_{non\text{-}cr}$(TCNF 0.2 wt%) = 3.075*10^{-3}
$I_{non\text{-}cr}$(TCNFsc(0.3 wt%)) = 3.40*10^{-3}
$I_{non\text{-}cr}$(CMC(0.3 wt%)) = 4.05*10^{-3}

$$CI(TCNF(0.2\ wt\%)) = \frac{7.05-3.073}{7.05} \cdot 100\% = 56.4\%$$
$$CI(TCNFsc(0.3\ wt\%)) = \frac{7.3-3.40}{7.3} \cdot 100\% = 53.4\%$$
$$CI(CMC(0.3\ wt\%)) = \frac{7.4-4.05}{7.4} \cdot 100\% = 453.\%$$

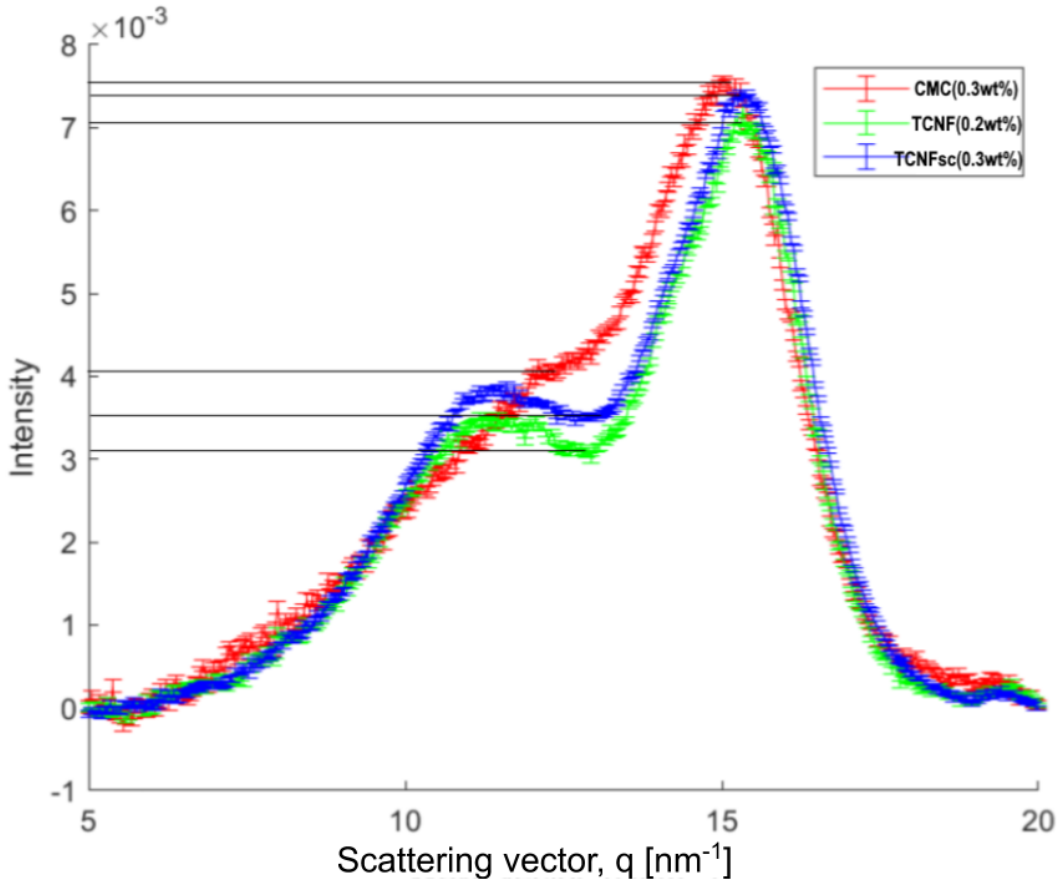

Figure AI. Shows what values have been used for calculating the crystallinity indices.

10.1.2 Calculation of orientation index

The widths of the graphs at half maximum (fwhm) for each graph was read from Fig.10, in section 6.2, as illustrated in Fig.AII below. These values were used in equation 8, written below) from section 2.4.2 in order to calculate the orientation indices.

$f_c = \frac{180^\circ - fwhm}{180^\circ}$, f_c = orientation index, fwhm = full width at half-maximum

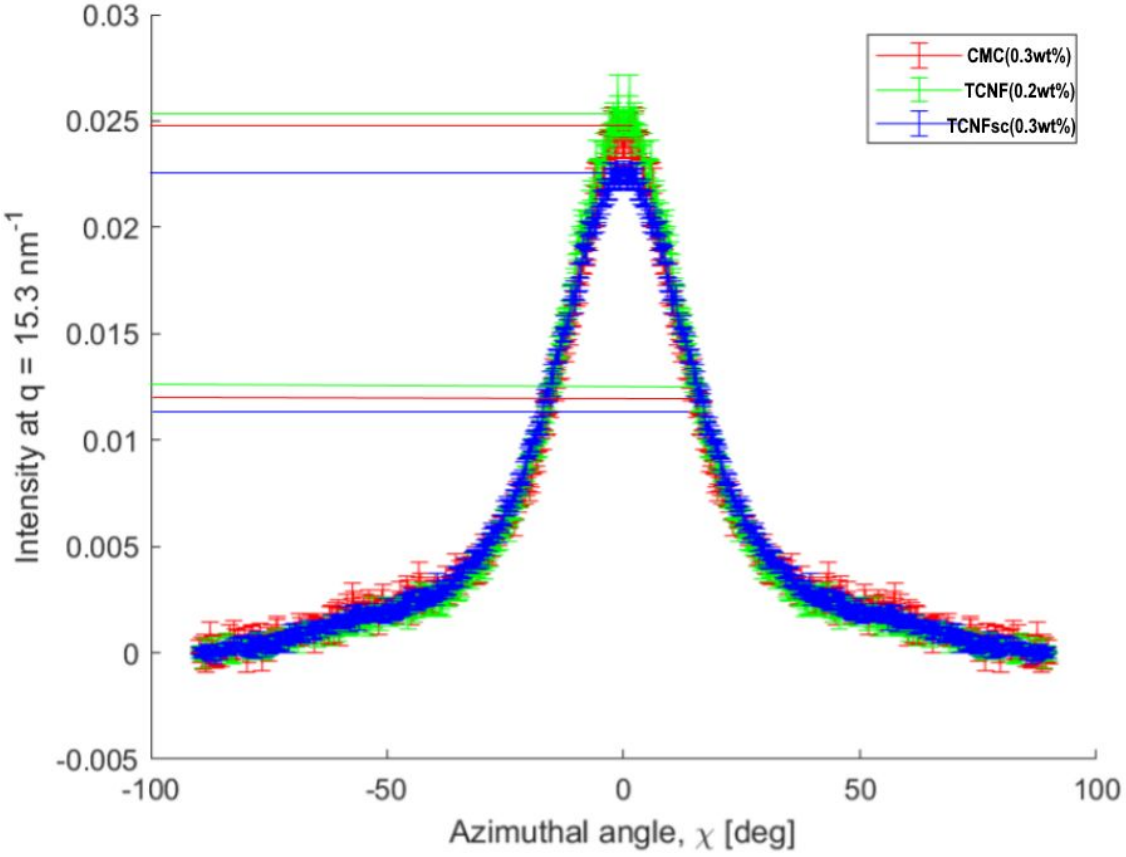

Figure AII. Shows what values that have been used to calculate the orientation indices.

$fwhm(TCNF(\ 0.2\ wt\%)) = 30.30\ nm^{-1}$
$fwhm(TCNFsc(\ 0.3\ wt\%)) = 34.85\ nm^{-1}$
$fwhm(CMC(\ 0.3\ wt\%)) \ = \ 31.82\ nm^{-1}$

$f_c(TCNF(0.2\ wt\%)) = \frac{180^\circ - 30.30}{180^\circ} = 0.832$
$f_c(TCNFsc(0.3\ wt\%)) = \frac{180^\circ - 34.85}{180^\circ} = 0.806$
$f_c(CMC(0.3\ wt\%)) = \frac{180^\circ - 31.82}{180^\circ} = 0.823$

10.2 Figures

10.2.1 Flow-stop results

The data collected through flow-stop analysis of 6 of the dispersions tested for spinning, as well as an additional 4 dispersions not tested for spinning, was analyzed in MatLab in order to construct mean value images and mean value intensity profiles for $D_{r,fast}$, $D_{r,slow}$ and birefringence, respectively. The meanings of $D_{r,fast}$ and $D_{r,slow}$ are presented in section 6.4 and the definition for birefringence is given in equation 1 in section 2.5.1. The mean value intensity profiles correspond to the results along the centerline of the flow-focusing channel used during flow-stop analysis. The resulting images and graphs for the dispersions tested for spinning are presented in section 10.2.1.1 below, and the resulting images and graphs for the dispersions not tested for spinning are presented in section 10.2.1.2.

10.2.1.1 Flow-stop results for dispersions tested for spinning

The resulting images and graphs for each of the analyzed dispersions that were tested for spinning are presented in Fig.AIII through AVIII below, where the results for $D_{r,fast}$ are shown on the top of each figure, the results for $D_{r,slow}$ are shown in the middle and the results for birefringence are shown on the bottom of each figure. The colour legend to the right of the images shows that a red colour represents a high value and a blue colour represents a low value. In the images for $D_{r,fast}$ and $D_{r,slow}$ this refers to the rate of dealignment and in the birefringence image it refers how much birefringence there is at different parts along the channel.

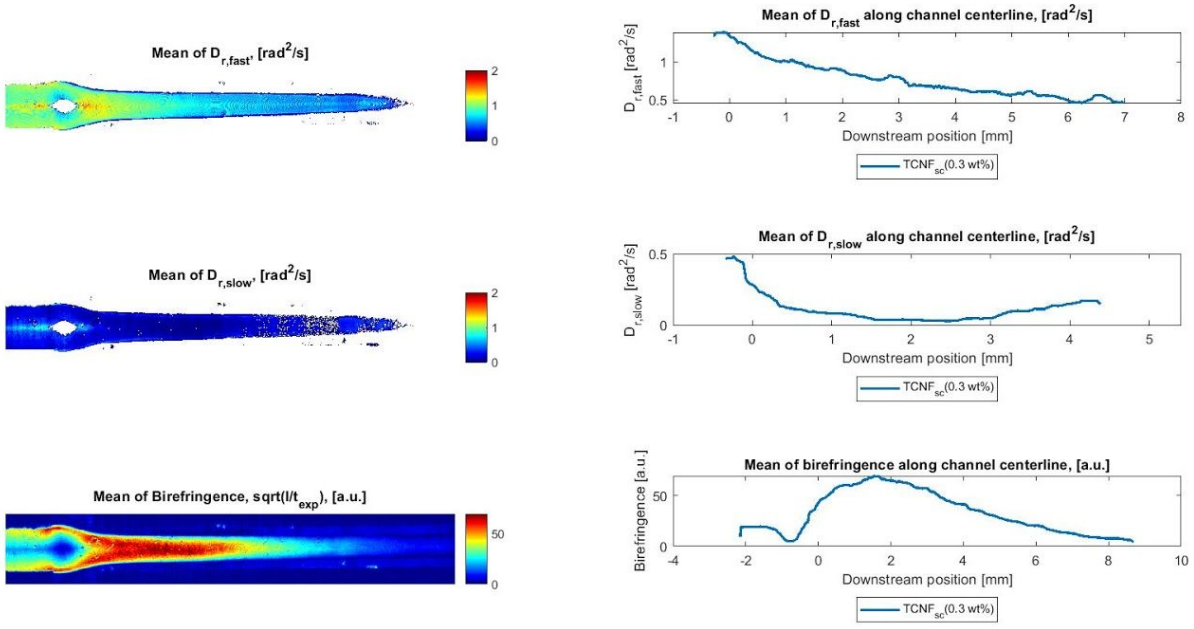

Figure AIII. The figure shows the resulting images and graphs given by flow-stop analysis of $TCNF_{sc}$(0.3 wt%), which was tested for spinning. The left side of the figure shows mean value images for $D_{r,fast}$, $D_{r,slow}$ and birefringence, and the right side shows mean value intensity profiles for the middle of the flow-focusing channel, for each of the mentioned variables. The images and graphs follow the same order, where the results for $D_{r,fast}$ are shown on top, the results for $D_{r,slow}$ are shown in the middle and the results for birefringence are shown on the bottom.

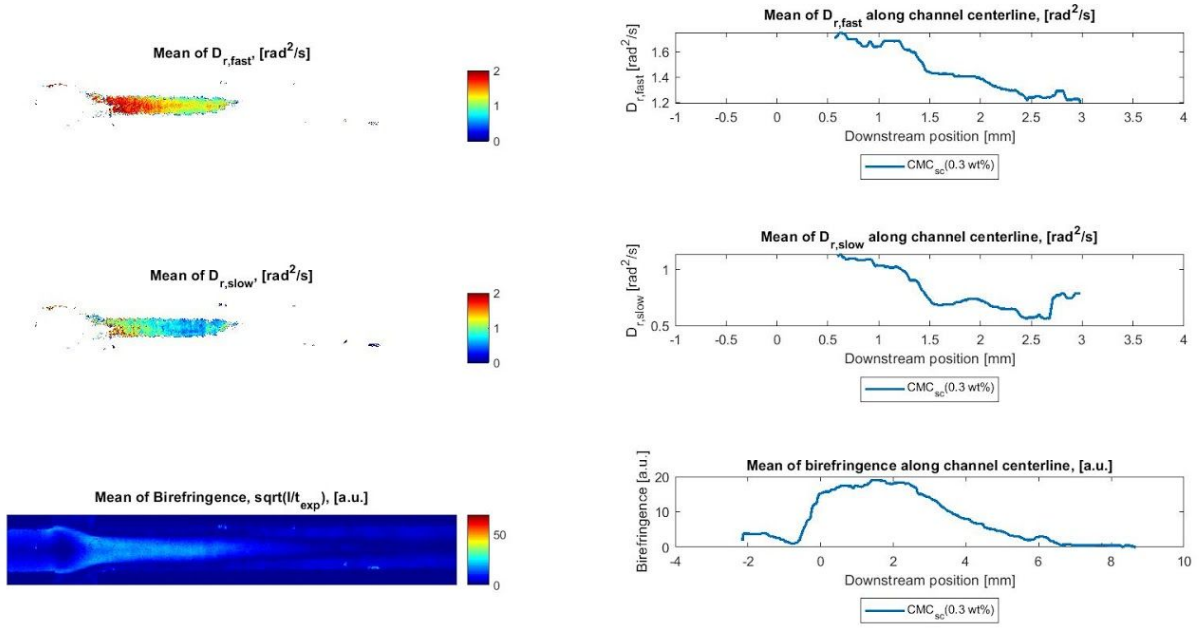

Figure AIV. The figure shows the resulting images and graphs given by flow-stop analysis of CMC_{sc}(0.3 wt%), which was tested for spinning. The left side of the figure shows mean value images for $D_{r,fast}$, $D_{r,slow}$ and birefringence, and the right side shows mean value intensity profiles for the middle of the flow-focusing channel, for each of the mentioned variables. The images and graphs follow the same order, where the results for $D_{r,fast}$ are shown on top, the results for $D_{r,slow}$ are shown in the middle and the results for birefringence are shown on the bottom.

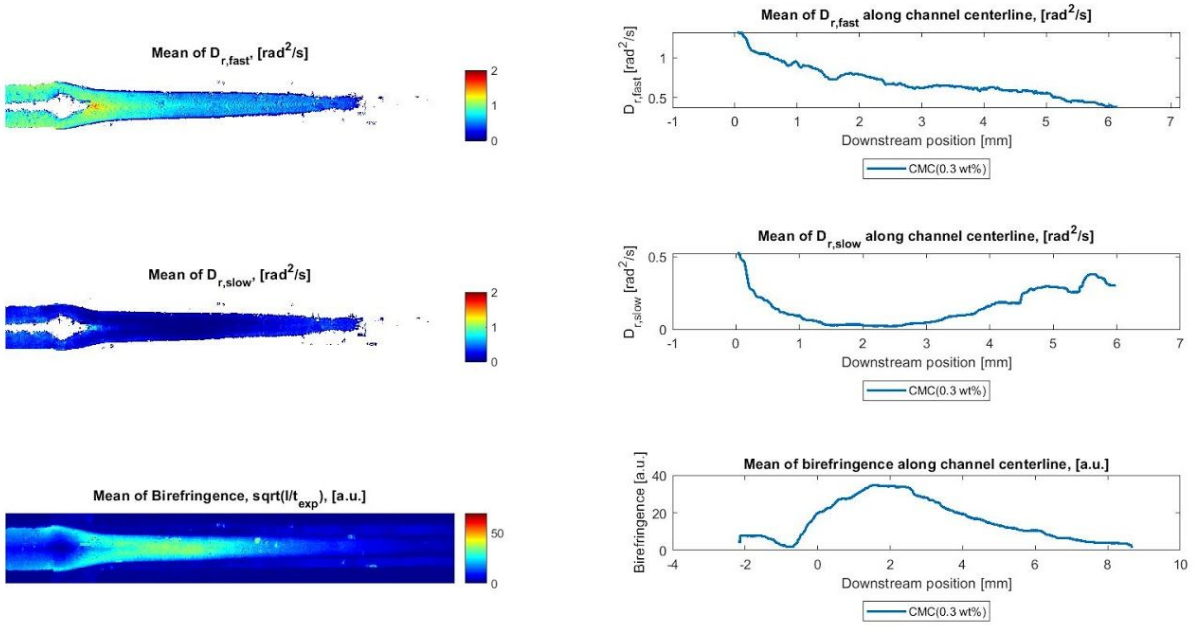

Figure AV. The figure shows the resulting images and graphs given by flow-stop analysis of CMC(0.3 wt%), which was tested for spinning. The left side of the figure shows mean value images for $D_{r,fast}$, $D_{r,slow}$ and birefringence, and the right side shows mean value intensity profiles for the middle of the flow-focusing channel, for each of the mentioned variables. The images and graphs follow the same order, where the results for $D_{r,fast}$ are shown on top, the results for $D_{r,slow}$ are shown in the middle and the results for birefringence are shown on the bottom.

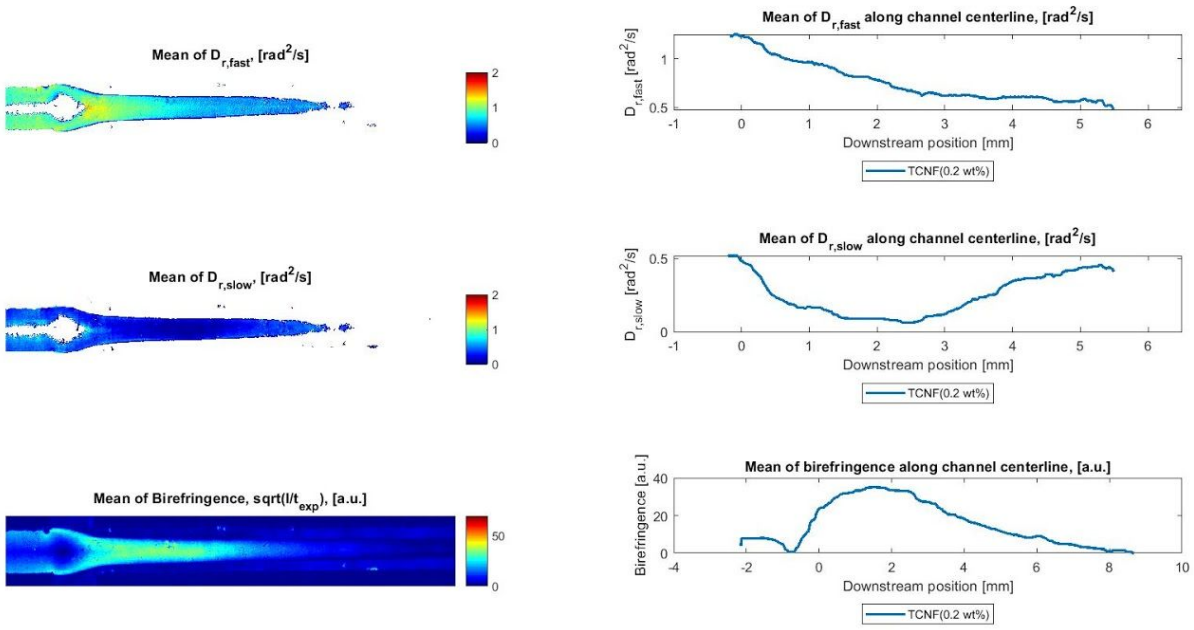

Figure AVI. The figure shows the resulting images and graphs given by flow-stop analysis of TCNF(0.2 wt%), which was tested for spinning. The left side of the figure shows mean value images for $D_{r,fast}$, $D_{r,slow}$ and birefringence, and the right side shows mean value intensity profiles for the middle of the flow-focusing channel, for each of the mentioned variables. The images and graphs follow the same order, where the results for $D_{r,fast}$ are shown on top, the results for $D_{r,slow}$ are shown in the middle and the results for birefringence are shown on the bottom.

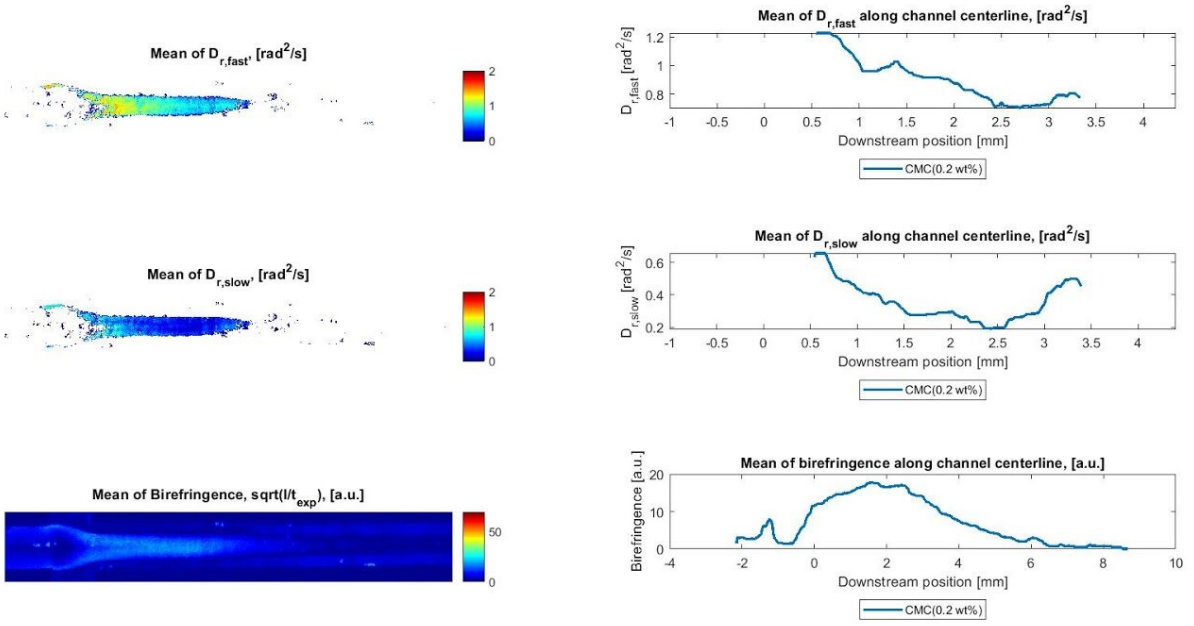

Figure AVII. The figure shows the resulting images and graphs given by flow-stop analysis of CMC(0.2 wt%), which was tested for spinning. The left side of the figure shows mean value images for $D_{r,fast}$, $D_{r,slow}$ and birefringence, and the right side shows mean value intensity profiles for the middle of the flow-focusing channel, for each of the mentioned variables. The images and graphs follow the same order, where the results for $D_{r,fast}$ are shown on top, the results for $D_{r,slow}$ are shown in the middle and the results for birefringence are shown on the bottom.

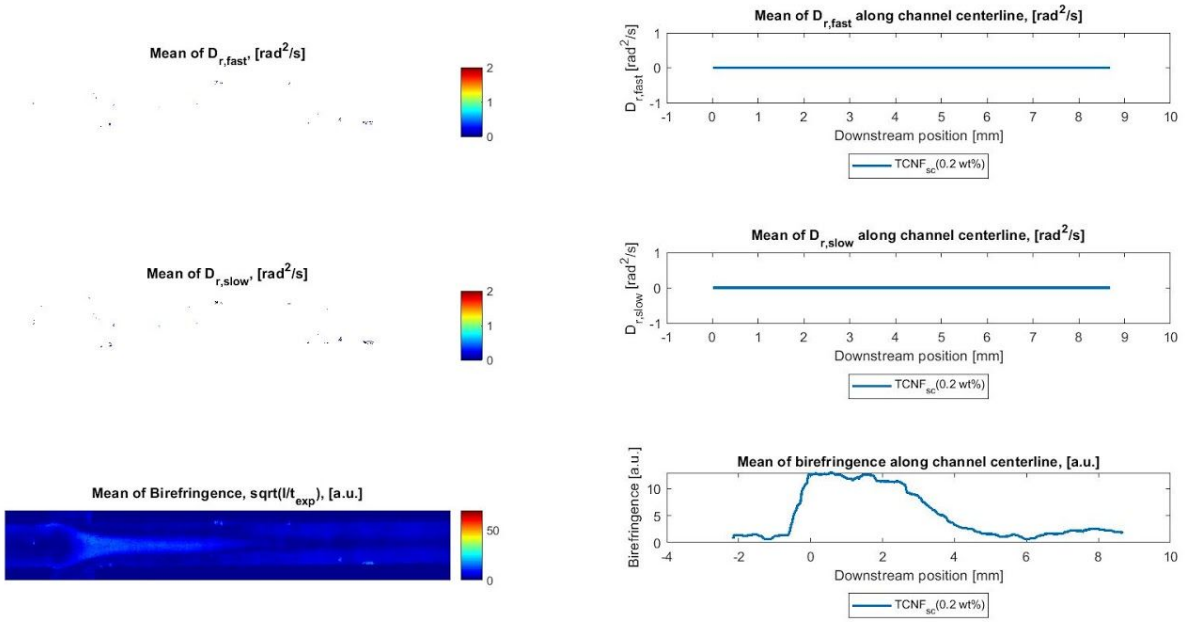

Figure AVIII. The figure shows the resulting images and graphs given by flow-stop analysis of $TCNF_{sc}$(0.2 wt%), which was tested for spinning. The left side of the figure shows mean value images for $D_{r,fast}$, $D_{r,slow}$ and birefringence, and the right side shows mean value intensity profiles for the middle of the flow-focusing channel, for each of the mentioned variables. The images and graphs follow the same order, where the results for $D_{r,fast}$ are shown on top, the results for $D_{r,slow}$ are shown in the middle and the results for birefringence are shown on the bottom.

10.2.1.2 Flow-stop results for dispersions not tested for spinning

The resulting images and graphs for the analyzed dispersions that were not tested for spinning are presented in Fig.AIX through AXII below, where the results for $D_{r,fast}$ are shown on the top of each figure, the results for $D_{r,slow}$ are shown in the middle and the results for birefringence are shown on the bottom of each figure. The colour legend to the right of the images shows that a red colour represents a high value and a blue colour represents a low value. In the images for $D_{r,fast}$ and $D_{r,slow}$ this refers to the rate of dealignment and in the birefringence image it refers how much birefringence there is at different parts along the channel. The star following a dispersion name marks that the dispersion in question was not tested for spinning.

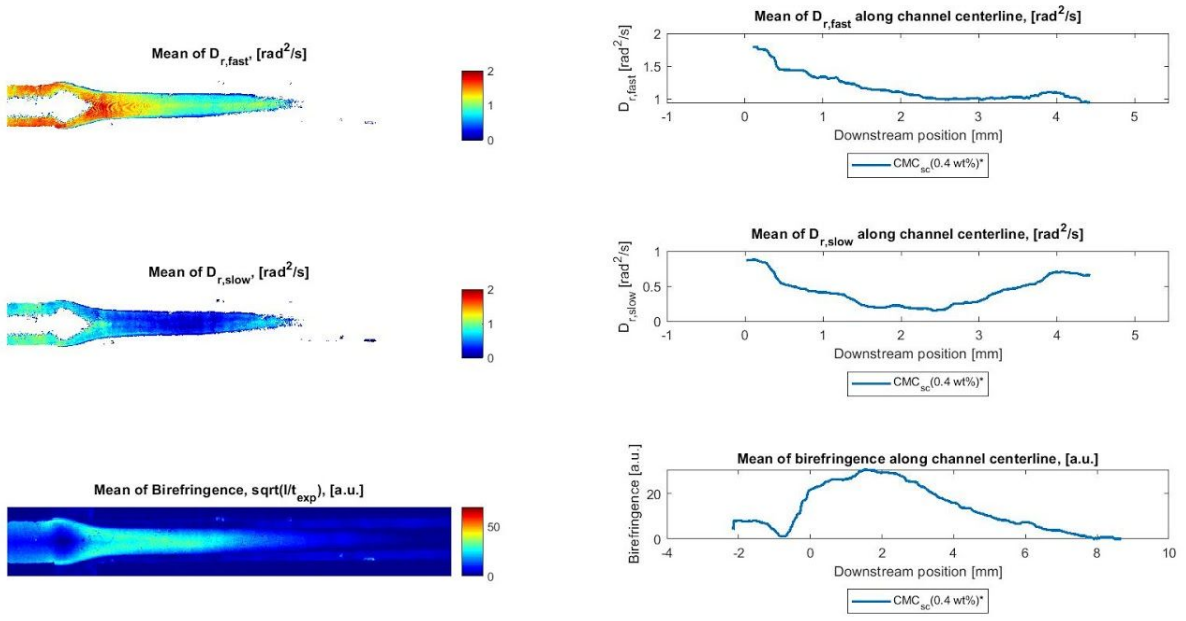

Figure AIX. The figure shows the resulting images and graphs given by flow-stop analysis of CMC_{sc}(0.4 wt%)*, where the star is marking that the dispersion was not tested for spinning. The left side of the figure shows mean value images for $D_{r,fast}$, $D_{r,slow}$ and birefringence, and the right side shows mean value intensity profiles for the middle of the flow-focusing channel, for each of the mentioned variables. The images and graphs follow the same order, where the results for $D_{r,fast}$ are shown on top, the results for $D_{r,slow}$ are shown in the middle and the results for birefringence are shown on the bottom.

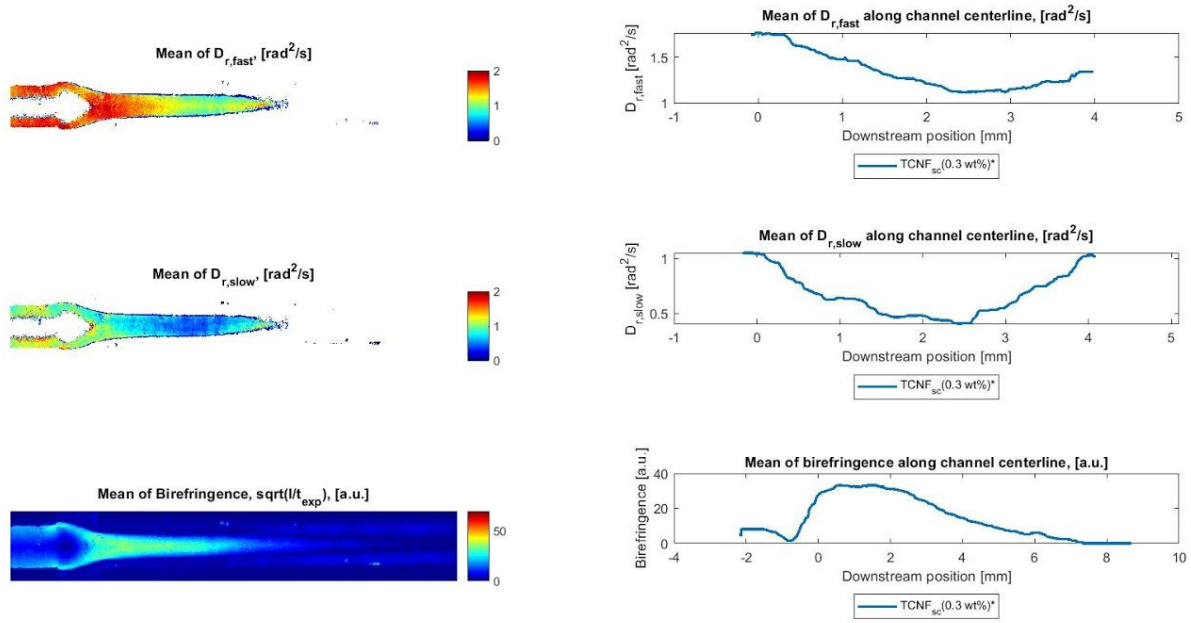

Figure AX. The figure shows the resulting images and graphs given by flow-stop analysis of $TCNF_{sc}$(0.3 wt%)*, where the star is marking that the dispersion was not tested for spinning. The left side of the figure shows mean value images for $D_{r,fast}$, $D_{r,slow}$ and birefringence, and the right side shows mean value intensity profiles for the middle of the flow-focusing channel, for each of the mentioned variables. The images and graphs follow the same order, where the results for $D_{r,fast}$ are shown on top, the results for $D_{r,slow}$ are shown in the middle and the results for birefringence are shown on the bottom.

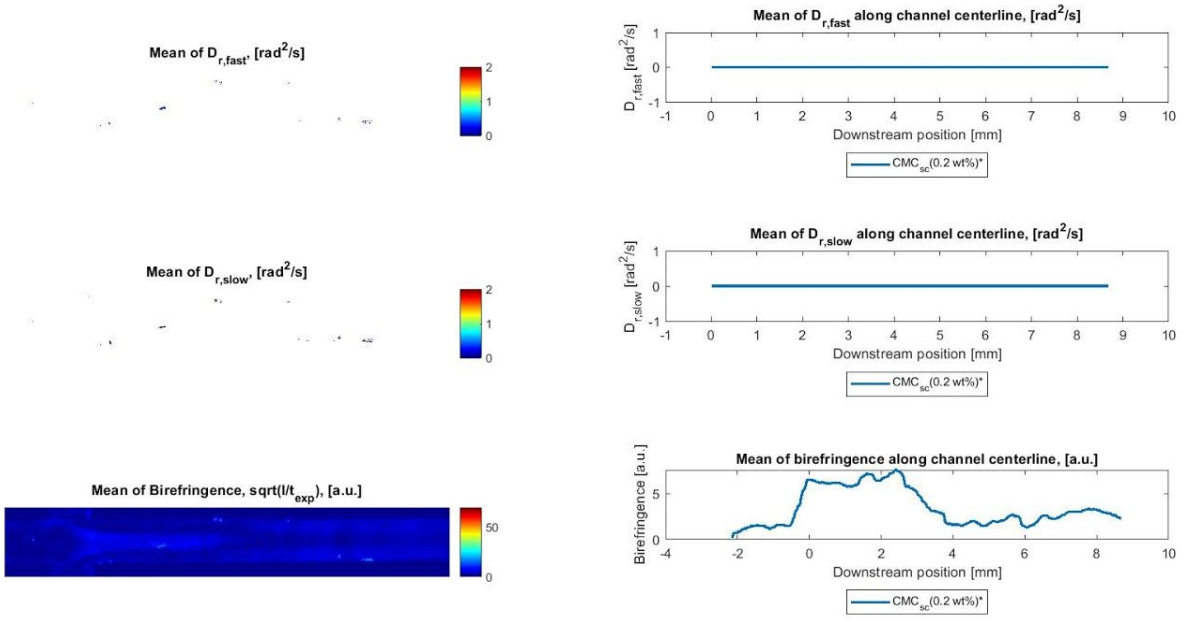

Figure AXI. The figure shows the resulting images and graphs given by flow-stop analysis of CMC_{sc}(0.2 wt%)*, where the star is marking that the dispersion was not tested for spinning. The left side of the figure shows mean value images for $D_{r,fast}$, $D_{r,slow}$ and birefringence, and the right side shows mean value intensity profiles for the middle of the flow-focusing channel, for each of the mentioned variables. The images and graphs follow the same order, where the results for $D_{r,fast}$ are shown on top, the results for $D_{r,slow}$ are shown in the middle and the results for birefringence are shown on the bottom.

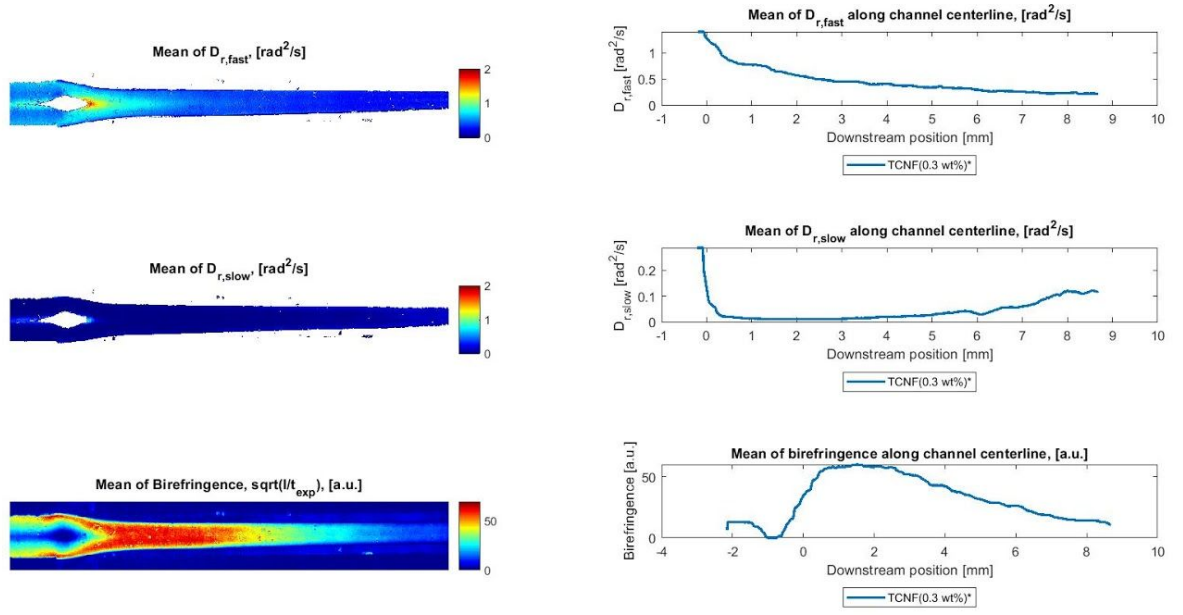

Figure AXII. The figure shows the resulting images and graphs given by flow-stop analysis of TCNF(0.3 wt%)*, where the star is marking that the dispersion was not tested for spinning. The left side of the figure shows mean value images for $D_{r,fast}$, $D_{r,slow}$ and birefringence, and the right side shows mean value intensity profiles for the middle of the flow-focusing channel, for each of the mentioned variables. The images and graphs follow the same order, where the results for $D_{r,fast}$ are shown on top, the results for $D_{r,slow}$ are shown in the middle and the results for birefringence are shown on the bottom.

10.2.2 Tensile results

The figures below, Fig.AXIII-AXVI, are the results of the MatLab processed data from the tensile tests of each sample of the different dispersions. Were the slope of the linear parts of the graphs are used to calculate the E-modulus, which is the samples' ability of reversible deformation. The end-point, the point with highest stress-strain value, determines the ultimate stress. Toughness of a sample is determined through the integral of the graph. All information of each value and sample is illustrated in the legends of the graphs.

The first, steeper part of the slopes in the graphs were determined to receive values representing the elastic modulus of the samples, namely the samples' ability to be reversibly deformed. The slope of the graphs changes distinctly when the deformation of the samples is large enough for it to be irreversible. The breaking point is where the graphs end. A breaking point at a higher stress-strain value indicates that the sample can withstand higher stress before breaking. In this case the ultimate stress of the samples coincide with the breaking points since both of them are at the highest point of the curves. The toughness of the samples was determined by calculating the area under the graphs.

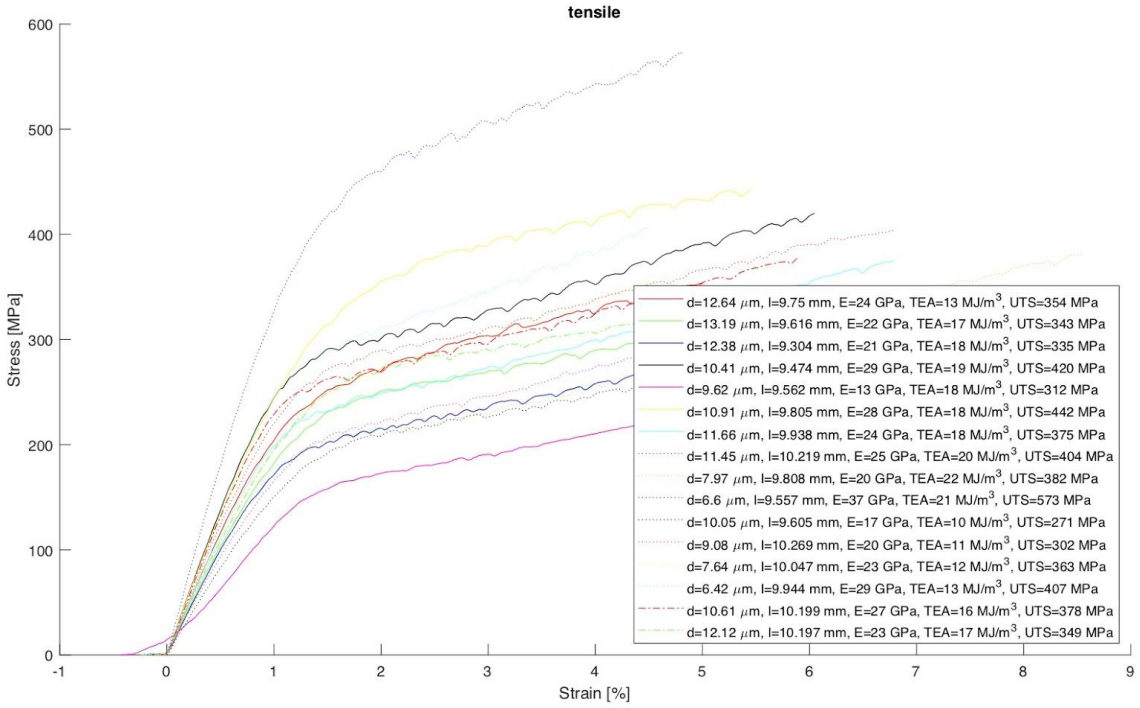

a)

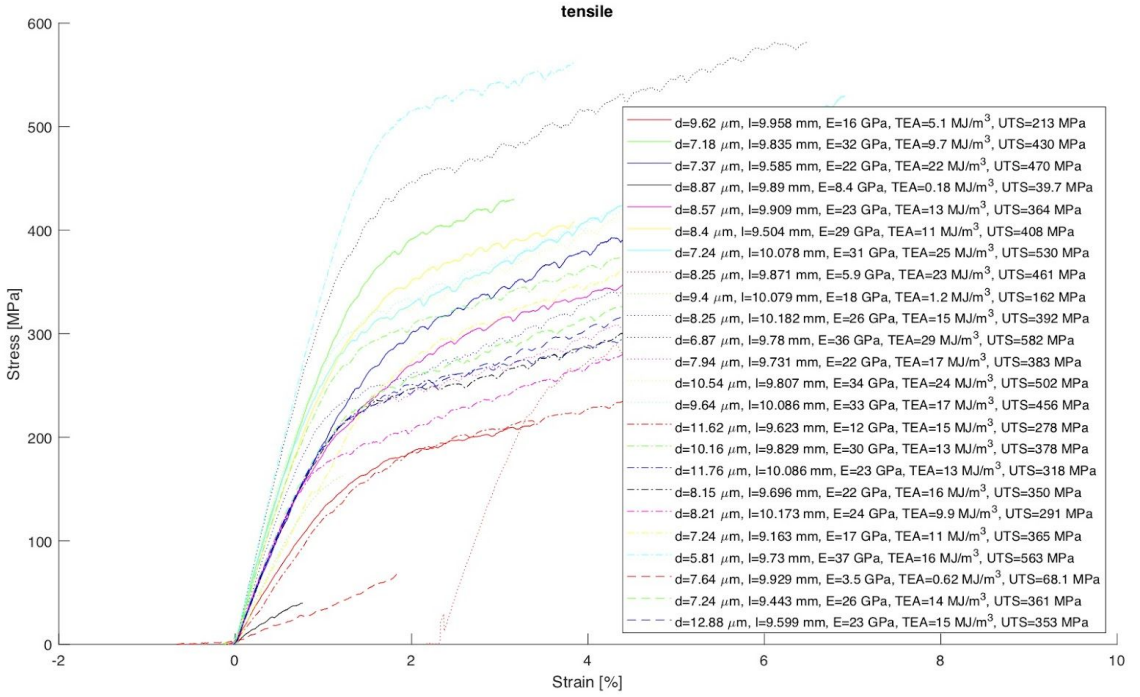

b)

Figure AXIII. Results from tensile testing of filaments spun from $TCNF_{sc}$(0.3 wt%). The minimum width, the length, the elastic modulus, the toughness and the ultimate stress of each filament is presented in order in the legend. Figure a) shows the results for the first half of the filament samples and figure b) shows the results for the second half.

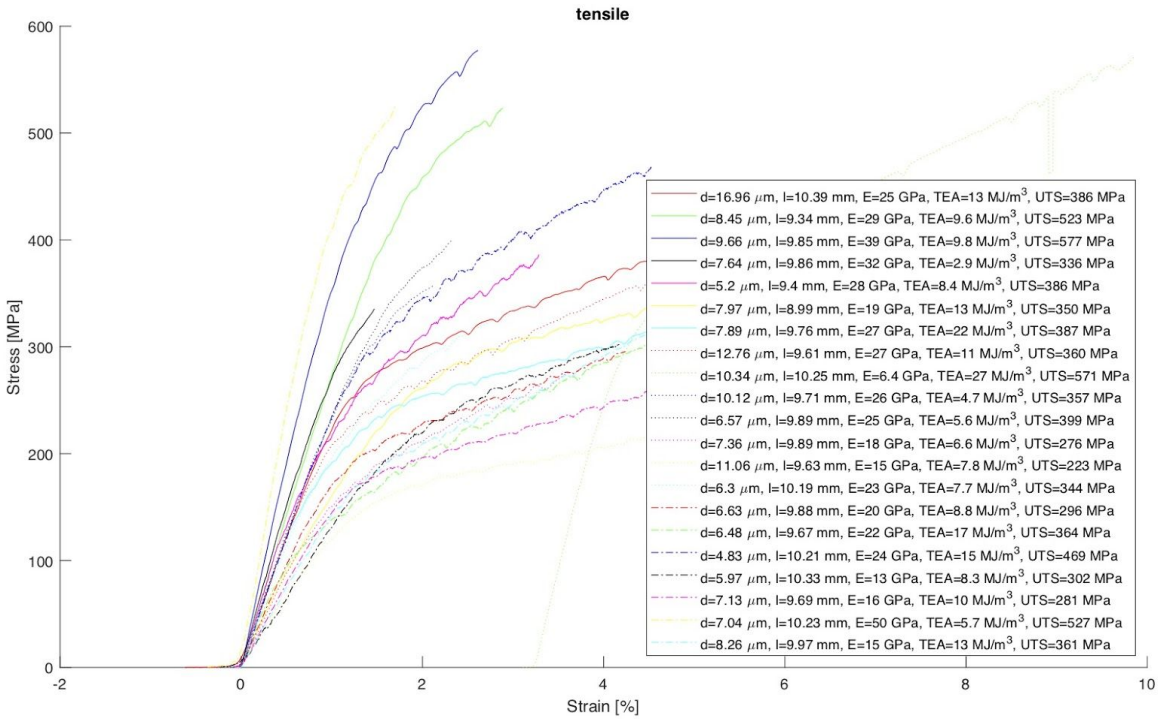

a)

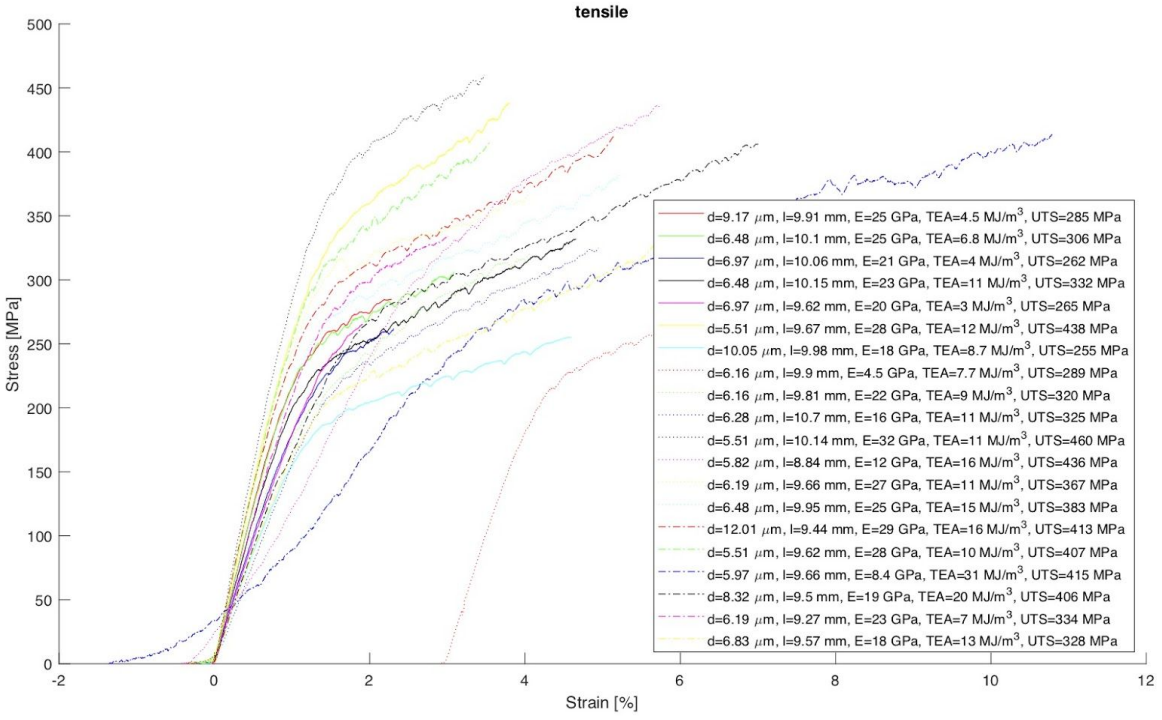

b)

Figure AXIV. Results from tensile testing of filaments spun from TCNF(0.2 wt%). The minimum width, the length, the elastic modulus, the toughness and the ultimate stress of each filament is presented in order in the legend. Figure a) shows the results for the first half of the filament samples and figure b) shows the results for the second half.

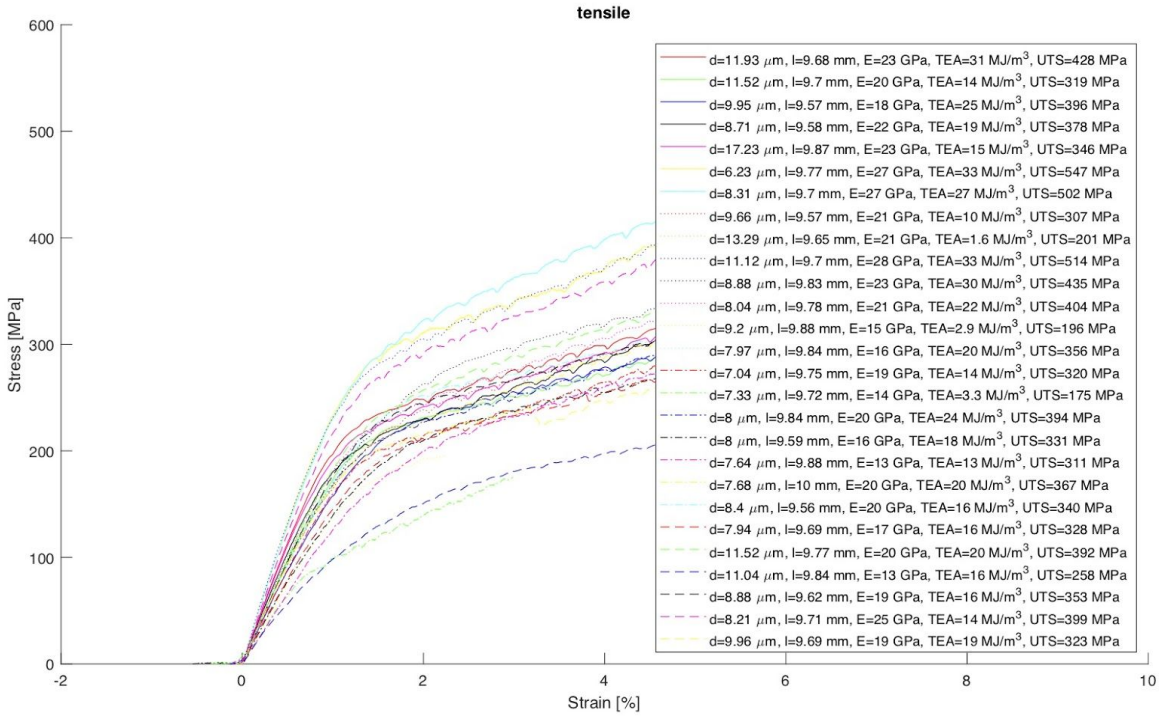

a)

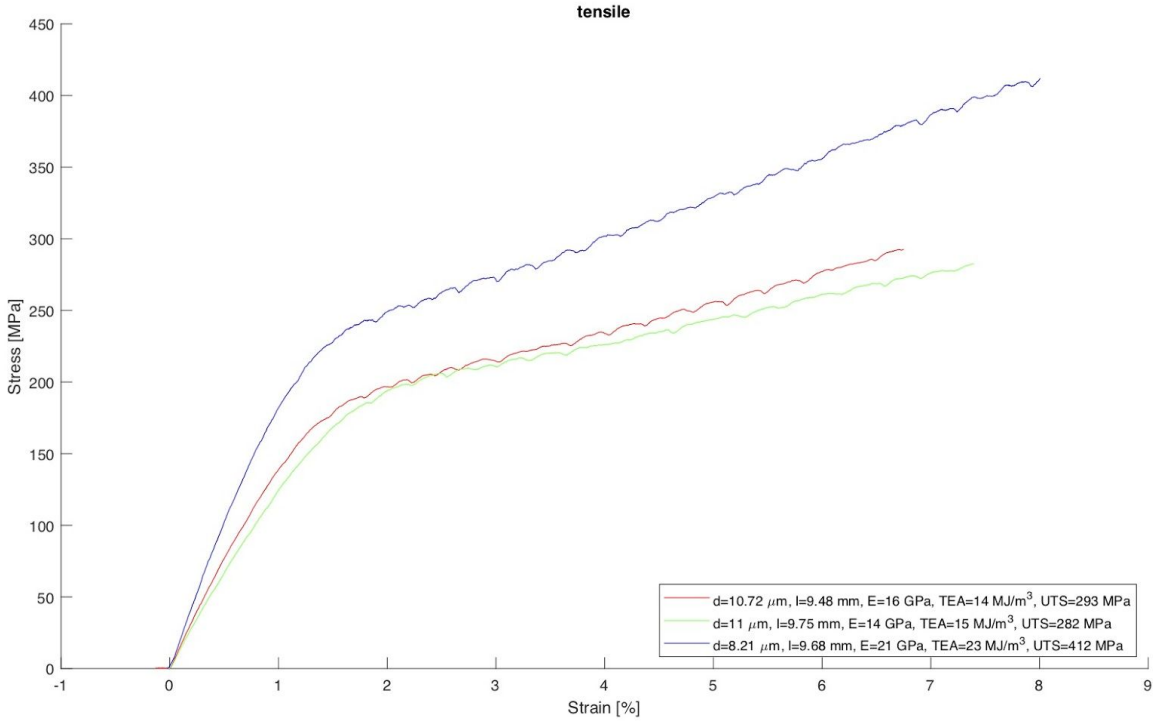

b)

Figure AXV. Results from tensile testing of filaments spun from CMC(0.3 wt%). The minimum width, the length, the elastic modulus, the toughness and the ultimate stress of each filament is presented in order in the legend.

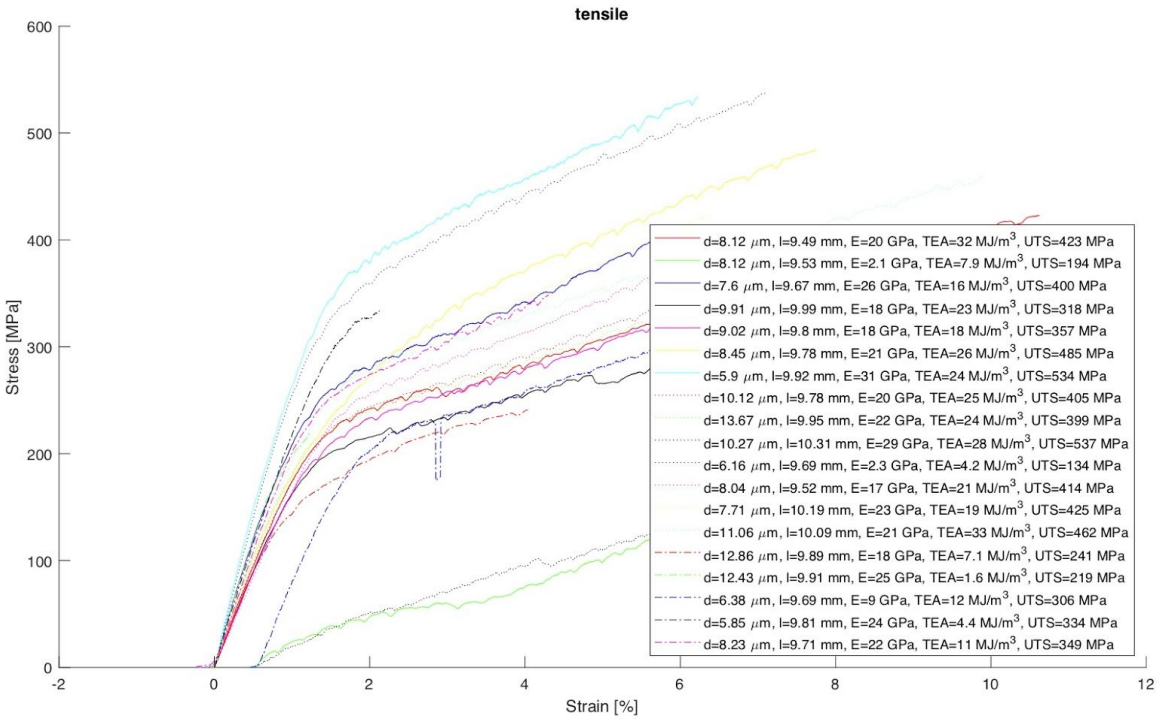

Figure AXVI. Results from tensile testing of filaments spun from CMC(0.2 wt%). The minimum width, the length, the elastic modulus, the toughness and the ultimate stress of each filament is presented in order in the legend.

10.3 Tables

The tables AI through AIV below show the data for the spun filaments samples that has been collected through tensile testing and optical microscopy. Comments have been written both in english and swedish. The rows marked in red indicate samples discarded in calculations as they have not fulfilled requirements mentioned in section 6.5. Rows that are blue contain samples that have been sent to another laboratory for further testing and therefore, tensile testing was not performed on them.

Table AI. The data gathered from tensile testing and optical microscopy for $TCNF_{sc}$(0.3 wt%).

Sample	Width [um]	Abnormalities	Length [mm]	Name at tensile tool	position of breakage	comment	Long comment	Name for Matlab	Elastic modulus, GPa	Ultimate stress, MPa	Strain at break, %	Toughness, MJ/m3
1	9.62	clean	9.958	Test1	at the grip	good		1	16.24744742	212.8029763	3.393090083	5.1
2	10.09	clean	9.388	Test2	at the grip	bad						
3	7.18	clean	9.835	Test3	middle	good		2	32.39047575	430.1169308	3.163395389	9.7
4	7.37	clean	9.585	Test4	middle	good		3	21.85738128	469.601265	6.657661007	22
5	8.87	aggregate, contamination	9.89	Test5	at the grip	bad		4	8.402910364	39.70942245	0.766349485	0.18
6	8.57	clean	9.909	Test6	middle	good		5	23.35086073	363.7520377	5.129755483	13
7	8.4	aggregate, contamination	9.504	Test7	middle	good		6	28.97225854	408.0093673	3.842723977	11
8	7.24	clean	10.078	Test8	middle	good		7	31.46335243	529.8018702	6.913743536	25
9	8.25	clean	9.871	Test9	middle	good	delete last points	8	5.887676934	460.6648952	9.385539166	23
10	9.4	clean	10.079	Test10	at the grip	good		9	17.90810423	162.4064384	1.219780425	1.2
11	8.25	clean	10.182	Test11	middle	good		10	26.39469053	392.1811757	5.66370869	15
12	6.87	clean	9.78	Test12	middle	good		11	36.20285274	581.5308302	6.481304464	29
13	7.94	clean	9.731	Test13	middle	good		12	22.36078514	382.5138611	6.461057442	17
14	11.88	aggregates	9.169	Test14	at the grip	bad						
15	10.54	clean	9.807	Test15	middle	good		13	33.82420745	502.4633349	6.689771413	24
16	9.64	contamination, aggregate	10.086	Test16	middle	good		14	32.63352807	455.776588	5.198427576	17
17	11.62	aggregate	9.623	Test17	middle	good		15	12.32528599	278.2667131	7.442029267	15
18	10.16	clean	9.829	Test18	middle	good		16	29.62888384	378.3698502	4.549331912	13
19	11.76	clean	10.086	Test19	middle	good		17	22.70826044	317.6579564	5.552135126	13
20	8.15	clean	9.696	Test20	middle	good		18	22.31058192	350.2654384	6.405712246	16
21	8.21	clean	10.173	Test21	middle	good		19	23.89177254	291.3920814	4.765517825	9.9
22	7.24	clean	9.163	Test22	middle	good		20	16.90711698	365.3150587	4.461287037	11
23	5.81	clean	9.73	Test23	middle	good		21	36.73337677	562.5424824	3.848735356	16
24	9.08	clean	9.989		middle	good						
25	6.73	bad fixation, clean	9.699	Test24	at the grip	bad						
26	7.64	aggregate	9.929	Test25	middle	good		22	3.466902719	68.08832473	1.846477524	0.62
27	7.24	contamination	9.443	Test26	middle	good		23	25.54258211	360.7978582	5.397899735	14
28	12.88	contamination	9.599	Test27	middle	good		24	23.0357837	352.6685359	5.826330717	15
29	12.64	contamination	9.75	Test28	at the grip	good		1	23.89714628	353.9725082	5.004552998	13
30	13.19	contamination	9.616	Test29	middle	good		2	21.93827538	342.6597061	6.625314574	17
31	12.38	clean	9.304	Test30	at the grip	good		3	20.66992524	335.1341748	7.588340235	18
32	10.41	aggregate	9.474	Test31	middle	good		4	28.56043928	419.8018739	6.047058246	19
33	9.02	clean	9.902	Test32	at the grip	bad						
34	9.62	aggregate	9.562	Test33	at the grip	good		5	12.51114635	312.298629	8.668188802	18
35	8.25	contamination	9.944	Test34	at the grip	bad						
36	11.46	aggregates	9.485	Test35	at the grip	bad						
37	10.91	aggregate	9.805	Test36	middle	good		6	28.24195381	442.2836915	5.452627936	18
38	11.66	aggregate, contamination	9.823	Test37	at the grip	bad						
39	11.66	aggregates	9.938	Test38	middle	good		7	24.39400832	374.6450821	6.797830117	18
40	11.45	clean	10.219	Test39	middle/at the grip	good		8	25.3431544	403.6451122	6.787108997	20
41	7.97	clean	9.808	Test40	middle	good		9	19.64651098	381.5927441	8.545978423	22
42	6.6	clean	9.557	Test41	middle	good		10	37.30980316	573.1449029	4.819156971	21
43												
44												
45												
46												
47												
48			3D nanotomography									
49												
50												
51												
52												
53												
54	10.05	aggregate, contamination	9.605	Test42	at the grip	good		11	17.0217331	270.6458373	5.238174578	10
55	9.08	aggregate, contamination	10.269	Test43	middle	good		12	20.31941039	301.8003123	5.089099945	11
56	7.64	aggregate, contamination	10.047	Test44	middle	good		13	22.95752739	363.1699217	4.72739671	12
57	6.42	contamination	9.944	Test45	middle	good		14	28.92817908	406.8666467	4.497956717	13
58	10.61	aggregate	10.199	Test46	middle	good		15	26.78085109	378.4023962	5.900601616	16
59	11.84	contamination	10.098	Test47	at the grip	bad						
60	12.12	aggregate	10.197	Test48	middle	good		16	23.16238707	348.8456305	6.382458008	17

Table AII. The data gathered from tensile testing and optical microscopy for TCNF(0.2 wt%).

Sample	Width [um]	Abnormalities	Length [mm]	Name at tensile tool	Position of breakage	Comment	Long comment	Name for Matlab	Elastic modulus, GPa	Ultimate stress, MPa	Strain at break, %	Toughness, MJ/m3
1	16.96	Aggregate	10.39	Test1	middle	good		1	24.72610726	386.3363221	4.618716783	13
2	13.68	Aggregate, skräp	9.85	Test2	middle	bad	paper pieces were in touch,					
3	11.02	Aggregate	9.89	Test3	at the grip	bad	it could be a reason for disturbances in data collection					
4	8.45	Aggregate	9.34	Test4	middle	good		2	28.56569757	523.4505202	2.888385116	9.6
5	8.71	skräp	9.73	broken								
6	6.19	skräp, aggregate	9.27									
7	9.66	Aggregate, skräp	9.85	Test5	next to grip	ok	strange ending, slipped out?	3	38.93379355	577.3677838	2.613105388	9.8
8	7.64	skräp	9.86	Test6	next to grip	good		4	31.9636994	335.545663	1.469966623	2.9
9	9.79	skräp, aggregate	10.41	Test7	next to grip	bad	strange beginning					
10	5.2	ser ut att vara twistad	9.4	Test8	at the grip	good		5	28.36027991	386.3418335	3.285584939	8.4
11	7.97	skräp	8.99	Test9	middle	good		6	19.36162935	349.8569689	5.093061664	13
12	11.29	Skräp	10.02	3D nanotomography								
13	8.91	Aggregate	8.85									
14	6.53		9.06	Trasig								
15	9.78	Skräp (mycket, typ damm)	9.54	3D nanotomography								
16	6.23	aggregate	8.84	dublicates								
17	6.83	aggregate	9.57									
18	7.89		9.76	Test10	next to grip	good		7	26.53778164	386.8399587	7.742936646	22
19	7.79	skräp	9.04	Test11	next to grip	bad	strange shape					
20	12.76	skräp	9.61	Test12	middle	good		8	26.65209412	360.2499268	4.479827539	11
21	10.34	aggregate	10.25	Test13	middle	good	remove last points	9	6.371159346	571.4384038	9.865026124	27
22	8.64	lös, skräp	10.4	3D nanotomography								
23	10.12		9.71	Test14	very close to grip	good		10	25.518574	357.2164231	2.122650457	4.7
24	6.57	skräp	9.89	Test15	at the grip	good		11	24.69799495	399.2539509	2.318445529	5.6
25	7.36	skräp	9.77	Test16	middle	good		12	17.91007076	276.2833039	3.613452448	6.6
26	11.06		9.63	Test17	middle	good		13	14.51474531	223.2374854	4.870715664	7.8
27	6.42		9.84	Test18	at the grip	bad	strange ending, dublicate, slipped out?					
28	6.11	trasig	9.74	Trasig								
29	6.3	aggregate, skräp	10.19	Test19	at the grip	good		14	23.27793402	343.5094276	3.298104589	7.7
30	5.48	aggregate	10.1	snurrad så svårt att se	Test20	at the grip	bad	strange ending, dublicate, slipped out?				
31	6.63		9.88	Test21	middle	good		15	19.87027059	295.7064172	4.240730347	8.8
32	6.48		9.67	Test22	at the grip	good		16	21.69085433	363.8345634	6.866697814	17
33	4.83		10.21	Test23	middle	good		17	24.39370461	468.5038248	4.522441051	15
34	Trasig			Trasig								
35	5.97	aggregate	10.33	Test24	middle	good		18	13.15073691	302.1814136	4.173746722	8.3
36	6.83		9.43	Test25	middle	bad	strange beginning					
37	3.68	aggregate, skräp, lös, *buk	10.57	Olika bredder vid upp- och nedbuktningar etc, svårt att mäta	Test26	at the grip	bad					
38	7.13		9.69	Test27	middle	good		19	15.89126904	280.6444309	5.346329369	10
39	7.04		10.23	Test28	at the grip	good		20	49.84958664	526.7910578	1.708311707	5.7
40	8.26	aggregate	9.97	twistad som fan	Test29	at the grip	good	21	14.93368466	361.1325881	5.656103645	13
41	trasig		10.17	Trasig								
42	9.17	aggregate	9.91	Test1	at the grip	good		1	24.82056135	284.8634037	2.28230274	4.5
43	6.48	lös tråd	10.1	Test2	at the grip	good		2	24.64328005	306.0672518	3.087729215	6.8
44	6.97		10.06	Test3	middle	good		3	20.87026636	261.993502	2.307544666	4
45	6.48		10.15	Test4	middle	good		4	22.69562895	331.9008745	4.658621034	11
46	6.97		9.62	Test5	at the grip	good		5	20.1517178	265.2044998	1.91006709	3
47	trasig		10.38	Trasig								
48	5.51	skräp	9.67	Test6	at the grip	ok	something strange in the beginning, data points can be deleted	6	28.32820171	438.4113692	3.808125377	12
49			Trasig	Trasig								
50	10.05		9.98	Test7	middle	good		7	18.21776454	255.2829142	4.59340012	8.7
51	6.16	knut/skräp? förgrening/da	9.9	Test8	middle	good	delete last points	8	4.507546723	289.4582489	6.72009715	7.7
52	6.16	skräp	9.81	Test9	middle	good		9	21.67775096	320.249303	4.059558492	9
53	6.28	skräp	10.7	Test10	middle	good	filament is too curved	10	15.67375913	324.9644199	4.945788978	11
54	5.51	skräp	10.14	Test11	middle	good		11	31.96830297	459.8934387	3.478436482	11
55	5.82	skräp	8.84	Test12	middle	good		12	11.9431814	436.2262913	5.735085348	16
56	6.19		9.66	Test13	middle	good		13	27.11933883	366.6503772	4.037076944	11
57	6.48	skräp	9.95	Test14	middle	good		14	24.51560918	382.089333	5.226097898	15
58	12.01	skräp, aggregat	9.44	Test15	middle	good		15	29.39975873	412.6861041	5.155671779	16
59	9.2		9.53	3D nanotomography								
60	5.51	aggregat	9.62	Test16	middle	good		16	28.25532408	406.8666954	3.541039656	10
61	5.97	aggregat	9.66	Test17	middle	good	strange yielding, multithread?	17	8.356763773	414.6780074	10.80422804	31
62	8.32		9.5	Test18	middle	good		18	18.55549988	406.3243218	6.999973836	20
63	5.9		9.82	3D nanotomography								
64	6.16	skräp	9.95	Test19	at the grip	bad	strange ending					
6	6.19	skräp, aggregate	9.27	Test21	middle	good		19	22.69169148	334.1674118	3.006539497	7
16	6.23	aggregate	8.84	Test22	middle	bad	brittle crush in the beginning of the curve, multifilament?					
17	6.83	aggregate	9.57	Test23	middle	good		20	17.65929955	327.956194	5.694231265	13

For table AIII the light yellow marking indicates clean samples, while red marking indicates discarded samples.

Table AIII. The data gathered from tensile testing and optical microscopy for CMC(0.3 wt%).

Sample	Width (um)	Abnormalities	Length (mm)	Name at tensile tool	Position of breakage	Comment	Long comment	Name for Matlab	Elastic modulus, GPa	Ultimate stress, MPa	Strain at break, %	Toughness, MJ/m3
1	11.93		9,68	Test1	middle	good		1	23.26348459	428.4129188	9.846853534	31
2	11.52	aggregat, skräp	9,70	Test2	middle	good		2	19.85416397	318.9260301	5.991860367	14
3	9.95	aggregat	9,57	Test3	at the grip	good		3	18.08161911	395.5286713	9.121749644	25
4	8.71		9,58	Test4	middle	good		4	21.65332126	378.0793196	7.285502575	19
5	14.8	aggregat	9,77	Test5	at the grip	bad	strange ending					
6	14.83	aggregat	9,79	Test6	at the grip	bad	strange ending					
7	16.08	aggregat, skräp	9,70	Test7	at the grip	bad	strange ending					
8	17.23	skräp, aggregat	9,87	Test8	middle	good		5	22.88626511	346.3835114	6.076798874	15
9	6.23		9,77	Test9	middle	good		6	26.74712146	547.2717498	8.862118673	33
10	8.31		9,70	Test10	middle	good		7	26.84745503	502.0815186	7.477338104	27
11	9.66		9,57	Test11	middle	good		8	20.55688441	306.6988819	4.710368783	10
12	13.29	aggregat, skräp	9,65	Test12	middle	good		9	20.63307781	200.6098993	1.380485996	1.6
13	11.12	skräp	9,70	Test13	middle	good		10	28.31558218	514.0854729	9.000119891	33
14	8.88	skräp	9,83	Test14	middle	good		11	22.93787566	434.6232166	9.438926432	30
15	9.11	abnormalcy	9,91	Test15	at the grip	bad	strange ending					
16	8.78	skräp	9,95	Test16	at the grip	bad	strange ending					
17	8.04		9,78	Test17	middle	good		12	21.39199387	404.0304231	7.794403672	22
18	9.2	aggregat	9,88	Test18	middle	good		13	15.00172787	195.9707118	2.252722265	2.9
19	8.31		9,74	Test19	at the grip	bad	strange ending					
20	7.25		9,66	Test20	at the grip	bad	strange ending					
21	7.64	aggregat	9,87	Test21	at the grip	bad	strange ending					
22	13.6		9,90	Test22	at the grip	bad	strange ending					
23	12.11	aggregate, dublicate	9,77	Test23	at the grip	bad	strange ending					
24	9,52	clean	9,90	Test24	at the grip	bad	strange ending					
25	7,97	aggregate	9,84	Test25	middle/grip	good		14	16.12311241	355.83883	7.934031641	20
26	7,04	clean	9,75	Test26	middle	good		15	19.04561699	320.459284	6.198580235	14
27	7,33	aggregate	9,72	Test27	middle	good		16	13.65387859	175.4121847	2.986862959	3.3
28	8,00	clean	9,84	Test28	at the grip	good		17	19.94439969	393.6805812	8.710407217	24
29	7,49	clean	9,82	Test29	at the grip	bad	strange ending					
30	8,00	clean	9,59	Test30	middle	good		18	15.89647313	330.9365419	7.805833411	18
31	7.64	aggregate/contamination	9.88	Test31	middle	good		19	13.17896876	311.0649975	6.047158424	13
32	7.68	aggregate	10	Test32	middle	good		20	19.90669386	366.7262415	7.486360891	20
33	8.4	aggregate, contamination	9.56	Test33	middle	good		21	19.87925659	340.1185787	6.269068982	16
34	7.94	clean	9.69	Test34	middle	good		22	16.75394697	327.5873489	6.920680381	16
35	11.52	aggregate	9.77	Test35	middle	good		23	19.66599307	391.6337819	7.218661043	20
36	13.75	aggregate	9.8	Test36	at the grip	bad	strange ending					
37	11.04	aggregate	9.84	Test37	at the grip	good		24	12.8182808	257.9249613	8.472316672	16
38	10.59	aggregate	9.82	Test38	at the grip	bad	strange ending					
39	8.88	clean	9.62	Test39	middle	good		25	19.48083839	352.8212623	6.379640068	16
40	8.21	aggregate	9.71	Test40	middle	good		26	25.03118925	399.1788634	5.086882914	14
41	11.04	clean	9.64	Test41	at the grip	bad	strange ending					
42	9.96	contamination, twist	9.69	Test42	middle	good		27	19.16198894	323.3238624	8.012225422	19
43	10.72	clean	9.48	Test43	at the grip	good		1	16.13158708	292.6428079	6.749993168	14
44	11	contamination	9.75	Test44	middle	good		2	14.07163536	282.4995231	7.395825587	15
45	17.59	aggregate, contamination	9.52	Test45	at the grip	bad	strange ending					
46	17.32	contamination, dublicate	9.81	Test46	at the grip	bad	strange ending					
47	16.69	aggregate, dublicate ?	9.74	Test47	at the grip	bad	strange ending					
48	8.21	clean	9.68	Test48	middle	good		3	21.14393189	412.0122928	8.005583883	21

For table AIV the red marks mean discarded samples and the yellow mark indicates the only clean samples obtained.

Table AIV. The data gathered from tensile testing and optical microscopy for CMC(0.2 wt%).

Sample	Width [um]	Abnormalities	Length [mm]	Name at tensile tool	Position of breakage	Comment	Long comment	Name for Matlab	Elastic modulus, GPa	Ultimate stress, MPa	Strain at break, %	Toughness, MJ/m3	
1	8.12		9,49	Test1	middle	good		1	19.98129088	423.0685616	10.62526741	32	
2	8.12	skräp	9,53	Test2	at the grip	good		2	2.061589383	193.8908744	8.639749726	7.9	
3	9.29	skräp	9,96	Test3	at the grip	strange endind							
4	8.45	aggregat	9,49	Test4	broken								
5	7.64	aggregat	9,67	Test5	middle	good		3	25.91567674	400.4724198	5.705980411	16	
6	9.91	skräp	9,99	Test6	middle	good		4	18.29056142	318.0340351	9.374132765	23	
7	9.02	aggregat	9,80	Test7	middle	good		5	17.81226326	356.6578932	7.256747009	18	
8	8.45	aggregat, skräp	9,78	Test8	middle	good		6	20.84818644	484.7168704	7.745771712	26	
9	5.9	clean	9,92	Test10	middle	good		7	31.27207125	534.298535	6.227218283	24	the only defectless filament
10	6.53		9,62	Test9	middle	bad							
11	10.12	skräp	9,78	Test11	middle	good		8	19.64168092	405.4129244	8.826513172	25	
12	13.67	aggregat	9,95	Test12	middle	good		9	21.76763397	399.3398275	8.658972328	24	
13	10.27	skräp, aggregat	10,31	Test13	middle	good		10	28.8204783	537.3285619	7.092370522	28	
14	6.16	aggregat, skräp	9,69	Test14	middle	good		11	2.313178371	133.6030239	6.076248998	4.2	
15	8.04	aggregat	9,52	Test15	middle	good		12	16.79193146	413.585749	7.333894153	21	
16	7.71	skräp	10,19	Test16	middle	good		13	23.31604279	425.1071047	6.390796387	19	
17	11.06	skräp, aggregat	10,09	Test17	middle	good		14	20.92121557	462.2194806	9.925648812	33	
18	12.86	skräp, aggregat	9,89	Test18	middle	good		15	18.48393163	240.9464508	4.038115511	7.1	
19	12.43	skräp, aggregat	9,91	Test19	middle	good		16	25.13656514	218.7937574	1.225921328	1.6	
20	10.86	aggregat	10,01	Test20	at the grip	bad	strange ending						
21	6.38		9,69	Test21	middle	good	delete last points	17	8.999952592	305.7998602	5.971951695	12	
22	5.85	aggregat	9,81	Test22	middle	good		18	24.07423247	333.8539725	2.128510222	4.4	
23	8.23	böjning, skräp, snurrning (7,55), agg	9,71	Test23	middle	good		19	21.73526712	348.6044438	4.302366766	11	